ELI-ALPS Research Institute
TOWARDS THE SHARP END OF ATTOSCIENCE

Atto-second pulses generation and amplification in laser plasmas

A.Andreev[1,2,3]

1. ELI-ALPS, Szeged, Hungary
2. St. Petersburg State University, St. Petersburg, Russia
3. Max-Born Institute, Berlin, Germany

SZÉCHENYI 2020
Hungarian Government
European Union
European Regional Development Fund
INVESTING IN YOUR FUTURE

Outline

- Motivation
- Atto-pulses production from gas/plasma by intense laser radiation
- Atto-pulses production from solid by high intense laser radiation
- Fast particle generation and atto-pulses production from nano-structure targets at ultra-high laser intensity
- Amplification of ultra-short pulses
- Conclusion

High intensity lasers and its applications

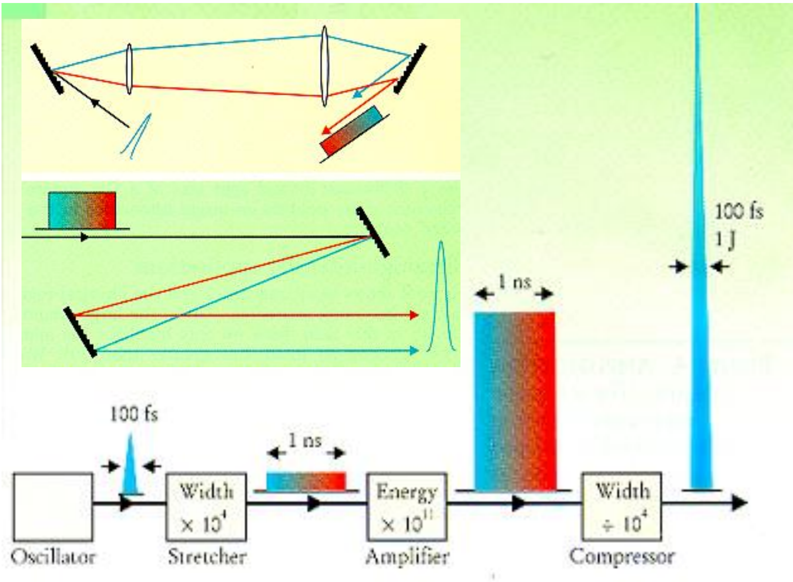

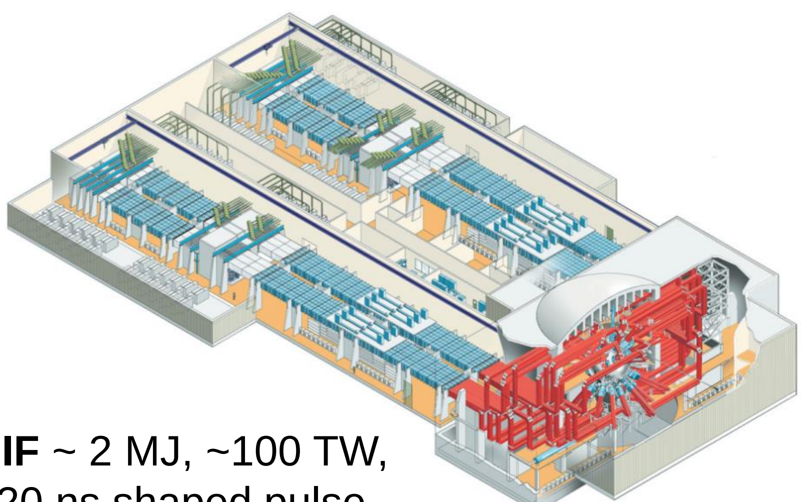

NIF ~ 2 MJ, ~100 TW, ~20 ns shaped pulse

$I_L=\varepsilon_L/t_L S_L$[Wcm-2], $E_L=(4\pi I_L/c)^{1/2}$

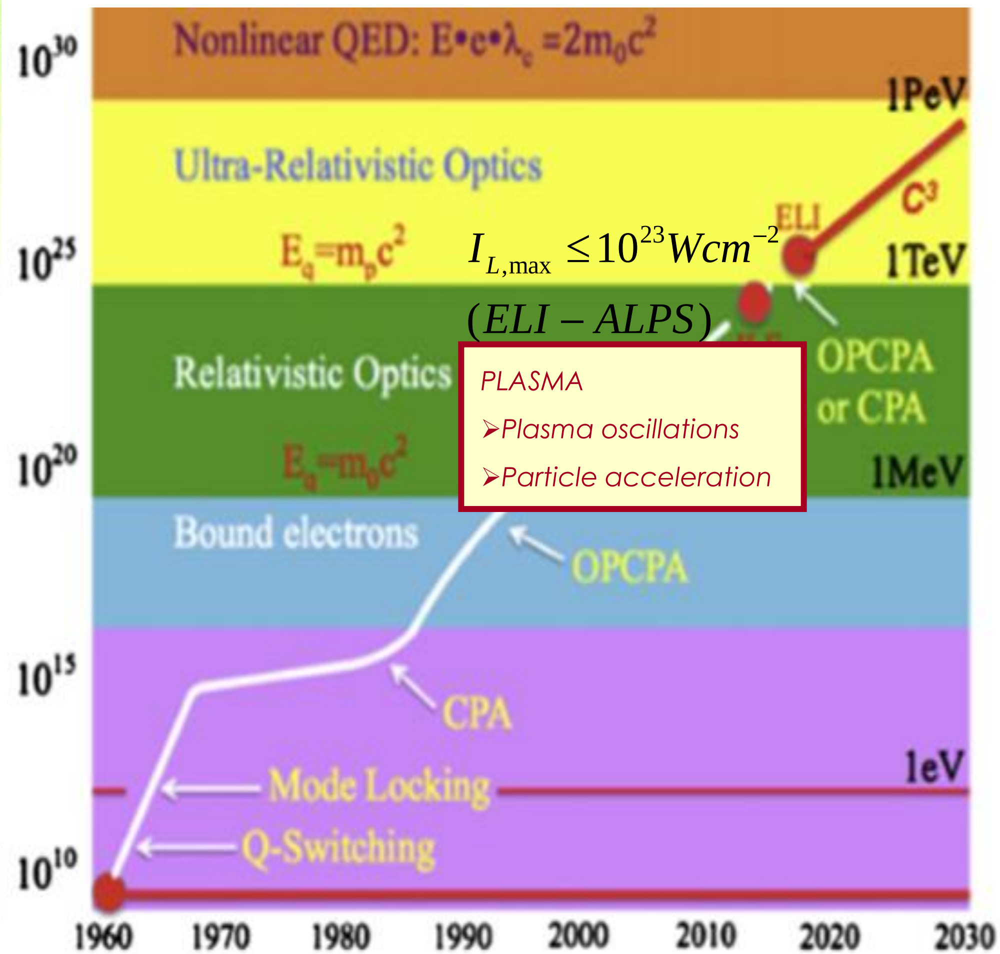

G.Mourou et al., 2006

Different regimes of laser matter interaction

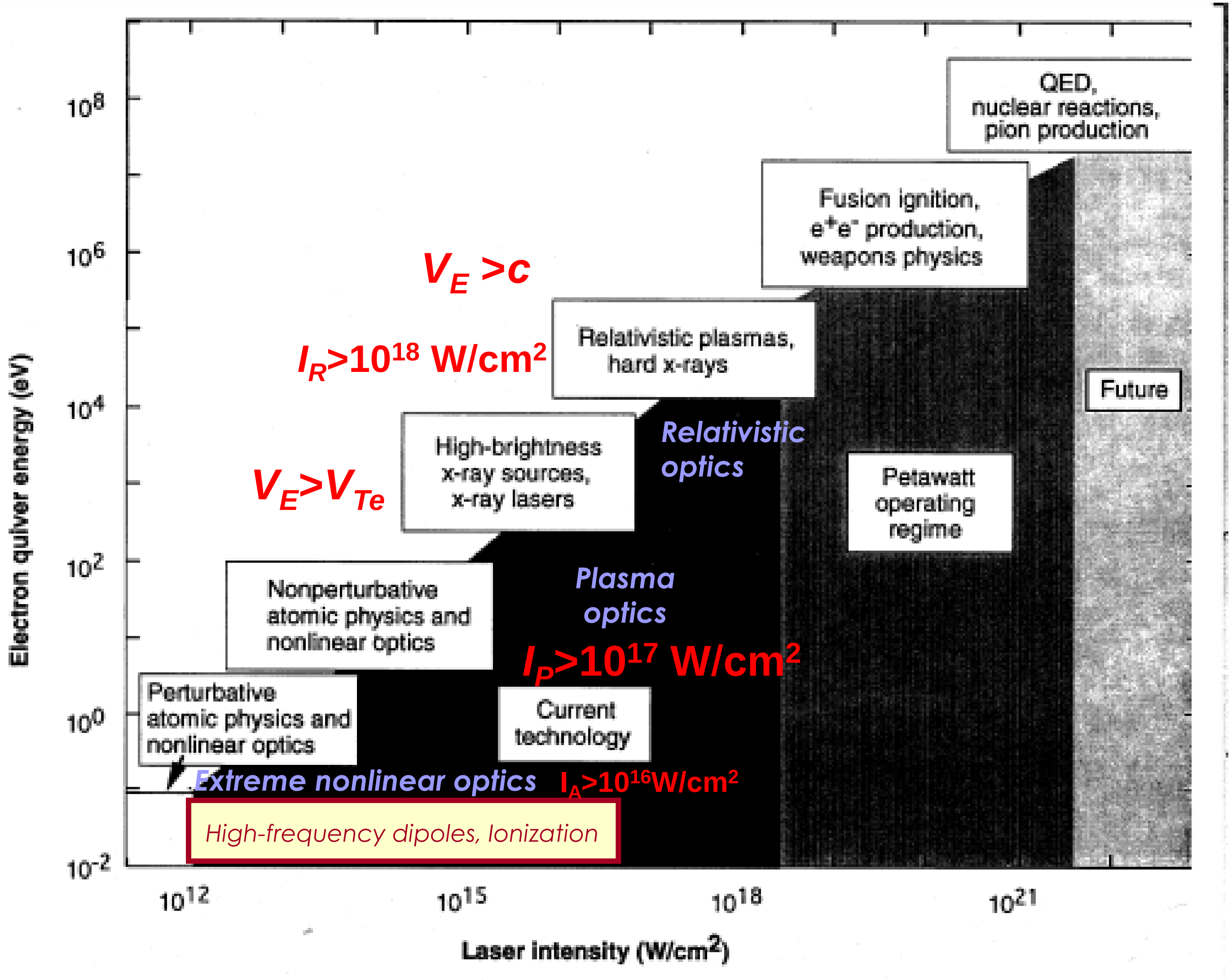

More Intense, Shorter Pulses

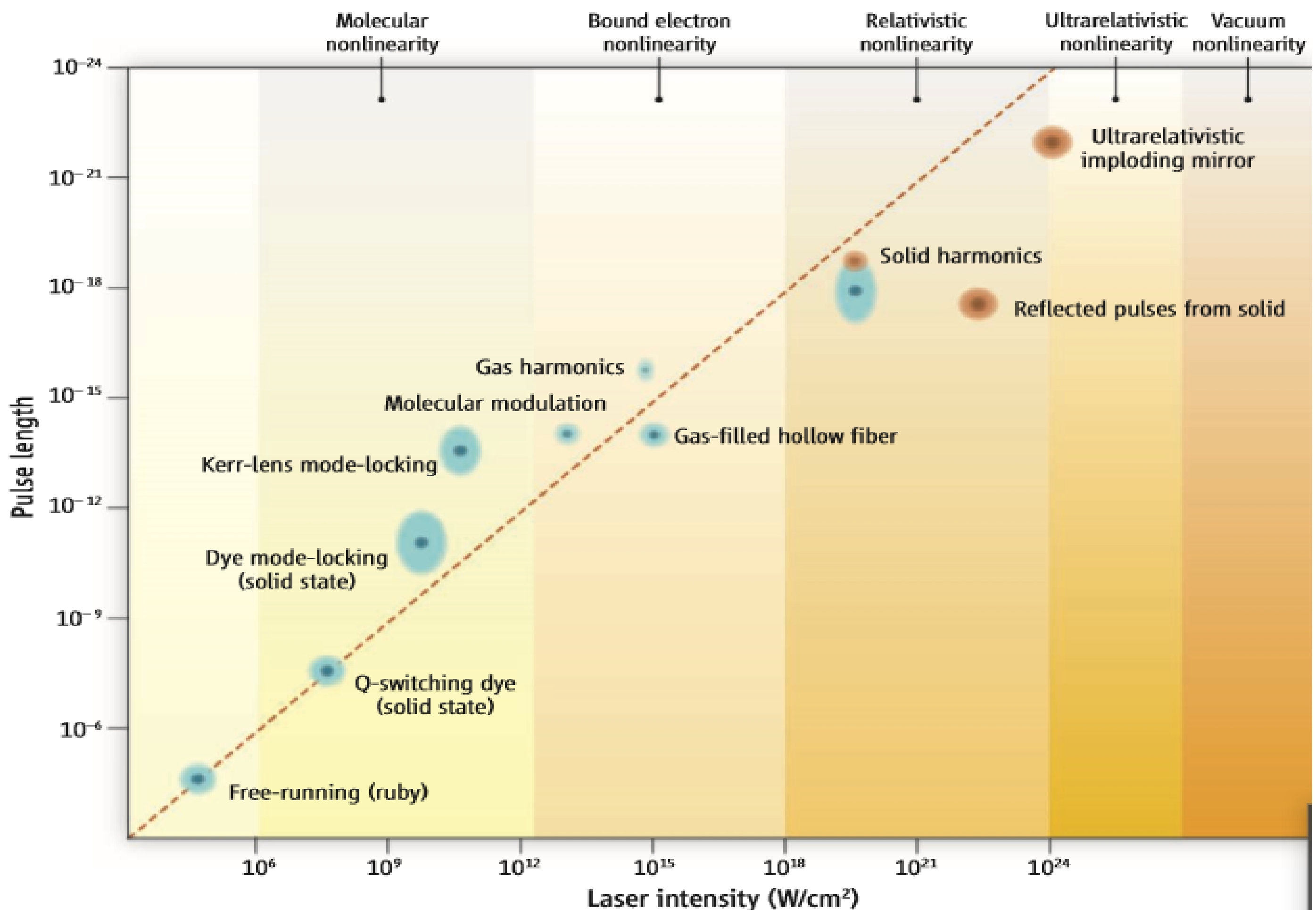

Shorter, more intense. An inverse linear dependence exists over 18 orders of magnitude between the puls duration of coherent light emission and the laser intensity. These entries encompass different underlyi physical regimes that exhibit molecular, bound atomic electron, relativistic plasma, ultrarelativistic, ar vacuum nonlinearities. Blue patches represent experimental data; red patches denote simulation or theory

G.Mourou et al., SCIENCE (2011)

Laser pulse harmonic generation in nonlinear media

$F \sim \sin(\omega t)$ $F << F_c$ $F_c = F_a \sim e^2/r^2_{Bohr}$

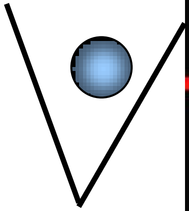

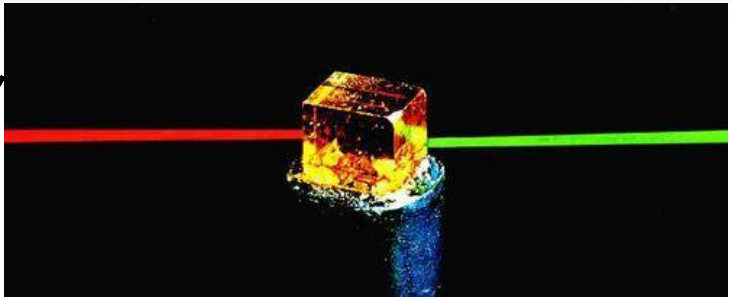

$x \sim \sin(\omega t) + \alpha_2 \sin(2\omega t) + \alpha_3 \sin(3\omega t) + \ldots$

$\alpha_n \sim (F/F_c)^n$

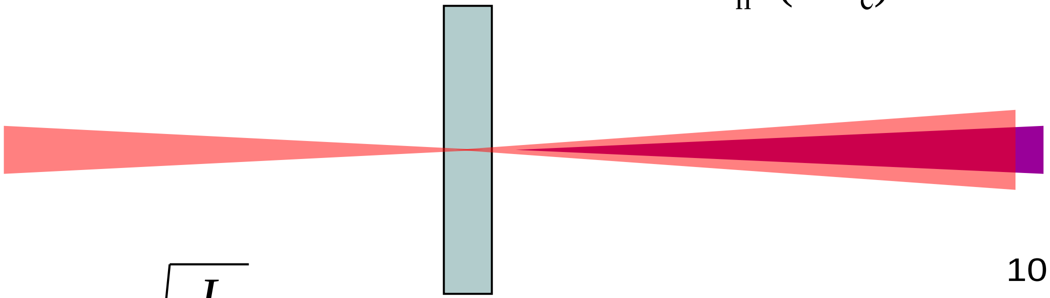

$$\gamma = \sqrt{\frac{I}{2U}}$$

Gas target

$\gamma < 1$

$$U = \frac{e^2 E^2}{4m\omega^2}$$

Pondermotive energy

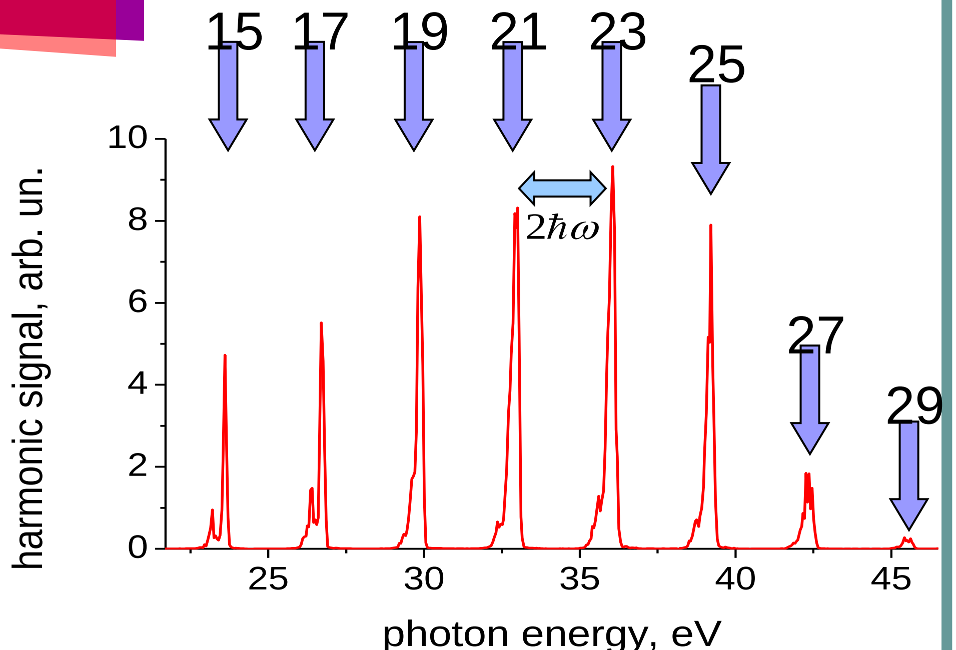

Experiment: Ar, Ti:Sapp laser

800 nm, 2 10^{14} W/cm^2

Three steps mechanism

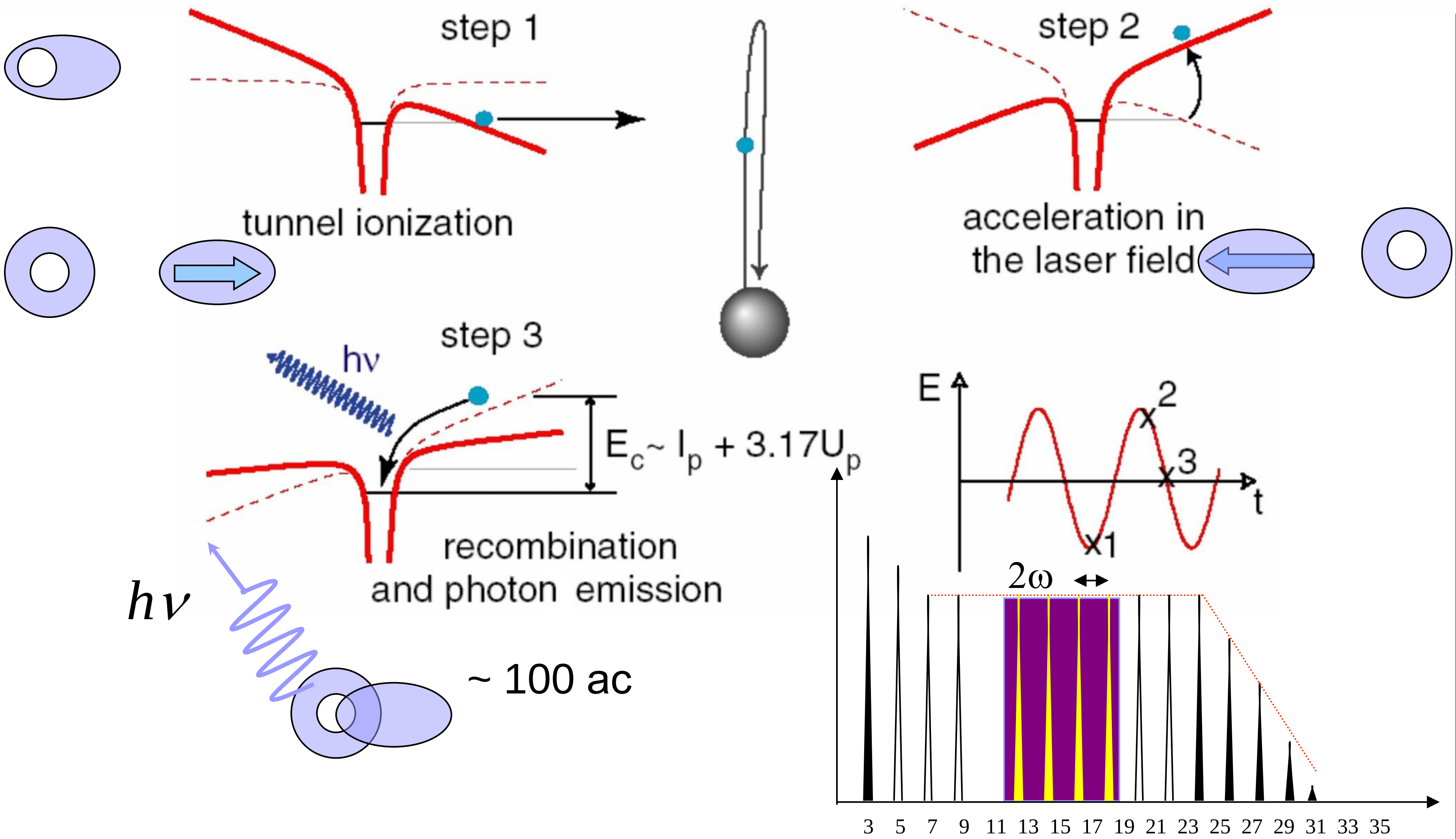

P.B. Corkum, PRL 71, 1994 (1993)

Simple model

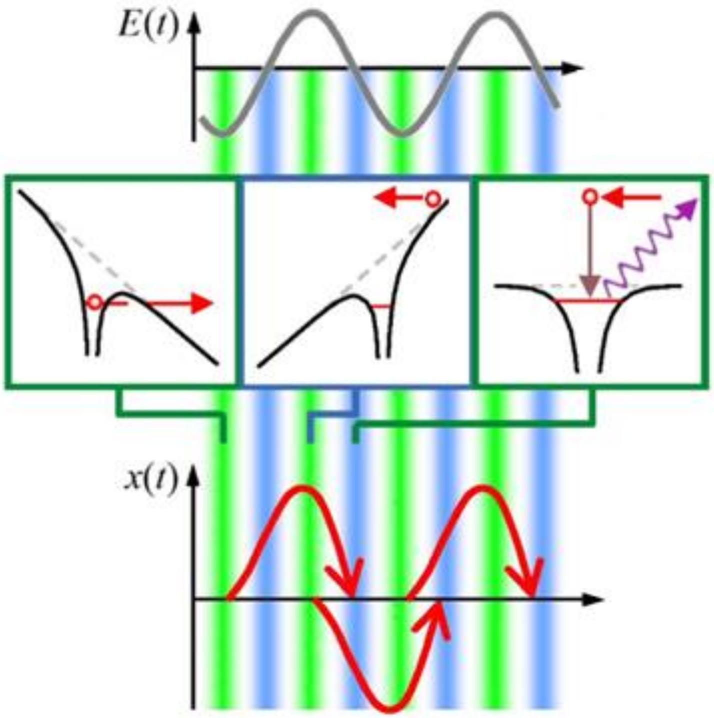

$$\ddot{x}(t) = -E(t) \qquad E(t) = E\sin\omega t$$

$$v(t) = \frac{E}{\omega}(\cos\omega t - \cos\varphi),$$

$$x(t) = \frac{E}{\omega^2}\left[(\sin\omega t - \sin\varphi) - (\omega t - \varphi)\cos\varphi\right],$$

$$x(t_r) = 0, \qquad \sin(\varphi+\tau) - \sin\varphi = \tau\cos\varphi,$$

$$\tau = \omega(t_r - t_0) \qquad \mathrm{tg}\,\varphi = \frac{\tau - \sin\tau}{\cos\tau - 1}.$$

$$E_{kin} = \frac{v(t_r)^2}{2} = \frac{E^2}{2\omega^2}\left[\cos(\varphi+\tau) - \cos\varphi\right]^2$$

$$\frac{E_{kin}}{U_p} = 2\left[\frac{C^2(\tau)\tau}{\tau - \sin\tau - C(\tau)}\right], \quad C(\tau) = \sin\tau - \frac{2(1-\cos\tau)}{\tau}.$$

$$E_{\max} \approx 3.17\,U_p \qquad \begin{array}{l}\tau = 4.09\ \ (234^\circ)\\ \varphi = 1.88\ \ (108^\circ).\end{array} \qquad N_{\max} \approx \frac{I_p + 3.17\,U_p}{\omega}$$

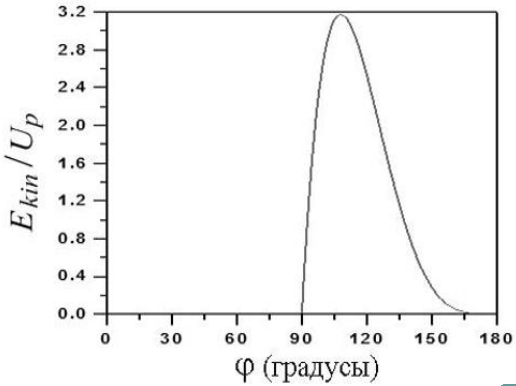

Wavelength dependence

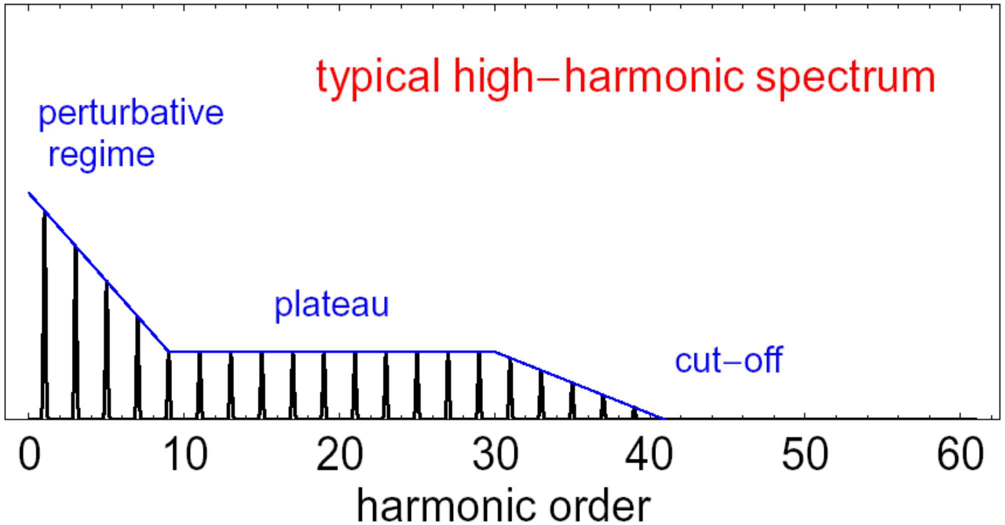

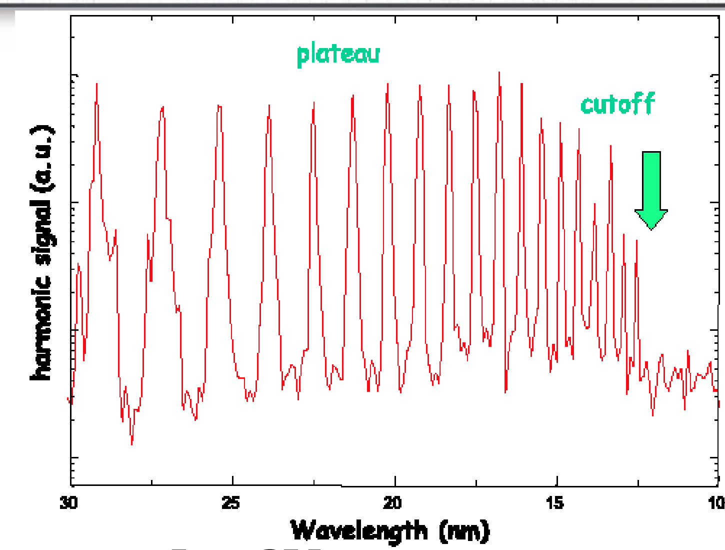

$$N_{\max} \approx \frac{I_p + 3U_p}{\hbar\omega_L}, U_p \propto I_L \lambda_L^2$$

$$I_L \neq I_{L,\max} : \quad I_{L,\max} = E_L / t_L S_{L,\min}$$

$$= E_L / t_L \alpha \lambda_L^2 \propto \lambda_L^{-2}$$

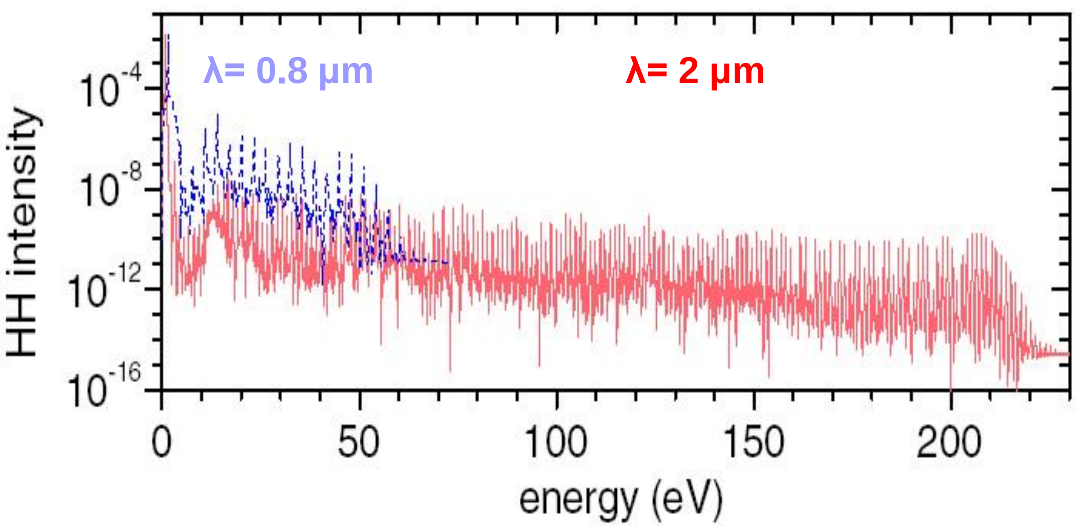

Two-color enhancement

L.Chipperfield, PRL (2009).

The color mixing, or wave front synthesis, of laser pulses has been proven to be a promising way to increase the efficiency of HHG.

Resonant harmonic enhancement: comparison of the experimental, numerical and analytical results

Resonant HHG: review of experiments

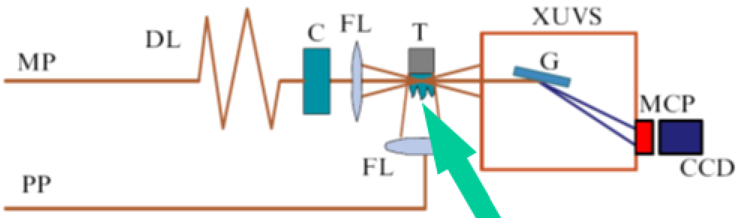

efficiency 10^{-4}

strong ellipticity dependence

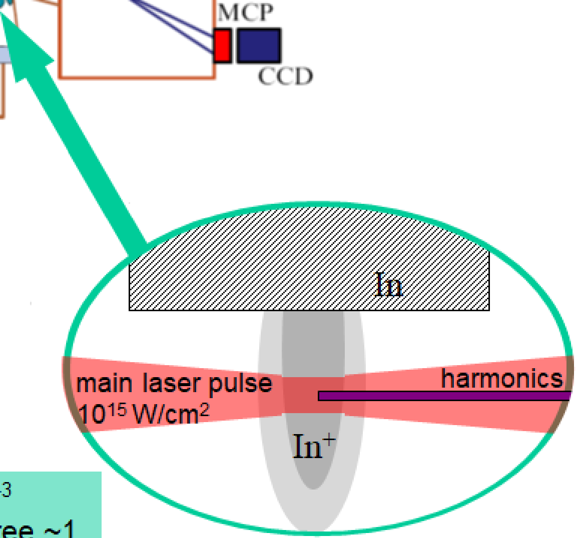

10^{17} – 10^{18} cm^{-3}
ionization degree ~1

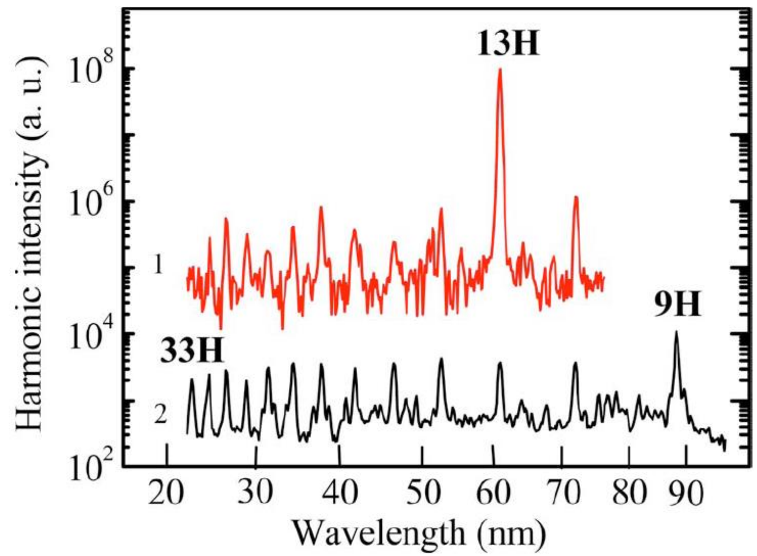

Resonant HHG model V. Strelkov, PRL, 2010

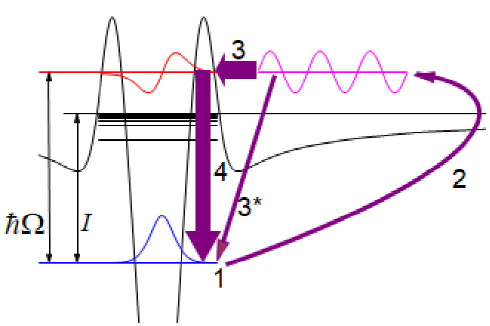

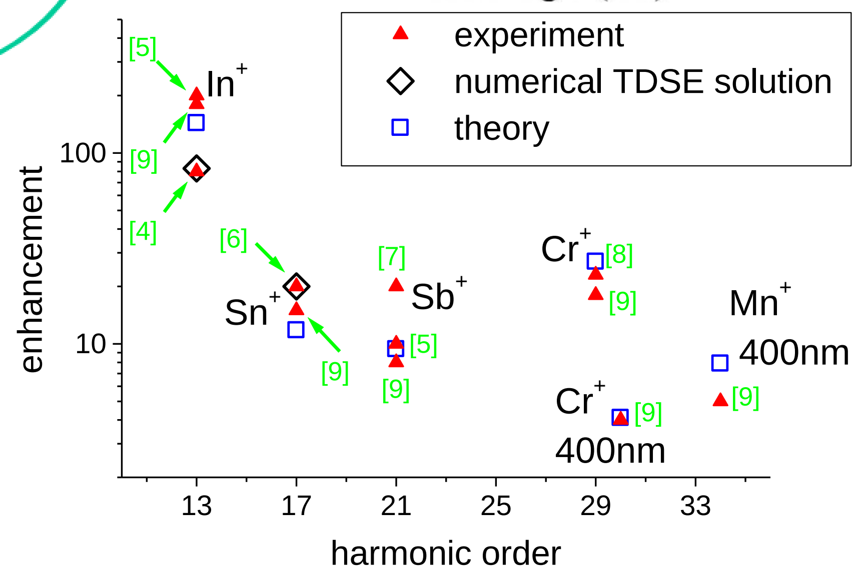

R. A. Ganeev, Physics-Uspekhi, **52**, 55 (2009).

Relativistic oscillating electron

$$\frac{\mathrm{d}\boldsymbol{p}}{\mathrm{d}t} = -e\boldsymbol{E} - \frac{e}{c}[\boldsymbol{v}\boldsymbol{H}], \qquad \boldsymbol{v}(0) = \boldsymbol{v}_0,\ \boldsymbol{r}(0) = \boldsymbol{r}_0.$$

$$E_x = E_0(x,y,\xi)\sqrt{\frac{1+\alpha}{2}}\cos\varphi,$$

$$E_y = \mp E_0(x,y,\xi)\sqrt{\frac{1-\alpha}{2}}\sin\varphi, \qquad \varepsilon = \lambda/(2\pi\rho_0)$$

$$E_z = -2E_0(x,y,\xi)\frac{\varepsilon}{\rho}\left(\sqrt{\frac{1+\alpha}{2}}\,x\sin\bar{\varphi} \pm \sqrt{\frac{1-\alpha}{2}}\,y\cos\bar{\varphi}\right),$$

$$H_x = -E_y,\ \ H_y = E_x, \qquad \rho(z) = \rho_0(1 + z^2/z_{\mathrm{R}}^2)^{1/2}.$$

$$H_z = 2E_0(x,y,\xi)\frac{\varepsilon}{\rho}\left(-\sqrt{\frac{1+\alpha}{2}}\,y\sin\bar{\varphi} \pm \sqrt{\frac{1-\alpha}{2}}\,x\cos\bar{\varphi}\right),$$

$$\varphi = \frac{2\pi c\xi}{\lambda} + \arctan\frac{z}{z_{\mathrm{R}}} - \frac{zr^2}{z_{\mathrm{R}}\rho^2} - \varphi_0;$$

$$\bar{\varphi} = \varphi + \arctan\frac{z}{z_{\mathrm{R}}}; \qquad \xi = t - z/c;\ z_{\mathrm{d}}$$

$$E_0(x,y,\xi) = \frac{E_m\rho_0}{\rho}\exp\left[-\left(\frac{\xi - z_{\mathrm{d}}/c}{\tau}\right)^q - \frac{x^2+y^2}{\rho^2}\right];$$

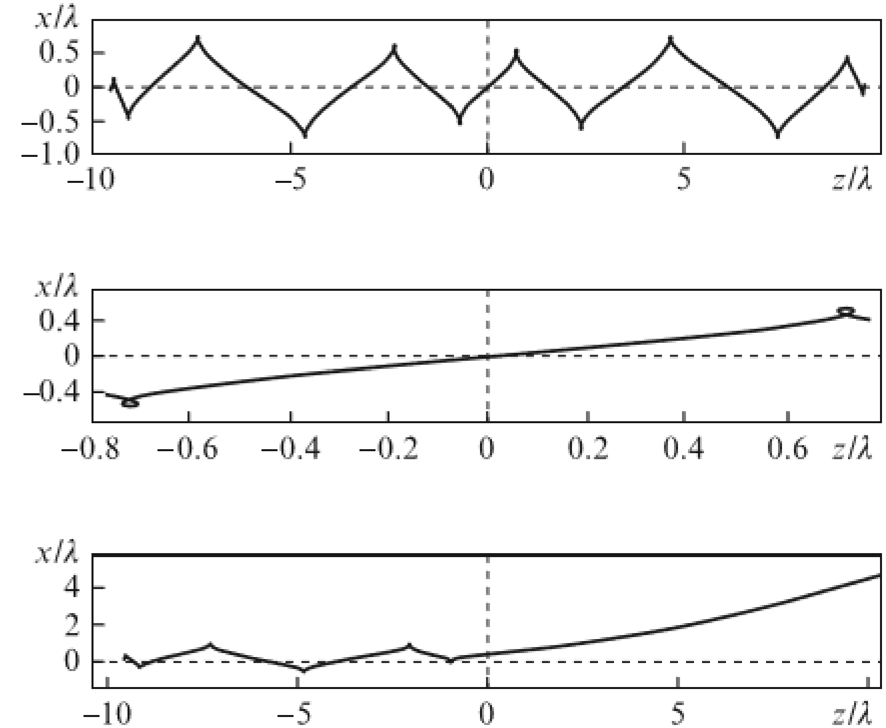

Electron trajectories for linear polarization: simmetrie trajectory for z0/l = –9.58 = z0 */l (a), central part of such trajectory (b) and trajectory at initial shift x0/l = 0.1 (c).

Wr/(mc2) = 128.

ct/l = 1.5 q = 2 r0/l = 1 Im/Ir = 5000

A. Andreev, QE (2011).

Radiation of zepto-second pulses

a)

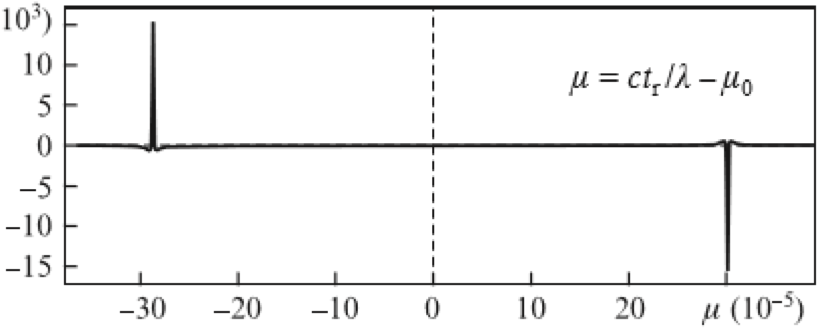

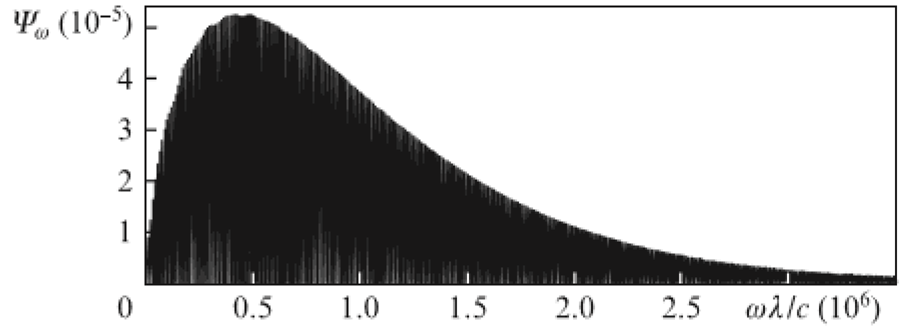

b)

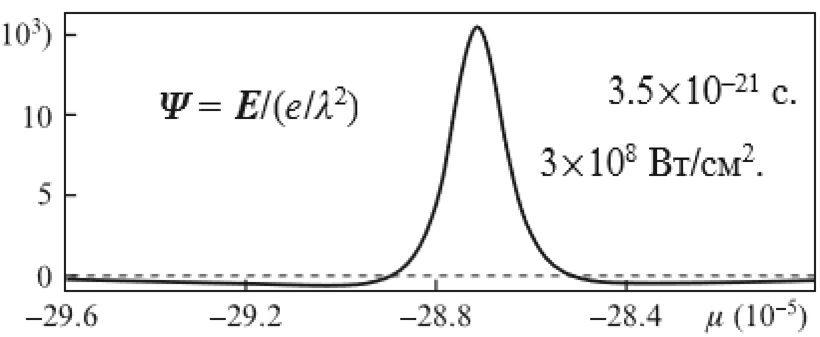

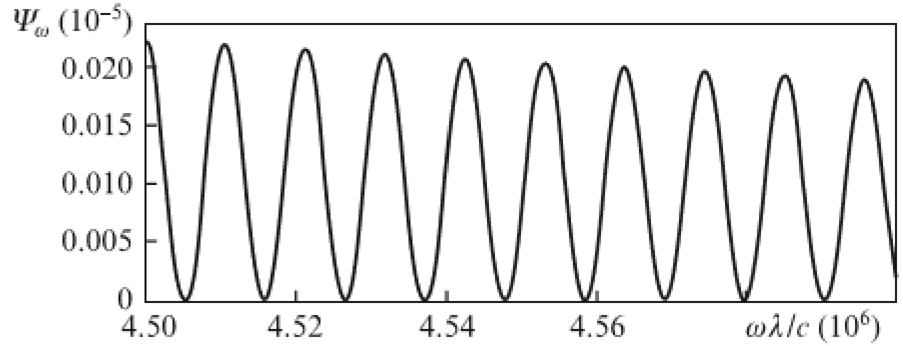

$$\boldsymbol{E} = -e\frac{1 - v^2/c^2}{(R - \boldsymbol{R}\boldsymbol{v}/c)^3}\left(\boldsymbol{R} - \frac{\boldsymbol{v}}{c}R\right)$$

$$-\frac{e}{c^2(R - \boldsymbol{R}\boldsymbol{v}/c)^3}\boldsymbol{R}\left[\left(\boldsymbol{R} - \frac{\boldsymbol{v}}{c}R\right)\boldsymbol{v}'\right],$$

$$\boldsymbol{r}(t) + \boldsymbol{R}(t) = \boldsymbol{R}_0;\ \boldsymbol{v} = \mathrm{d}\boldsymbol{r}/\mathrm{d}t;\ \boldsymbol{v}' = \mathrm{d}^2\boldsymbol{r}/\mathrm{d}t^2.$$

The spectra of pulses shown in a) and b) figures

$$\varphi_0 = \pi/6,\ \mu = ct_r/\lambda - \mu_0$$

High harmonic generation from solid

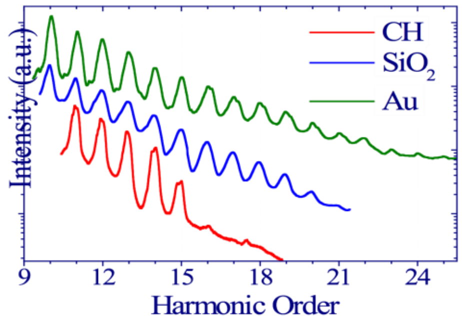

Thaury *et al*, Nature Physics 2007
60 fs, few 100mJ, 10^{18} W/cm^2

Nomura *et al.*, Nat. Phys. 2009
45fs, 700mJ, 10^{18} W/cm^2

Attosecond pulses

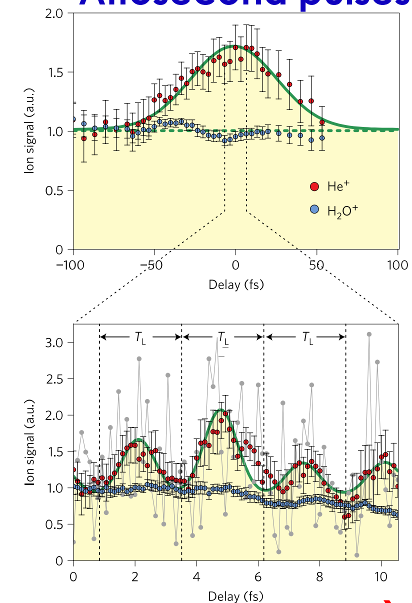

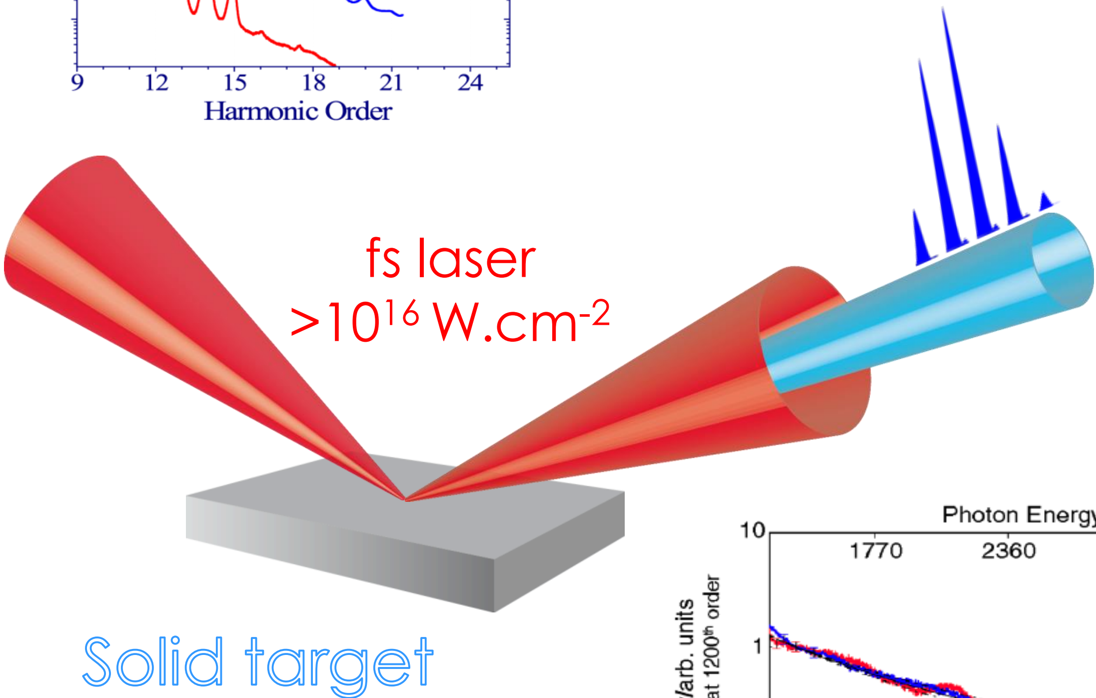

G.Tsakiris NJP (2006)

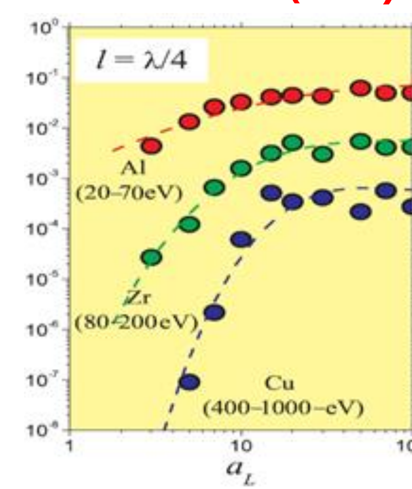

Dromey *et al*, Phys. Rev. Lett. 2007

500fs, tens of J, ~ 10^{20} W/cm^2

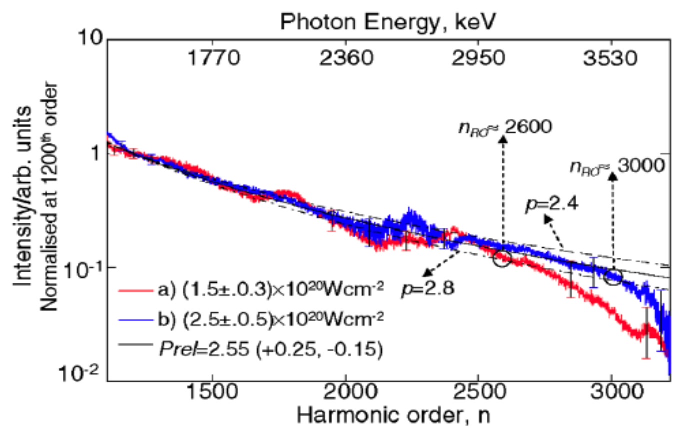

Nonlinear fluid model

The starting point for most theoretical analyses of HHG is the usual set of Lorentz-Maxwell equations for a preionized, quasineutral, collisionless plasma slab. The ions are assumed to form a fixed background density $Zn_i \equiv n_0$, where Z is the average ionization degree, ni is the ion density, and n0 is the initial electron density; the electrons are fluid-like and driven by the laser fields incident on the surface. For normally incident light, these fields can be represented by a vector potential $\mathbf{A} = (0, A_y\{x,t\}, 0)$,

In this geometry, the transverse electron momentum is $p_y = eA_y/c$,

$$\frac{1}{c^2}\frac{\partial^2 A_y}{\partial t^2} - \nabla^2 A_y = \frac{4\pi}{c} J_y. \qquad J_y = -en_e v_y = \frac{e^2 n_e}{mc}\frac{A_y}{\gamma}, \qquad \gamma = \left(1 + \frac{p_x^2 + p_y^2}{m_e^2 c^2}\right)^{1/2}.$$

$$\frac{dp_x}{dt} = e\frac{\partial \varphi}{\partial x} - \frac{e^2}{2m_e c^2 \gamma}\frac{\partial A_y^2}{\partial x}. \qquad \frac{\partial n_e}{\partial t} + \frac{\partial}{\partial x}\left(\frac{n_e p_x}{m_e \gamma}\right) = 0, \qquad \frac{\partial^2 \varphi}{\partial x^2} = 4\pi e(n_e - n_0)$$

Lorentz transformation of fluid variables to frame moving along the plasma surface with velocity $v_y = ck_y = c \sin \theta$ (

$$\frac{dp_x}{dt} = e\frac{\partial \varphi}{\partial x} - \frac{e^2}{2m_e c^2 \gamma}\frac{\partial A_y^2}{\partial x} + \frac{e}{m_e c \gamma} p_0 \frac{\partial A_y}{\partial x}, \qquad \gamma^{-1} = \frac{(1 + p_x^2/m_e^2 c^2)^{1/2}}{[1 + (|\mathbf{p}|^2/m_e^2 c^2)\cos^2 \theta - (p_y/m_e c)\sin 2\theta]^{1/2}}.$$

$$\mathbf{p}_0 = -\hat{\mathbf{y}} m_e c \tan \theta = -p_0 \hat{\mathbf{y}}$$

These equations form a closed set that is in principle sufficient to determine the reflected wave form Ay(x,t) for arbitrary laser amplitude at oblique incidence angle

Akhiezer and Polovin (1956); Bourdier (1983); Bulanov (1994); Lichters (1996); Gibbon (2005).

Coherent Wake Emission

Generated at $L < 0.1\lambda$, $0.1 < a_0 < 1$

Different electron trajectories:

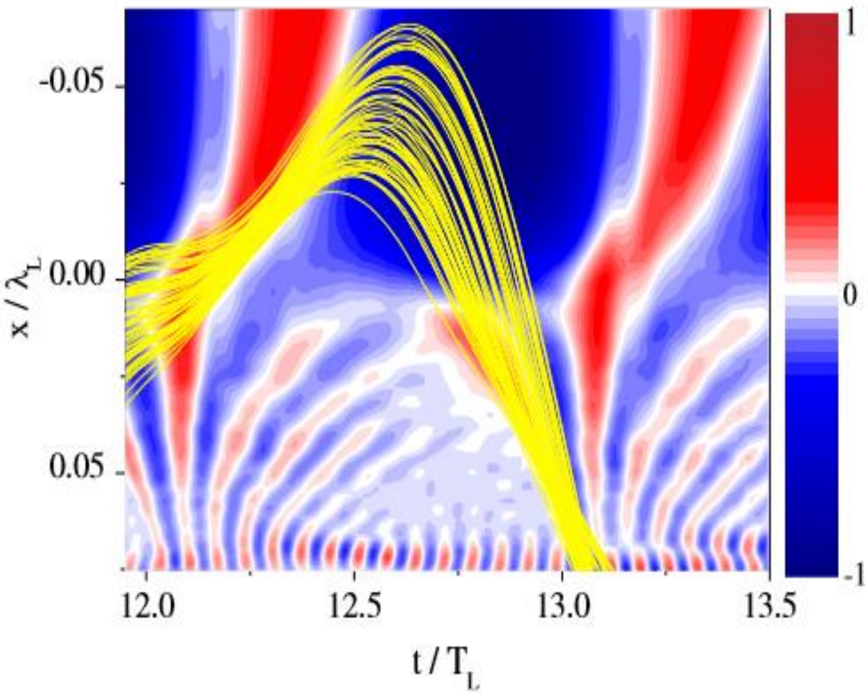

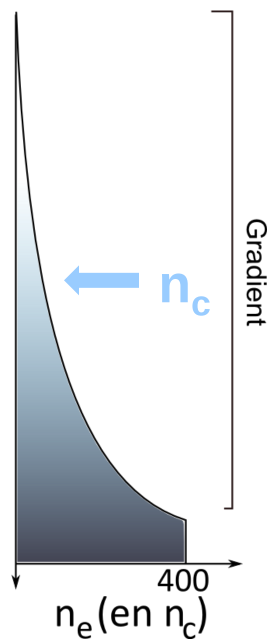

Excitation of plasma oscillations by Brunel electrons. The selected Brunel electrons, whose trajectories are shown by the yellow lines, cross in the density gradient and form a peak of electron density that travels through the plasma and excites in its wake plasma oscillations.

Quéré, Phys. Rev. Lett. 2006

$$N_{max} \approx \omega_{pe} / \omega_L$$

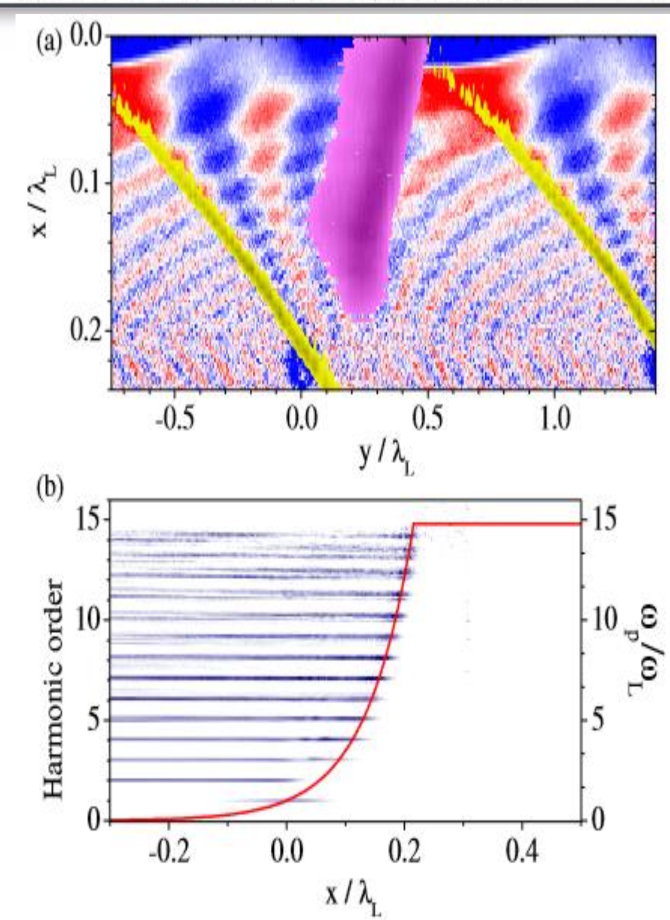

(a) Contour plot of the Bz field (purple), the plasma oscillations, which are initially longitudinal, acquire transverse component and can radiate e.m. wave
(b) Spatially resolved emission spectrum (blue) and plasma frequency profile (straight line)

Relativistic Oscillating Mirror

Generated at the critical surface, dominates for $a_0 >> 1$

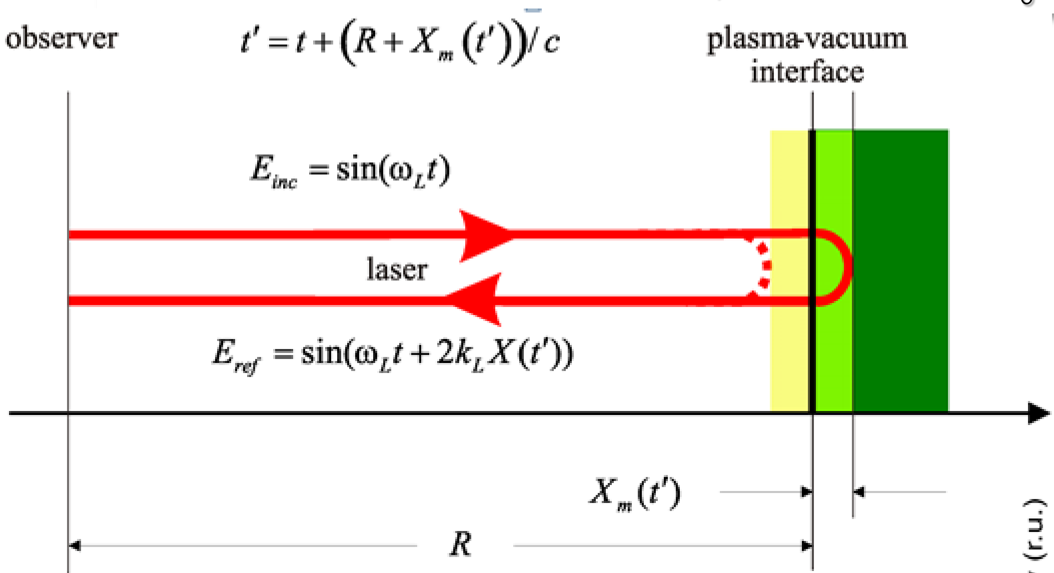

Figure 1. Scheme showing the basic idea of the oscillating mirror model. An E-M wave is incident on an electron surface oscillating around an immovable ion background. The phase of the reflected E-M wave as seen by the observer depends on the position of the electron surface at the moment of the reflection. This retardation effect gives rise to a distorted waveform rich in harmonics of the fundamental frequency.

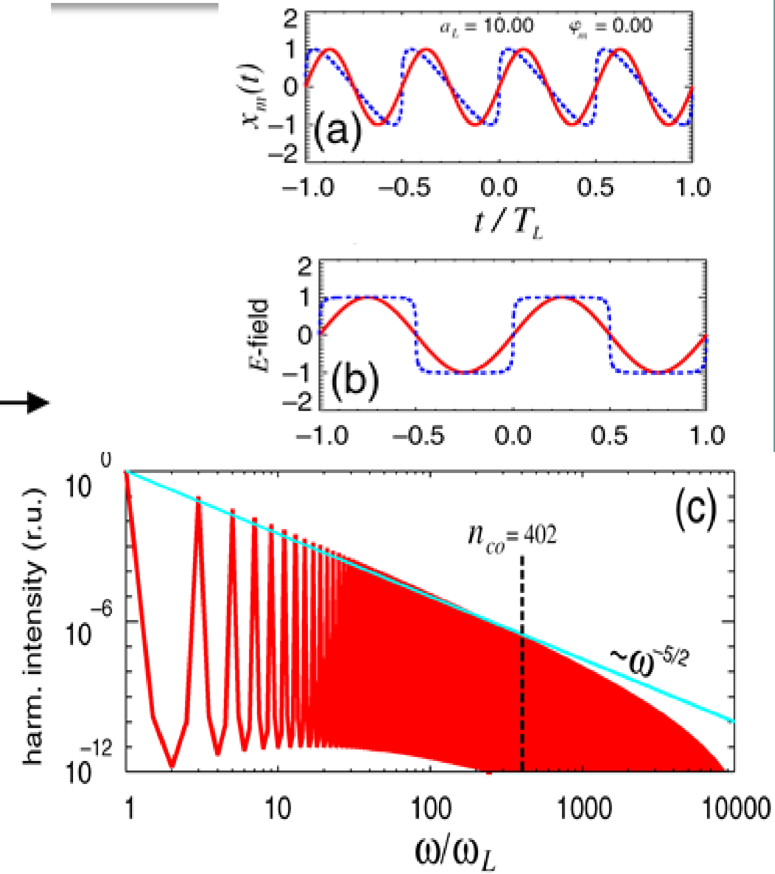

Bulanov *et al*, Phys. Plasmas (1994) $n_{cutoff} = 4\gamma^2_{max}$ $I_\omega \sim \omega^{-5/2}$

Baeva *et al*, Phys. Rev.E (2006) $n_{cutoff} = \sqrt{8\alpha}\gamma^3_{max}$

γ_{max} **is the maximum rel. factor of the surface**

$\alpha \sim 1$ **is related to the plasma-surface acceleration** $I_n \propto 1/n^{8/3}$

Figure 2. Predictions of the oscillating mirror model for $a_L = 10$. (a) Motion of the mirror in its own frame (———) and as seen by the incident wave (– – – –). (b) The incident (———) and the reflected (– – – –) E-M field as seen by the observer. (c) The power spectrum is obtained by Fourier transforming the reflected field. The roll-off follows closely the predicted power law $1/\omega^q$ with $q \approx 5/2$.

a >>1 Tsakiris NJP (2006)

Sliding mirror model

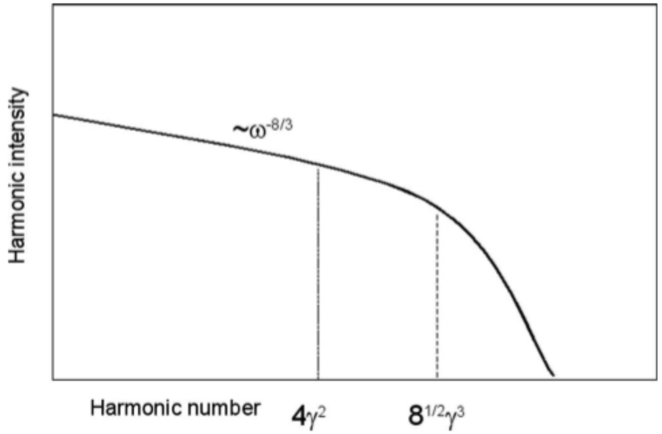

Physically the γ^3 cutoff originates from the finite time over which the mirror electrons are accelerated. In fact, there is a close analogy here with synchrotron radiation, which also contains harmonics up to a maximum $\omega_c \approx 3c\gamma^3 / R$

where R is the radius of curvature of the device.

A further variation on this approach is the sliding mirror model. This is valid for highly overdense, thin plasma slabs in which the electron motion along the density gradient can be neglected owing to the high charge-separation field. The only motion relevant for harmonic generation is then along the target surface. The figure of merit characterizing this regime is the so-called normalized plasma density

$$\varepsilon_p = \frac{\pi d n_e}{\lambda_0 n_c},$$

where *d* is the slab thickness. The sliding mirror regime is defined by $\varepsilon_p > a_0$
In this case, the spectrum is predicted to fall off as ω^{-2} up to a critical frequency $\omega_{cr} \approx a_0\omega_0$, after which it decays exponentially.

Pirozhkov, PoP (2006)

Coherent Synchrotron Emission

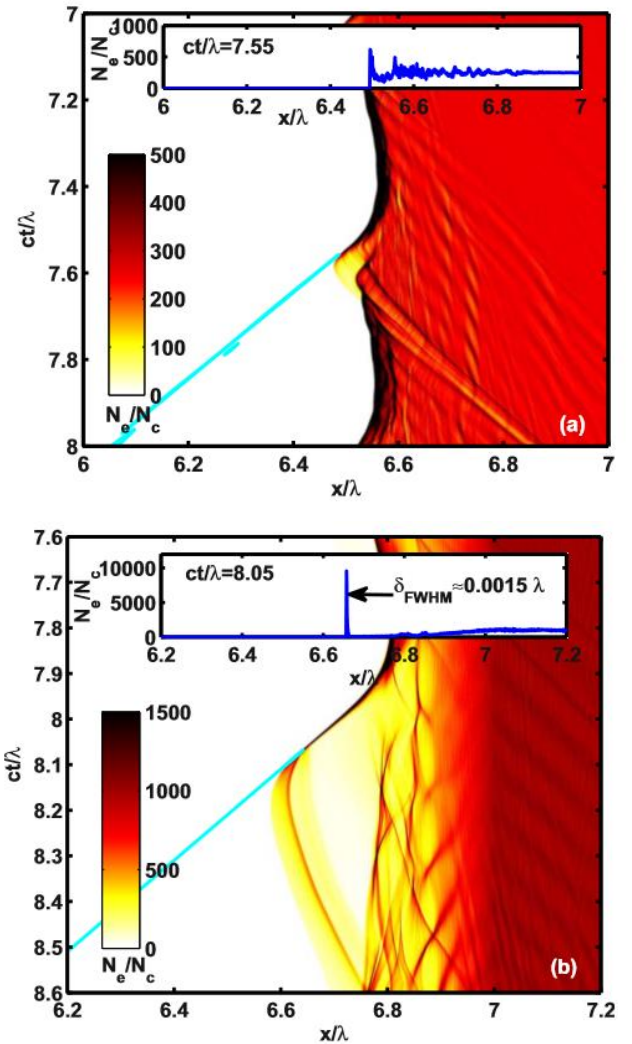

The electron density and contour lines (cyan) of emitted harmonics radiation for a) BGP and b) the synchrotron regime. Pukhov PoP (2010)

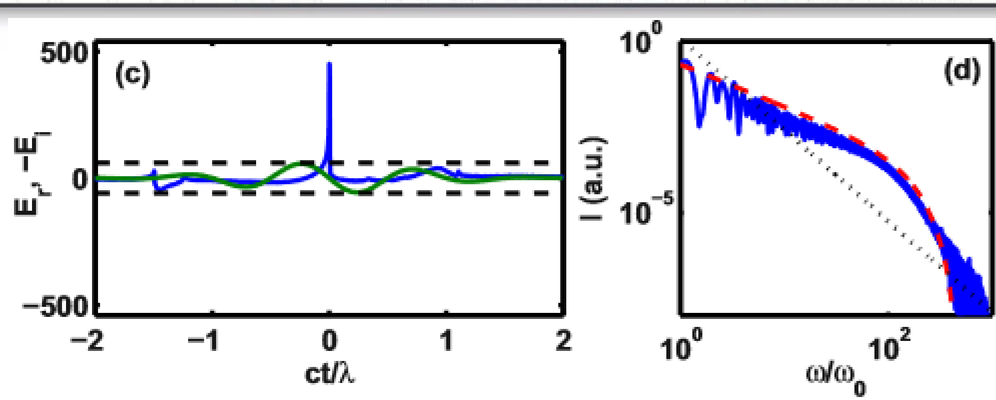

Radiation in time (c) and spectral (d) domain for the simulations: "normal" incidence, plasma density Ne=250Nc, sharp edged profile; (c) and (d) correspond to the nanobunching case: plasma density ramp up to a maximum density of Ne=95Nc laboratory frame, oblique incidence at 63° angle p-polarized. Laser field amplitude is a0 =60. In (d), the dotted black line represents an 8/3 power law, the light gray/red dashed line corresponds to the 1D synchrotron spectrum with

$$j(t,x) = j(t) f[x - x_{el}(t)],$$

$$E_{sy}(t,x) = \frac{2\pi}{c}\int_{-\infty}^{+\infty} j\left(t + \frac{x - x'}{c}, x'\right) dx'$$

$$j(t) = \alpha_0 t$$

$$\tilde{E}_{sy}(\omega) = 2\pi c^{-1} \tilde{f}(\omega) \int j(t) \exp\{-i\omega[t + x_{el}(t)/c]\} dt.$$

$$I(\omega) \propto |\tilde{f}(\omega)|^2 \omega^{-4/3} \left\{ \mathrm{Ai}'\left[\left(\frac{\omega}{\omega_{rs}}\right)^{2/3}\right]\right\}^2, \qquad x_{el}(t) = -v_0 t + \alpha_1 t^3/5.$$

$$\text{with } \omega_{rs} \approx 2^{3/2}\sqrt{\alpha_1}\gamma_0^3, \text{ where } \gamma_0 = (1 - v_0^2)^{-1/2}$$

Model for atto pulse generation

$c\sin(\theta_0)$ $\omega' = \omega_L \cos\theta_0$ $y' = (y - ct\sin\theta_0)/\cos\theta_0$ $t' = (t - y\sin\theta_0/c)/\cos\theta_0$

Moving frame

$$(\frac{\partial^2}{\partial\xi'^2} + \frac{\omega^2}{\omega_p^2})a'_{y1}(\xi') = (\theta(\xi') + \frac{\partial^2}{\partial\xi'^2}\sqrt{1+(a'_{y1}-tg\theta_0)^2}\,\frac{2}{\pi}E(\frac{\pi}{2};\frac{a'_{y1}-tg\theta_0}{\sqrt{1+(a'_{y1}-tg\theta_0)^2}}))\times$$

$$\times\frac{a'_{y1}-tg\theta_0}{\sqrt{1+(a'_{y1}-tg\theta_0)^2}}\frac{2}{\pi}F(\frac{\pi}{2};\frac{a'_{y1}-tg\theta_0}{\sqrt{1+(a'_{y1}-tg\theta_0)^2}})$$

Equation for first laser harmonic

$$m_e\frac{d}{dt'}\dot{x}'_s\sqrt{\frac{1+p'^2_y/m_e^2c^2}{1-\dot{x}'^2_s/c^2}} = -2\pi e^2\frac{Zn_0}{\cos\theta_0}x'_s(t) - \frac{ep'_y}{m_ec}\sqrt{\frac{1-\dot{x}'^2_s/c^2}{1+p'^2_y/m_e^2c^2}}\frac{\partial A'_y(x'_s,t)}{\partial x'_s}$$

$$p'_y = -eA'_y/c - m_ec\,tg(\theta_0), \quad A'_y = m_ec^2a_{y1}{}'(\omega_p x'_s/c)\cos(\omega' t')$$

Eq. of plasma surface dynamic

$$\frac{\partial^2 A'_{ry}(x',t')}{\partial x'^2} - \frac{1}{c^2}\frac{\partial^2 A'_{ry}(x',t')}{\partial t'^2} = j_y(x',t')$$

Eq. of atto pulse field

$$j_y(x',t') = -4\pi e n_e\theta(x'-x'_s(t))\theta(x'_s(t)-x'-l_s)\frac{p'_y}{m_ec}\sqrt{\frac{1-\dot{x}'^2_s/c^2}{1+p'^2_y/m_e^2c^2}}$$

atto pulse field

$$\frac{eE'_{yr}(x',t')}{m_ec\omega_L} = 2\frac{\omega_p}{\omega_L l_s}\int_0^{l_s}\frac{j_y(t^*,x')}{Zen_0}dx' \approx 2\frac{\omega_p}{\omega_L}\frac{j_y(t^*,x_s(t^*))}{Zen_0}$$

$$t' - t^* - |x' - x'_s(t^*)|/c = 0$$

Generation of electron nano-bunches from semi-limited foil at laser pulse oblique incidence

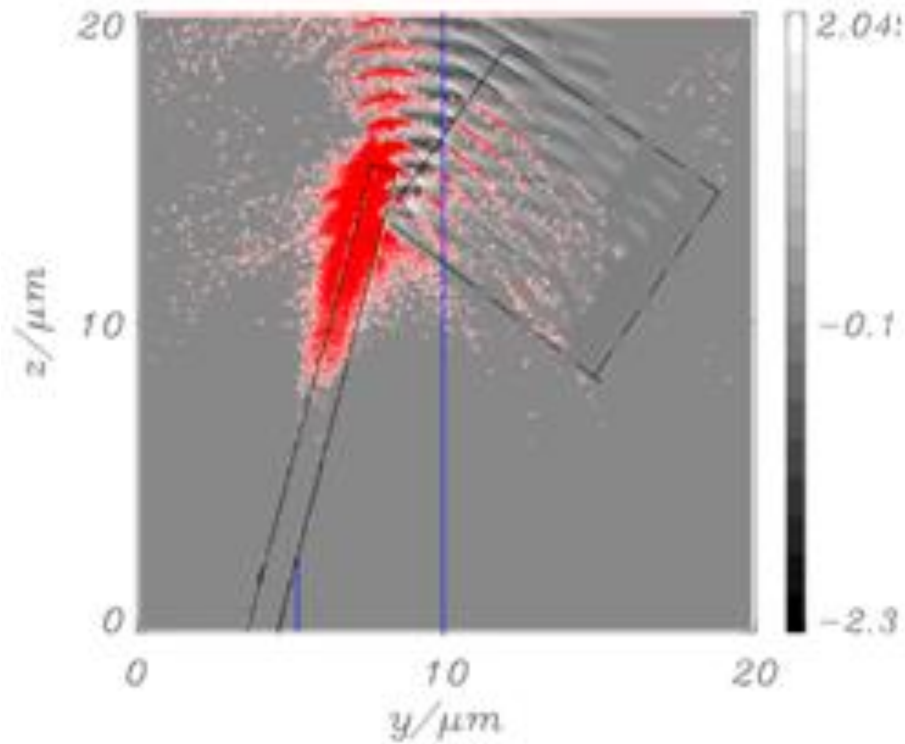

(a)

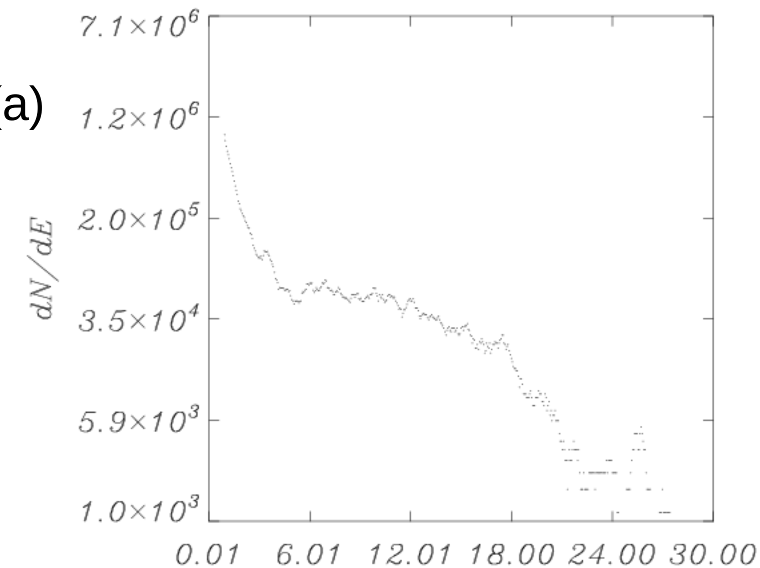

(b)

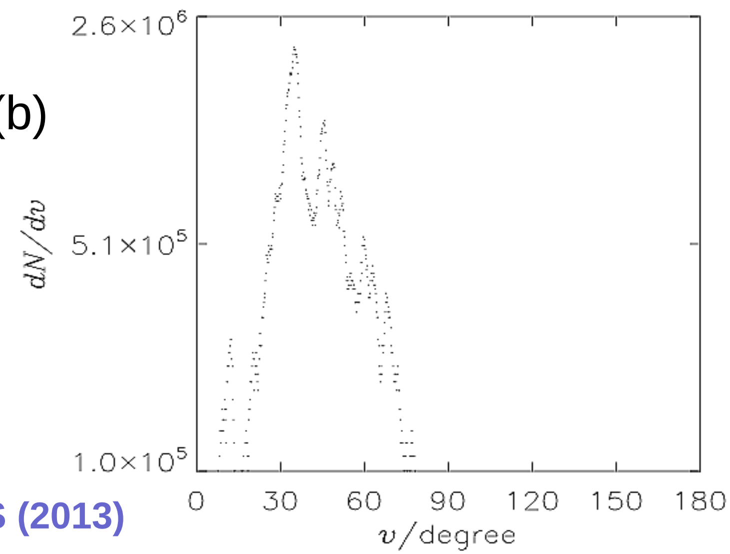

Laser field (white, black) and hot (>0.5MeV) electron density (red) at t=85 fs.

(a) electrons distribution function (in black rectangle) at 109 fs;
(b) its angular distribution

A.Andreev et al. O&S (2013)

Nano-scale electron bunch formation at oblique incidence of intense laser pulse on a foil

Length of electrons extraction

$$l_{extr} = E_0 \sin\theta_0 / en_e = 2\lambda_L \sin\theta_0 (n_c / n_e)\sqrt{1.37\, I_{18}}$$

Number of electrons in the bunch propagating in specular direction

$$N_b \approx n_e l_{extr} S \qquad S \approx d_L \cdot d_b$$

Angle of electron front in the target

$$\sin\theta_n = \frac{\cos\theta_e \sin\theta_0}{\sqrt{1+\sin^2\theta_0 - 2\sin\theta_e \sin\theta_0}}$$

$$\sin\theta_e \approx \sqrt{(\gamma-1)/(\gamma+1)}\sin\theta_0$$

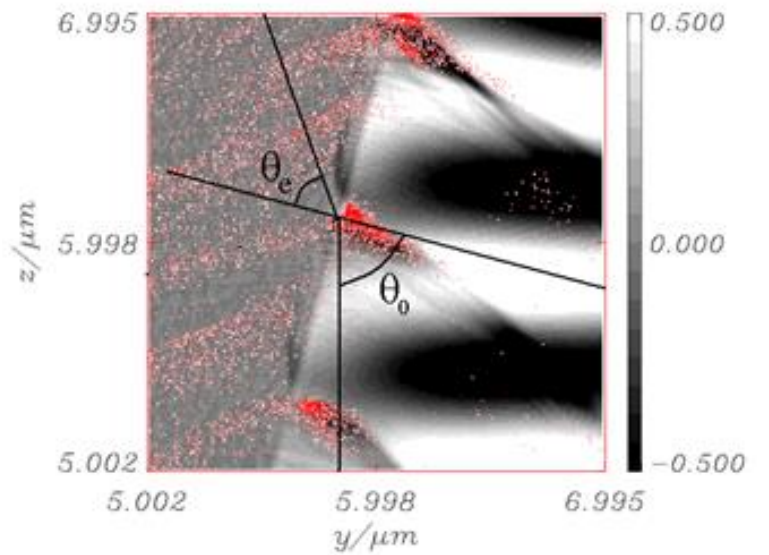

E/laser field (white, black), hot (>0.5 MeV) electron density (red) at t= 56 fs.

10^{20} W/cm^2 26 fs, linear pol, diameter 4 mkm, $C^{+6}H^{+1}$ target, density 6 10^{22} cm^{-3}, thickness1 mkm, 75 ^{0} angle

Electron bunch parameters

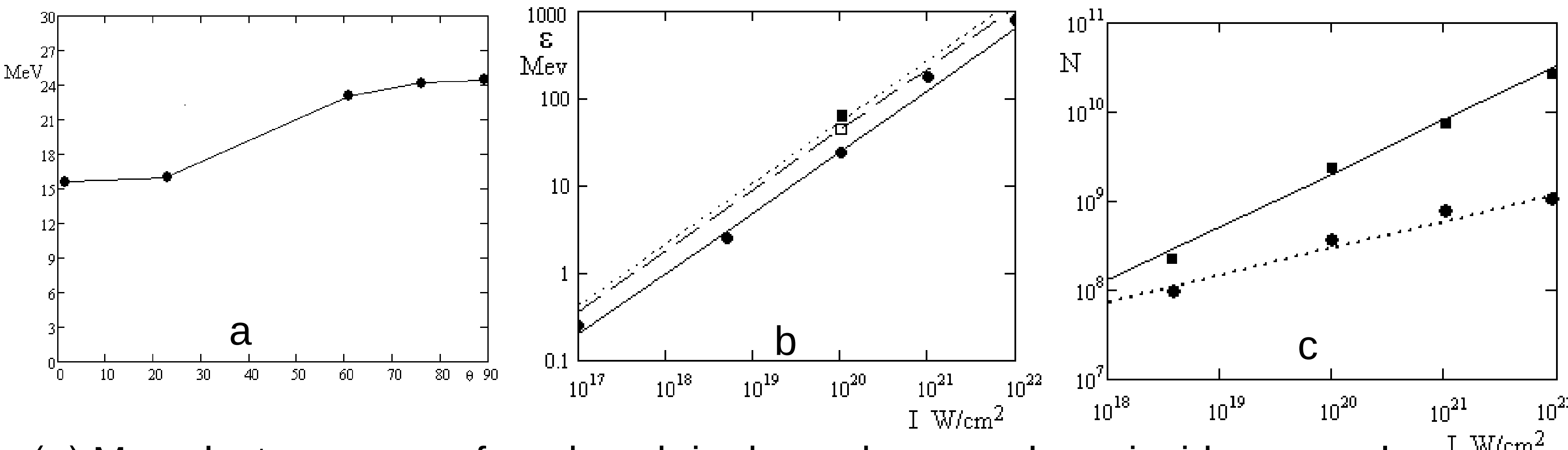

(a) Max electron energy for s-bunch in dependence on laser incidence angle

(b) Max electron energy in s-bunch on laser intensity (angle 75^0), solid line is limited target (of laser spot size), dot line – nonlimited, dash line (1.5 laser spot size)

(c) number of electrons in d-bunches (squares) and s-bunches (circles). Lines - scaling formulas.

s-bunches (specular direction)

$$\varepsilon_e(MeV) \approx 1.0\, I_{18}^{\;0.7}$$

d-bunches (laser beam direction)

$$\varepsilon_e(MeV) \approx 0.6 * I_{18}^{\;0.6}$$

Number of s-bunches=number of laser pulse periods, but number of d-bunches – two times more. Efficiency: 3.7% d-bunches, 0.3% s-bunches

Atto-pulses parameters

(a)

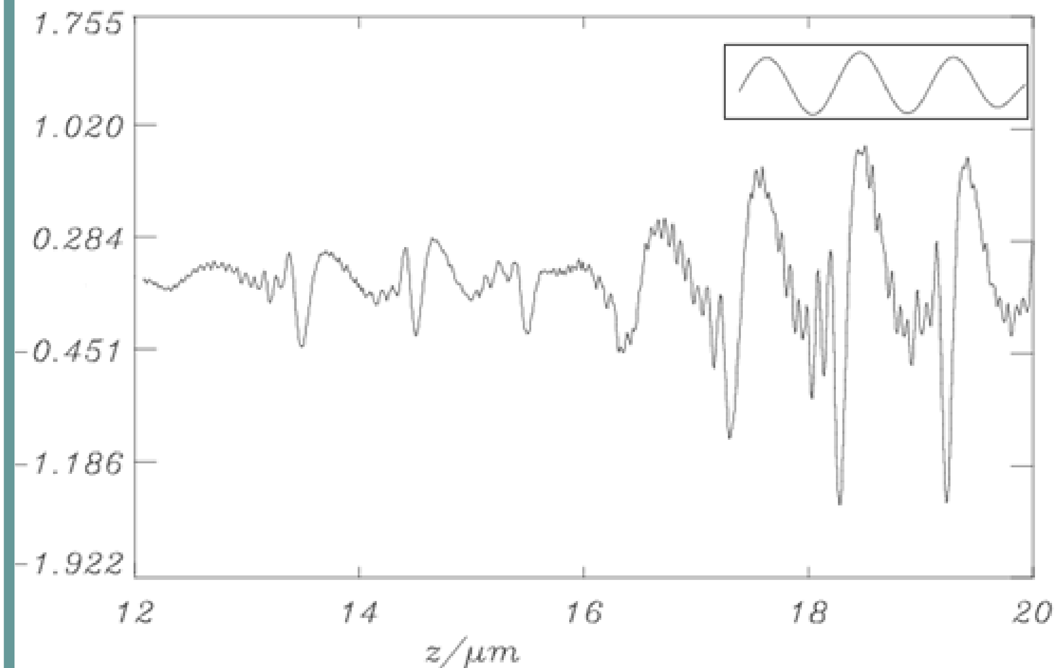

(b)

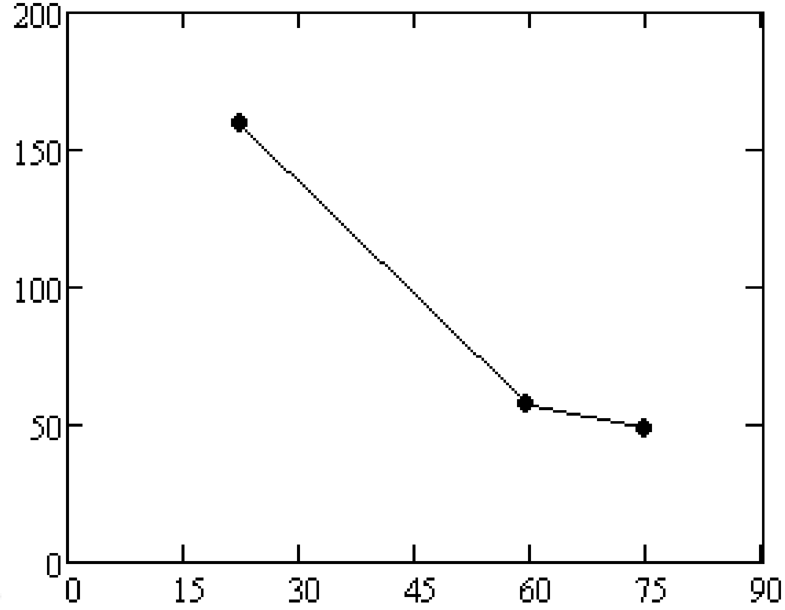

(a) The electric field of reflected pulse (y=12 mkm) at 85 fs.

The incident laser beam was located in the interval y=6-10mkm

b) The dependence of atto-pulse duration (in nm) on the angle

of laser beam incidence on the target

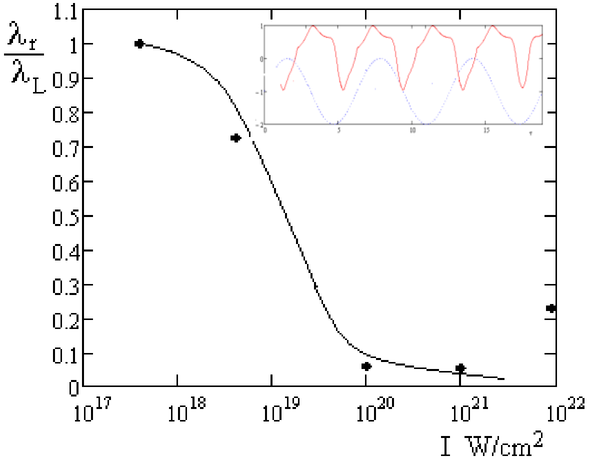

c) Dependence of atto-pulse duration on laser intensity. Points – simulation, line – analytical model. Incidence angle 75^0

Experimental set-up and results

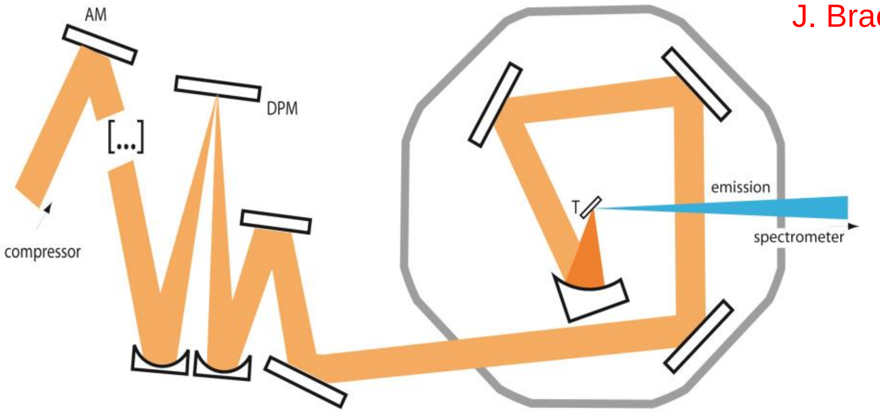

J. Braenzel, A. Andreev et al., PoP (2013)

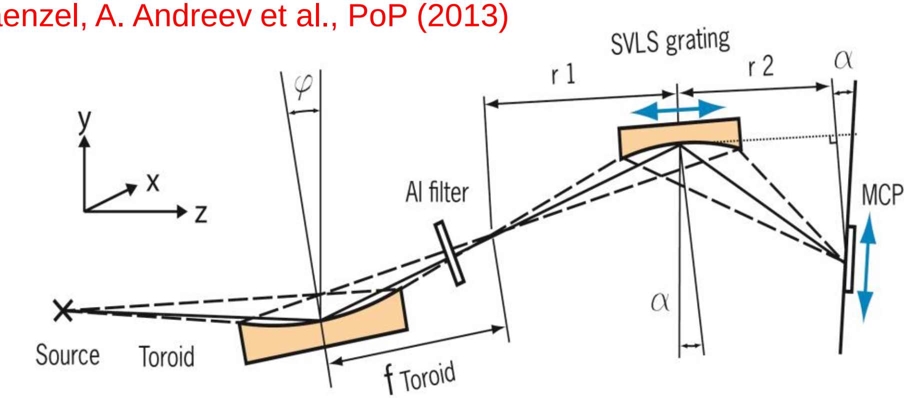

Adaptive Mirror (AM) and double plasma mirror (DPM) for wave front and contrast enhancement;
The laser pulse is focused by f/2.5 off axis parabola at 45 degrees on a polished target SiO_2 **;** $\tau_L = 45\,fs$
EUV spectrometer: a combination of a toroidal mirror and a SVLS Hitachi grating; allows the detection in a wide spectral range of 10nm to 80nm. The spectrometer has a spectral resolution of better than Δλ/λ=10^{-2} in the spectral range of 17nm-50nm. Kn ~10^{11}

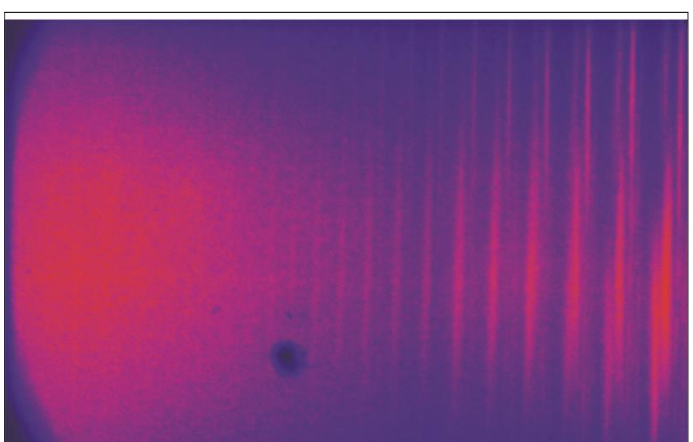

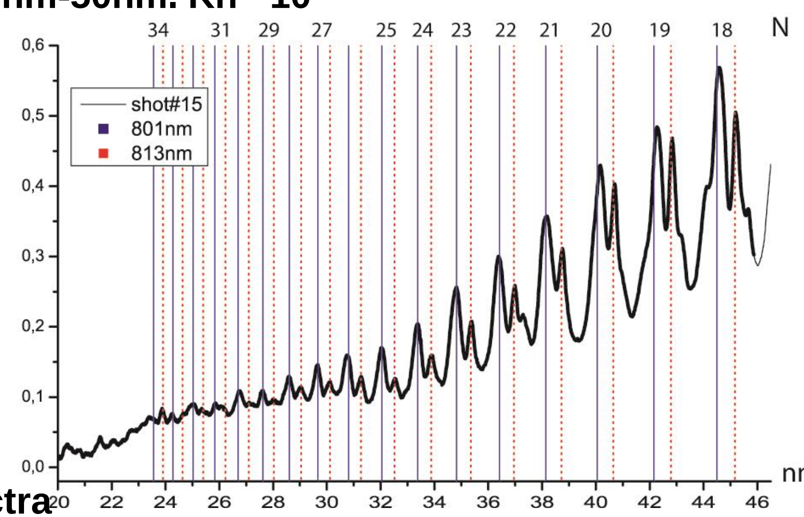

Photographed MCP detector and evaluated spectra

1D PIC simulation results for the experiment

The spatial-temporal electron (a,c) and ion (b,d) density distributions

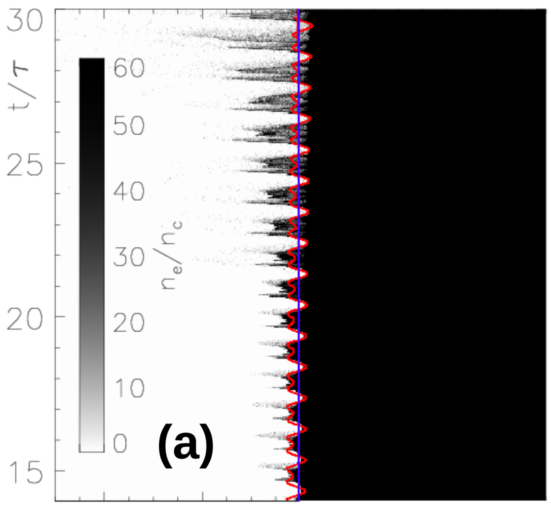

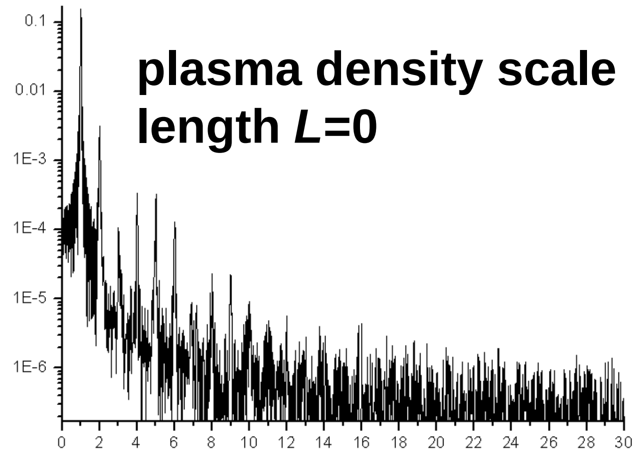

plasma density scale length *L*=0

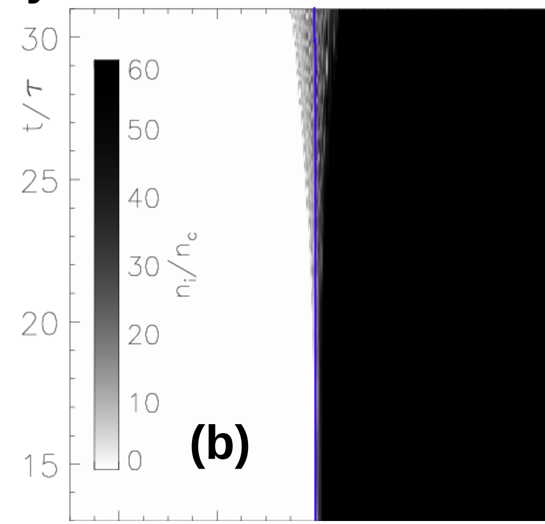

red line: $x'_s(t') = \lambda_L[\alpha_1 \sin(\omega'_L t') - \alpha_2 \sin^2(\omega'_L t') + \alpha_3 \omega'_L t' + \alpha_4 {\omega'_L}^2 {t'}^2]$

$L = 0: \alpha_1 = 0.04, \alpha_2 = 0.03, \alpha_3 = 2\cdot10^{-4}, \alpha_4 = 5\cdot10^{-6}$

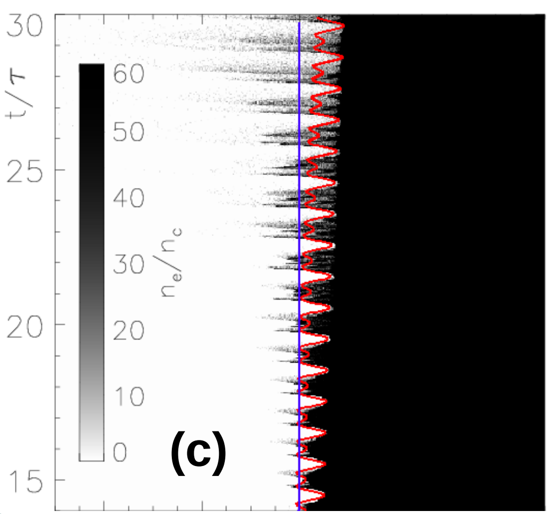

$L = 100nm: \alpha_i \approx 2\alpha_i(L=0); i = 1,..,4$

***L*=100nm**

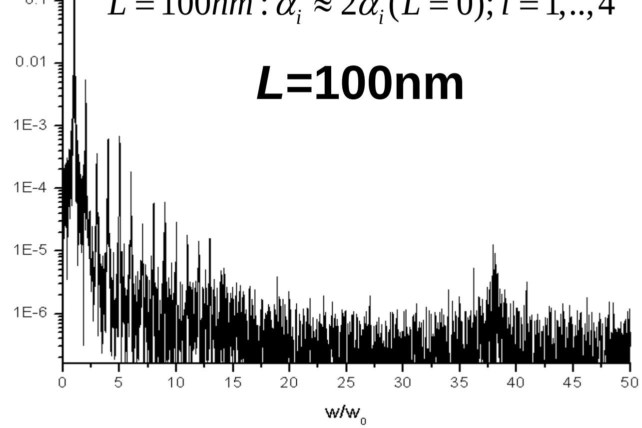

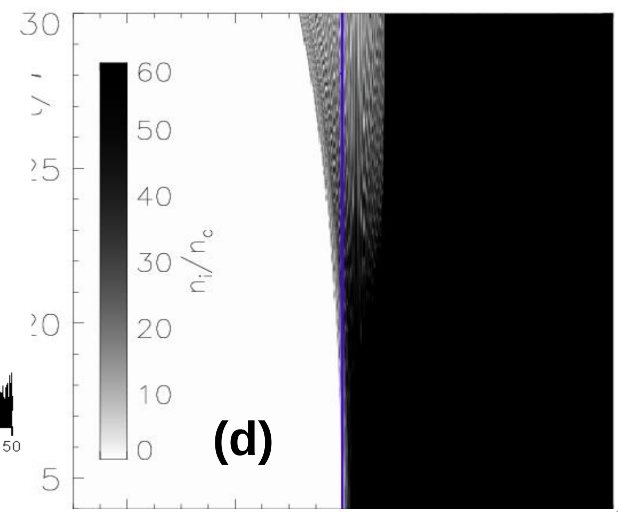

Substructure of high harmonics

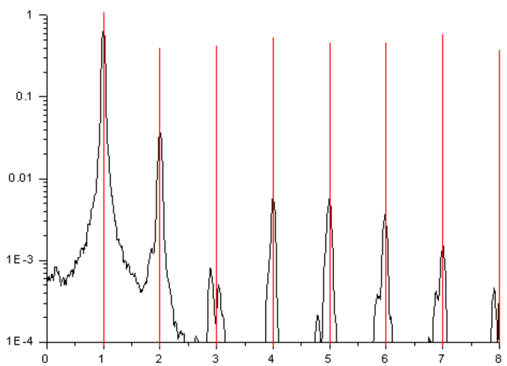

A.Andreev (2013)

Line splitting model

$$x_s \sim \upsilon_s t + g_s t^2 + \ldots$$

$$\omega'_{1,2} = \omega_{1,2} / \omega_L, \quad \delta\omega' = \omega'_1 - \omega'_2$$

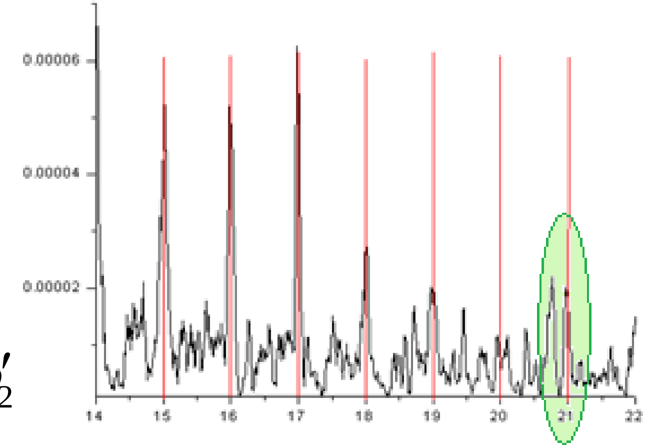

$$\frac{(\omega'_{1,2} - N - (N-p)v_0)^2 (\omega'_{1,2} - p)\varepsilon}{2((\omega'_{1,2} - p)^2 \varepsilon^2 + \tau_L{}^{-4})} - \frac{(\omega'_{1,2} - N - (N-n)v_0)^2 (\omega'_{1,2} - n)\varepsilon}{2((\omega'_{1,2} - n)^2 \varepsilon^2 + \tau_L{}^{-4})} \approx 2\pi k;$$

$$k = 0, \pm 1, ..; \quad p = 0, \pm 1, \ldots$$

$$k = 1 \qquad \varepsilon \geq \tau_L{}^{-2} / N \qquad \frac{(\delta\omega')^2 (p-n)}{(N-p)(N-n)} \approx 4\pi\varepsilon \qquad \frac{\delta\omega'}{N\omega'_L} = \frac{\delta\omega}{N\omega_L} \approx \sqrt{2\pi g / c\omega'_L}$$

$$v_0 \sim c\sqrt{I_L / \rho_s c^3} \qquad g \sim v_0 / t_L = \sqrt{I_L / t_L{}^2 \rho_s c}$$

$$N \approx 1 / \omega'_L t_L \sqrt{I_L / \rho_s c^3} \sim 10 \qquad \delta\omega \approx N\omega_L \sqrt{\frac{2\pi\sqrt{I_L / \rho_s c^3}}{\omega_L t_L}}$$

High harmonics enhancement in laser plasma

J.Bransel, A.Andreev et al. (2016)

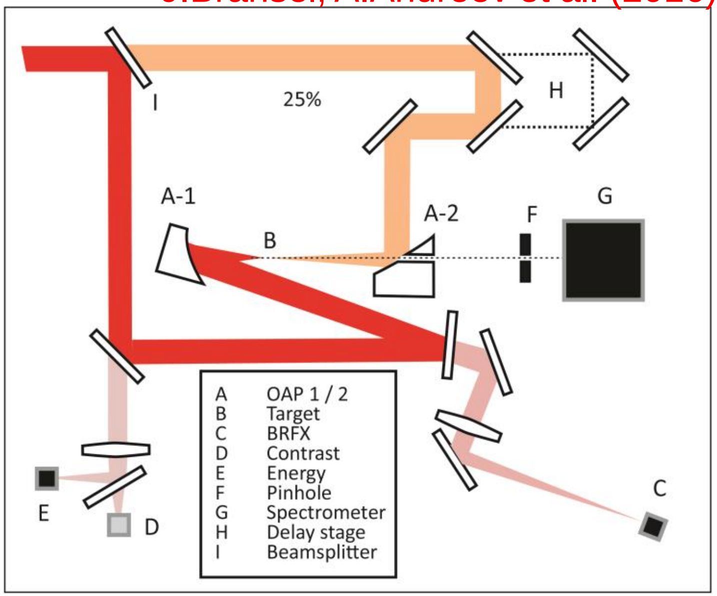

Setup for a two laser pulse experiment in counter-propagating geometry. The intensity of the drive pulse is 6x10^19 W/cm2 at ultrahigh laser contrast. The second, less intense laser pulse hits the targets backside.

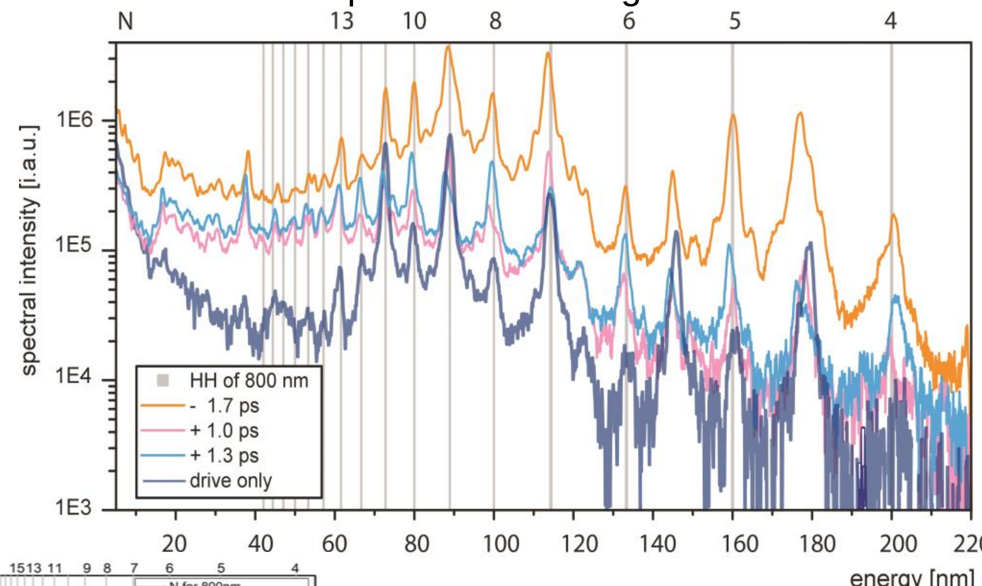

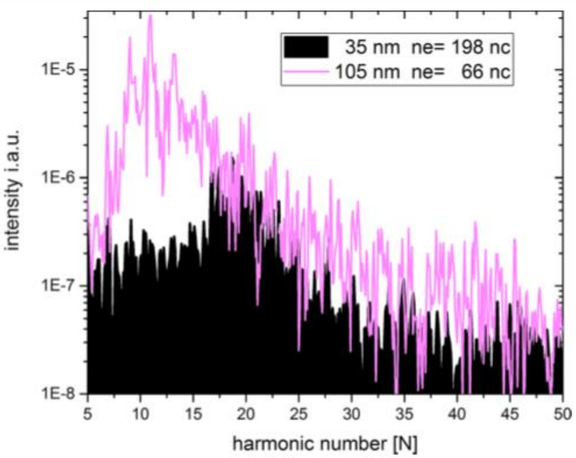

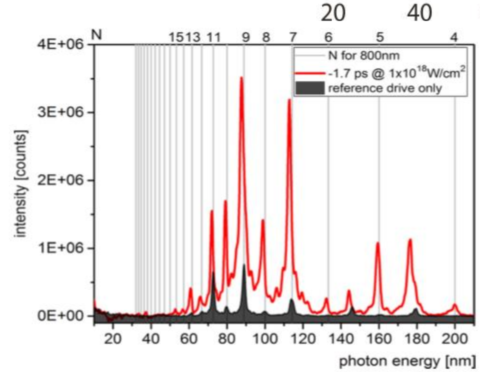

At a time difference of two laser pulses of about ps a remarkable enhancement of the harmonic emission in forward direction was found. The polarization is for both laser pulses linear perpendicular, the target is CH foil with D=35 nm

I_L=5x10^{19}Wcm^{-2}, t_L=35 fs, Rectangle profile, l_t=35/105 nm, C^{+6}, n_e= 198/66n_{cr}

Generation of electron bunch and atto-pulse from nano-foils (DREAM target)

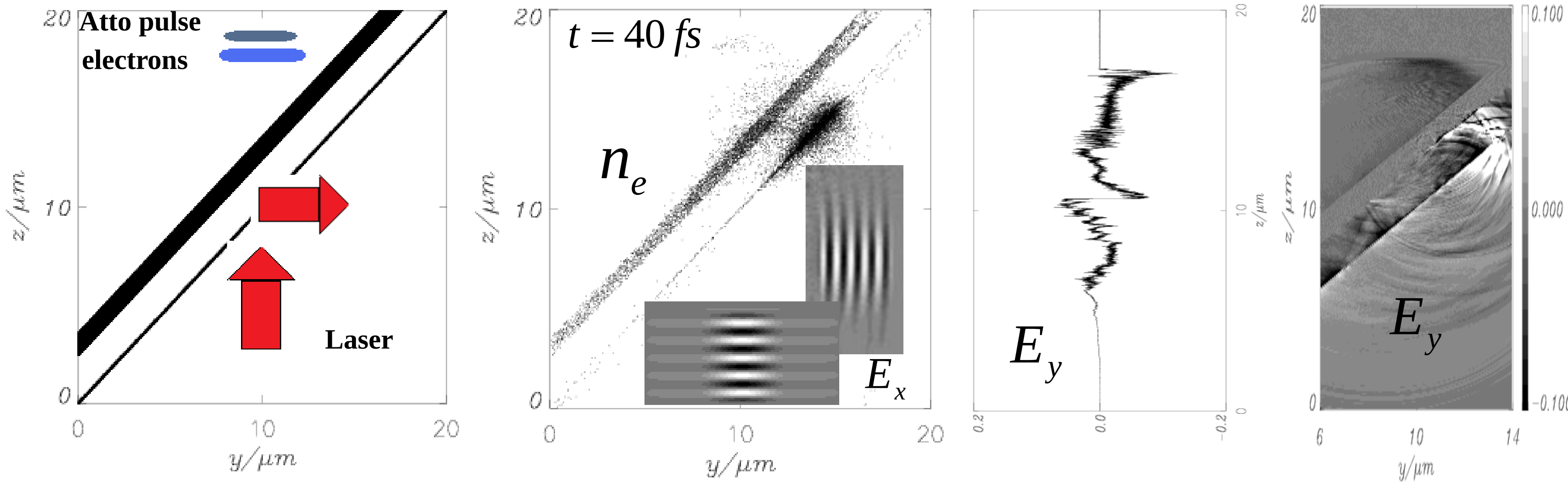

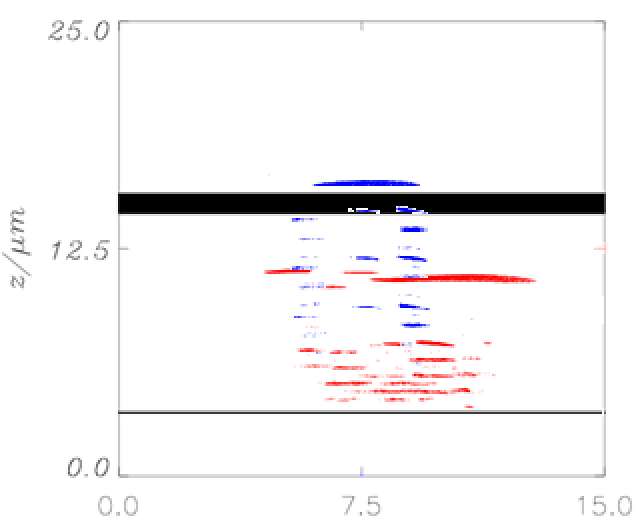

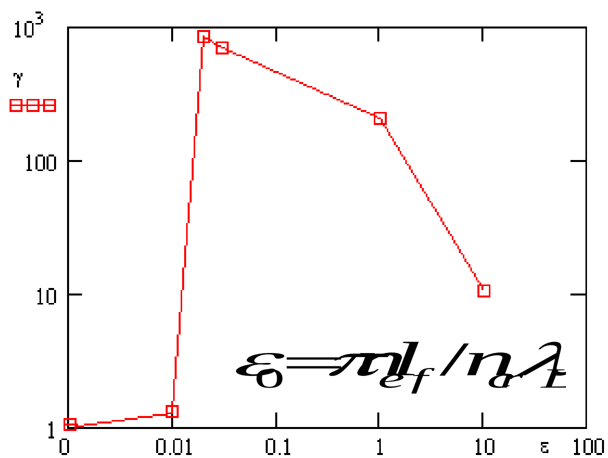

$I_L = 10^{20} Wcm^{-2}, t_L = 15\,fs, l_f = 5nm$

$C^{+6}, n_0 = 1.7 \cdot 10^{23} cm^{-3},$

$l_1 = 0.6nm, l_2 = 200nm,$

$I_L = 2 \cdot 10^{21} W / cm^2, t_L = 3T,$

$d_L = 4\mu m, SuperGauss,$

$s - pol, \theta = 30^\circ$

$$ct_{atto} \approx l_f + \frac{l_s}{2\gamma^2 \cos\theta}$$

K. Miyauchi, A.Andreev et al., PoP (2004) **H.Wu et al., Nature photonics (2012)** **A.Andreev et al. AplSci (2013)**

Generation of electron bunch and atto-pulse

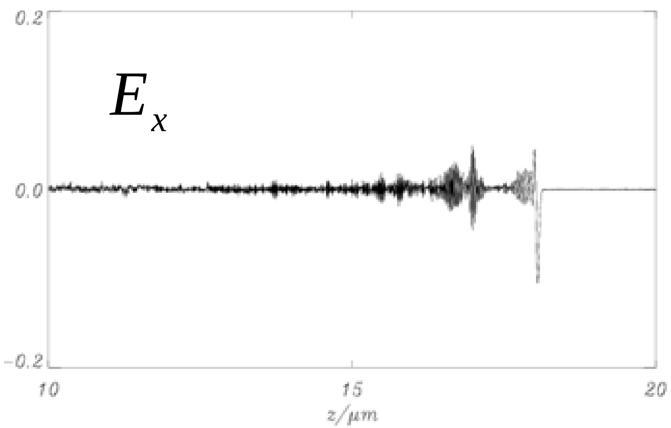

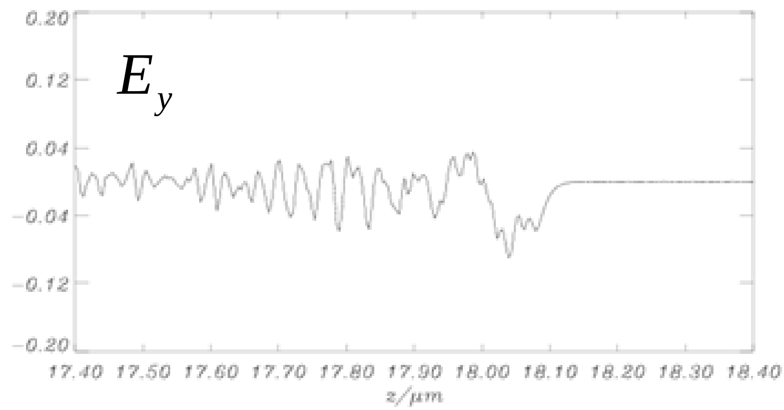

n_e

$y = 11\mu m$

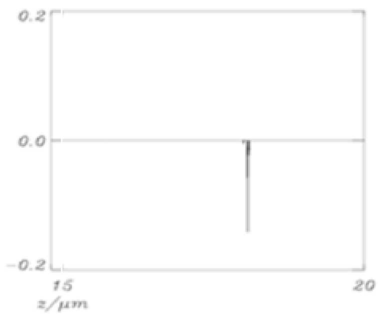

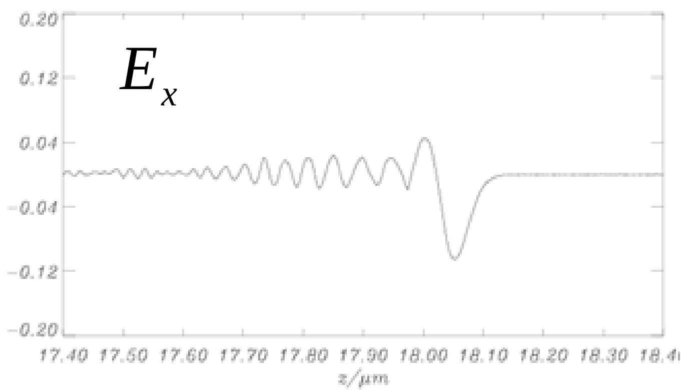

$$\frac{E_\eta}{E_L} \approx \frac{4\pi e n_e d_e \gamma tg\theta}{E_L} \approx \frac{2\pi\gamma}{a_0}\frac{n_e}{n_{cr}}\frac{d_e}{\lambda_L} = \frac{2\gamma\varepsilon_0}{a_0}$$

$$ct_{atto} \sim d_e + \frac{l_s}{2\gamma^2\cos\theta}$$

$$d_e \sim l_f$$

A.Andreev et al. AplSci (2013)

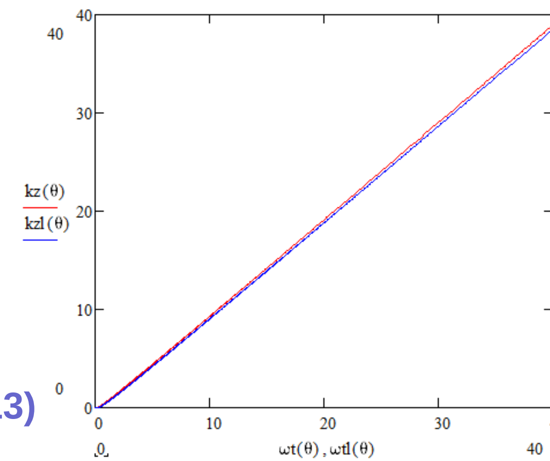

Atto-spiral generation upon interaction of circularly polarized intense laser pulses with cone-like targets

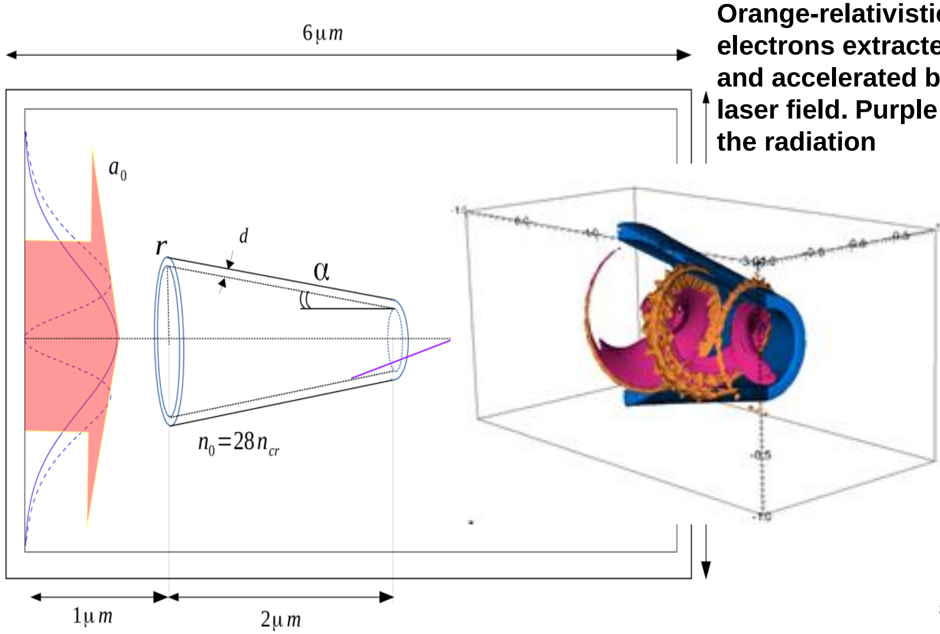

Orange-relativistic electrons extracted and accelerated by laser field. Purple: the radiation

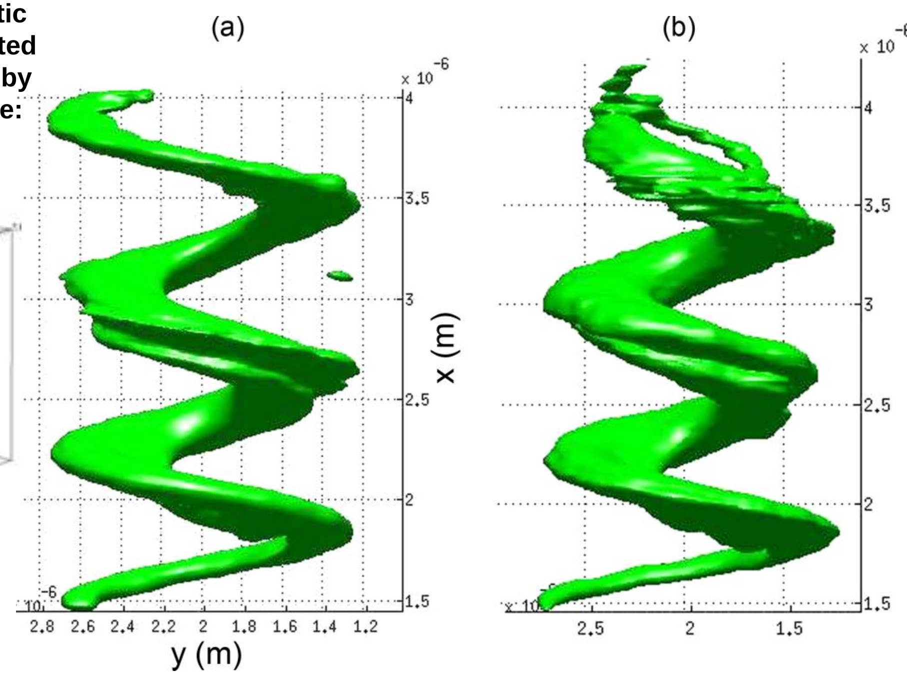

Sketch of the simulation domain and parameters.

The obtained atto-pulse (<100 as) generation and focusing with energy conversion efficiency of a few percent by cone-shaped target enables the peak intensity of the filtered fields in the focus to reach the value of the incident radiation. The calculated spectral intensity shows a much weaker decay (~ 1/n^2) with the harmonic number n than in the ROM and other models.

The calculated isosurface of the electromagnetic energy density produced with (a) cylinder and (b) cone targets is shown at *t* = 20 fs for the values: 3x10^13 J/m3 (a) and 12x10^13 J/m3 (b). Here a frequencies five times higher than the fundamental are included. The Gaussian laser pulse has 10 fs FWHM, with a peak intensity 10^20 *W/cm2,* wavelength is 0.8 *μm* and the focal spot size is 2 *μm.* **Z.Lech&A.Andreev PRE (2016)**

The comparison of cone and cylinder targets

(a)

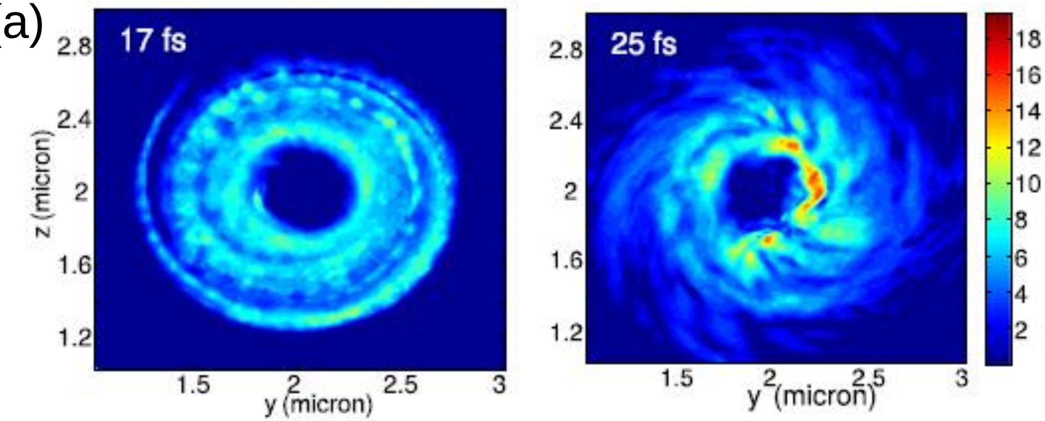

(d)

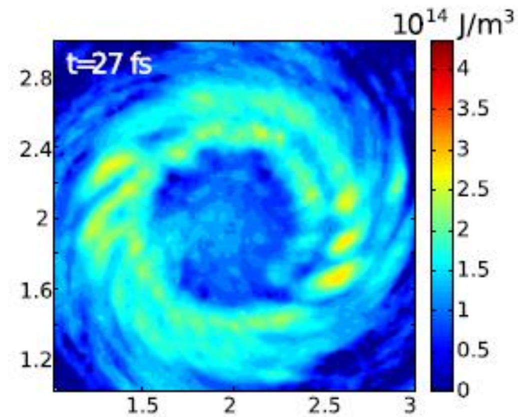

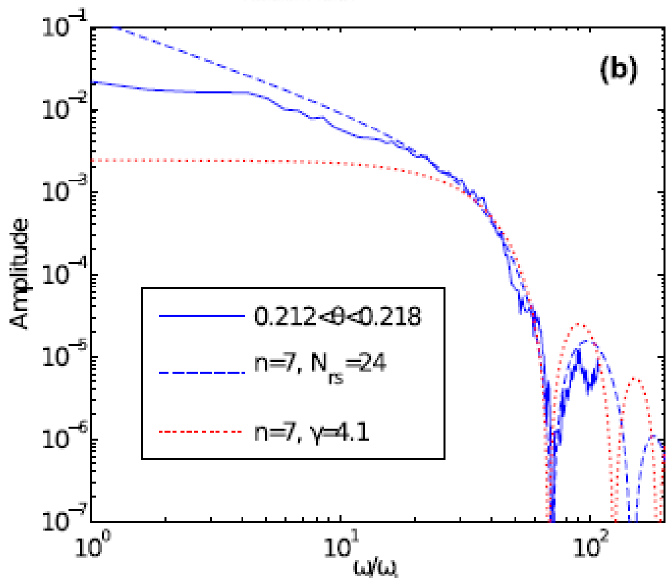

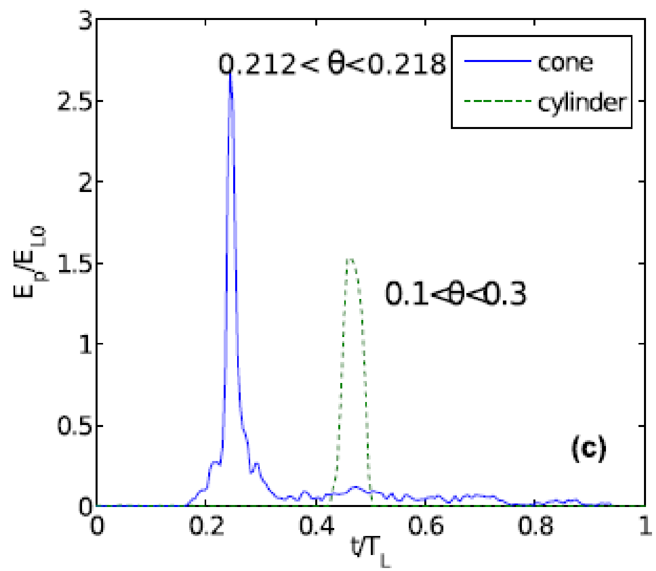

Averaged energy density distribution viewed from the direction of laser propagation corresponding to the cone (a) and cylinder (d) targets. In averaging, only grid cells with *u > 10*14 J/m3 are included.*

(b) Frequency spectra of the strongest pulses for cone targets;

(c) the corresponding normalized attopulses generated within the angle of coherent radiation.

Ultra-high temporal contrast with help of plasma mirrors and XPW

MBI TW Ti:Sa Laser

Initial Parameter

- pulse energy > 1.2 J
- pulse duration < 45 fs
- ns - ASE contrast: 10^{-6} - 10^{-7}

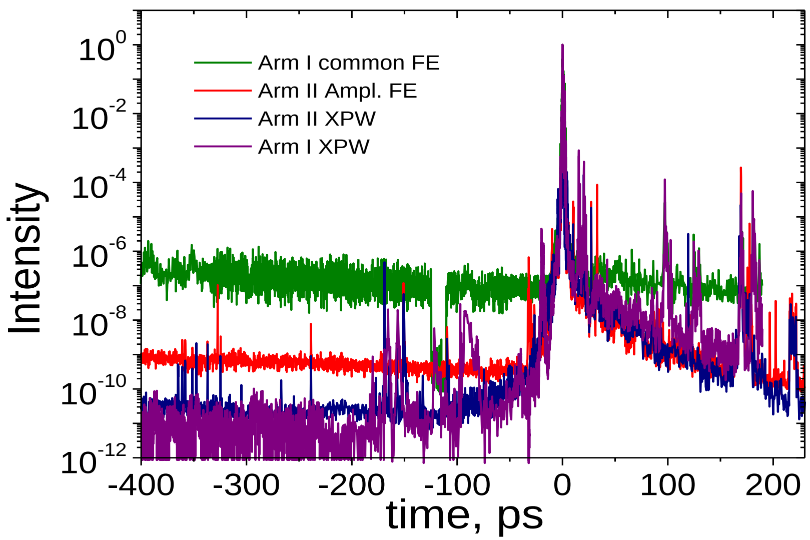

M.Kalashnikov, SPIE (2011)

Improvement of 10^4

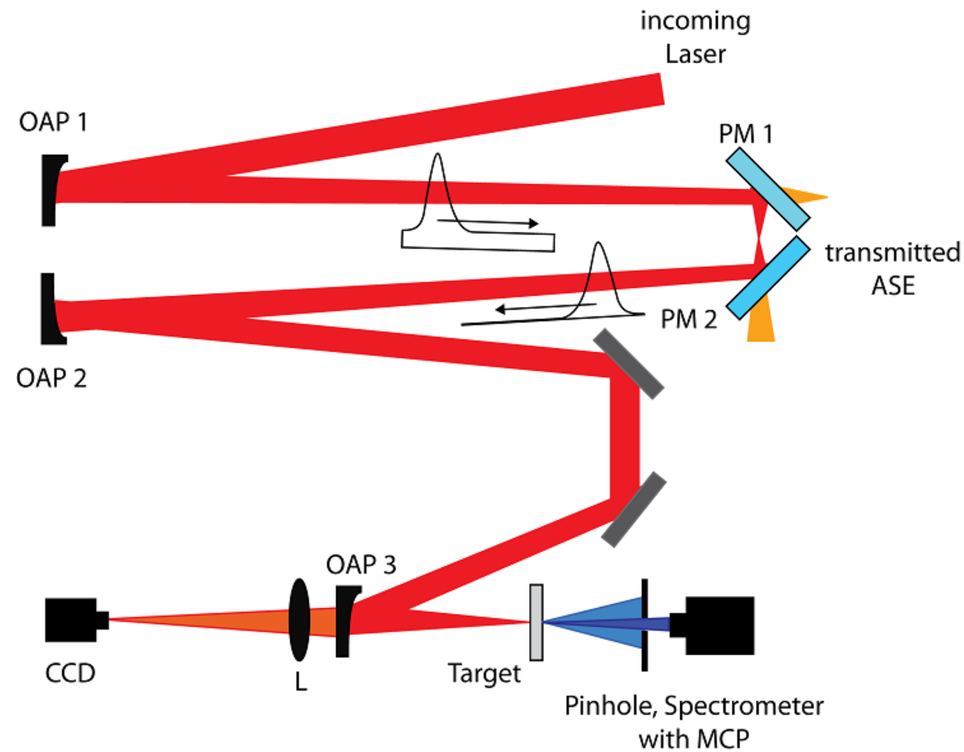

Double – Plasma Mirror (DPM)

- energy throughput ~65%
- no decrease of focusability

$$K_{PM+XPW} \approx 10^{-14}$$

$$K_{PM} \leq 10^{-10}$$

Fs laser induced quasi-periodic nanostructure

(a)

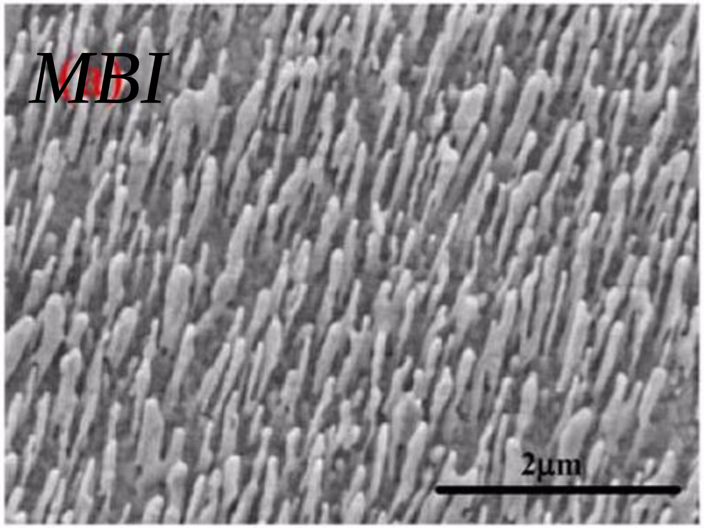

FESEM image of metal nanorods

S.Das, A.Andreev et al., APJ (2016)

(b)

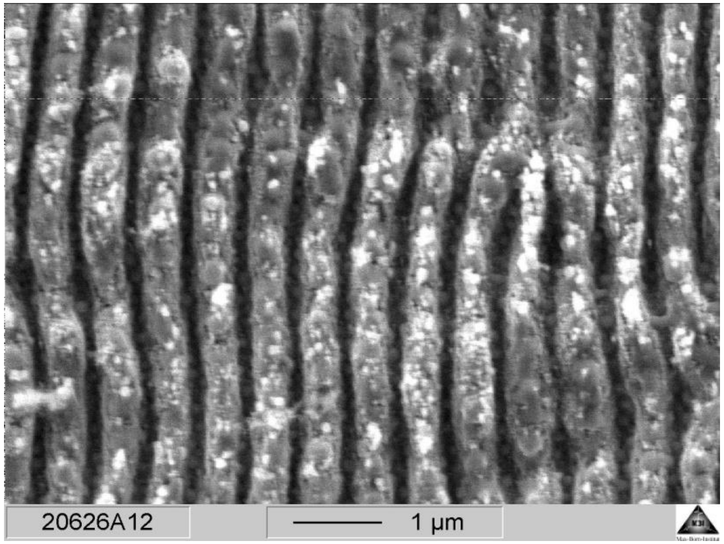

The results on ripples on Cu created with fs pulses at 800 nm.

a) The catalyst-free technique to grow nano-rods has been developed using two-stage buffer layers combined with high temperature vapor phase transport nano-rod deposition, which results in well-aligned long nano-rod arrays coverage over large areas.

$$d_1 \sim d_2 \sim 100nm, h \sim 1000nm$$

b) LIPSS - laser induced periodic surface structuring. $d_1 \sim d_2 \leq 300nm, h \leq 500nm$

A.Lubke, A.Andreev et al. Sci.Rep. (2017)

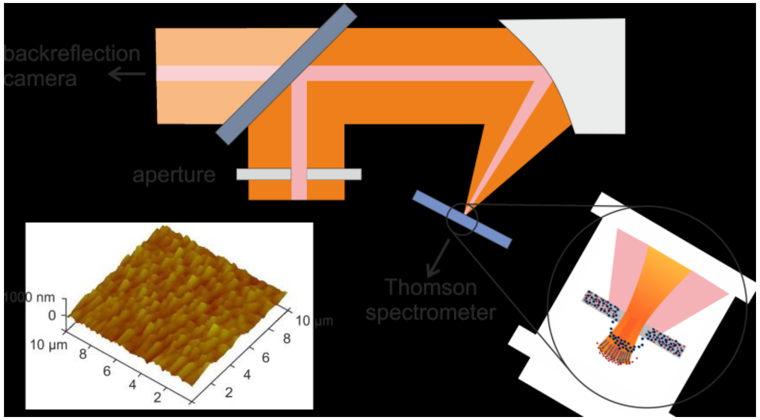

5 s exposure,10 μJ on target by reduction of beam diameter. Under these conditions we were able to generate LIPSS

Nano-structure (dynamic) target

(a) Schematic of the nanostructure target,

(b) Spatial distribution of electric field component normal to the target surface.

(a)

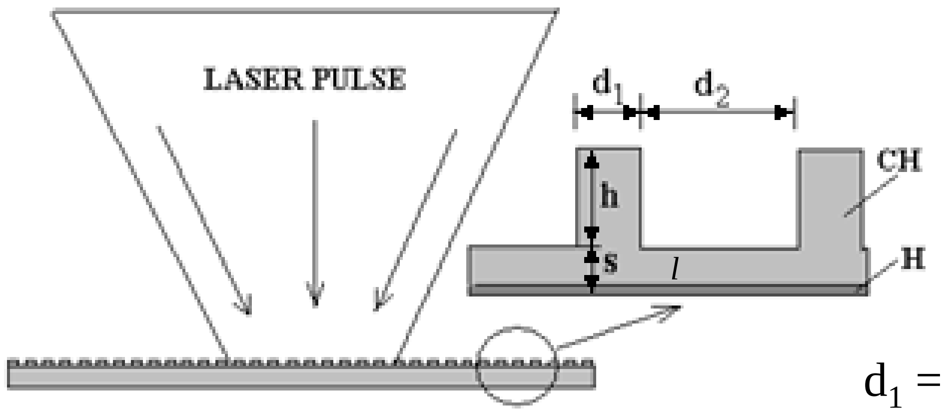

(b)

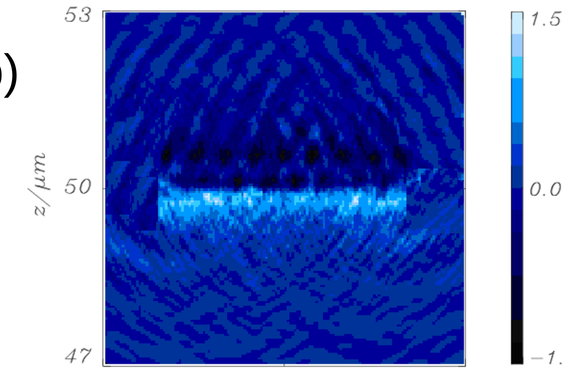

$d_1 = 0.15\ \mu m$; $d_2 = 0.35\ \mu m$; $h = 0.3\ \mu m$

c) Proton distribution function at the end of simulation (600 fs), (d) Phase space of accelerated protons at the same time.

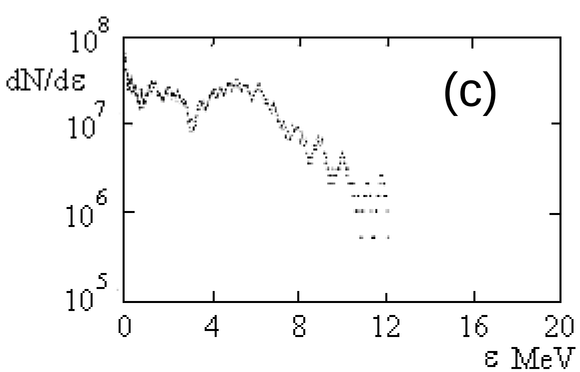

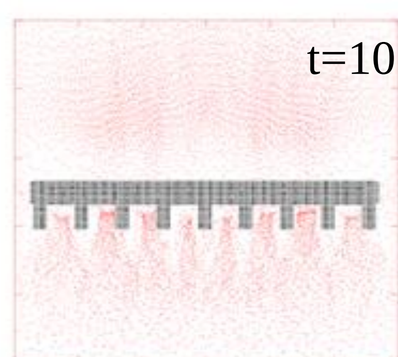

t=107fs

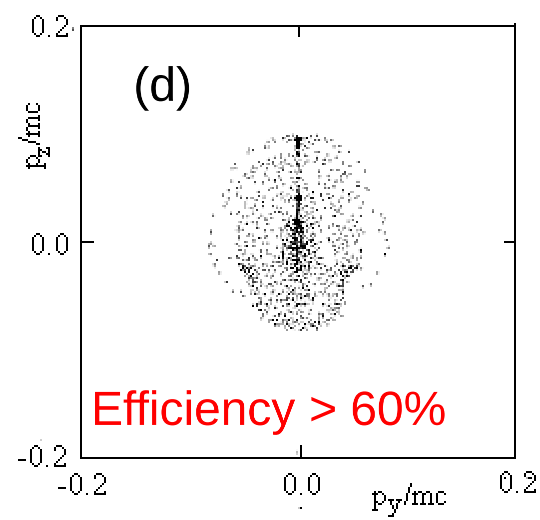

A.Andreev et al. PoP (2011)

Laser pulse 10^{20}W/cm^2, 15 fs, diameter 3 μm; target C^{+6} H^{+1}, density 0.4g/cm^3, finite 4x4μm

Efficiency of a structure targets

Absorption in the units of the plane 300 nm foil $C^{+6}H^{+1}$ 10^{20} W/cm^2,15 fs, 3 μm

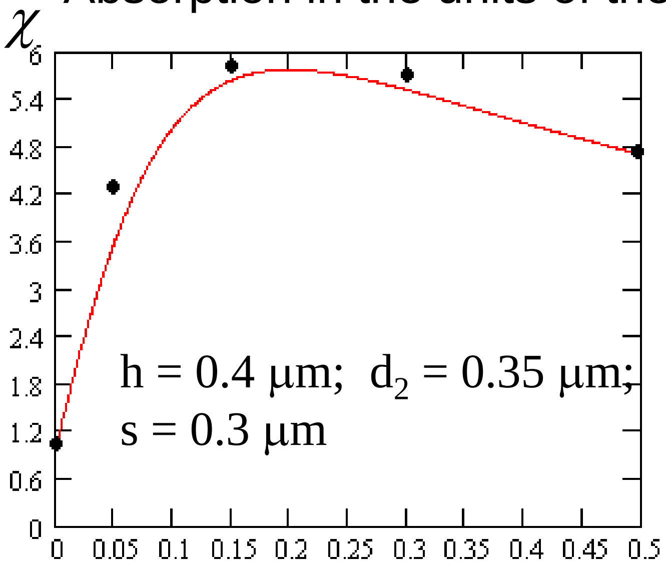

d_1 [μm]

ρ= 0.4 g/cm^3

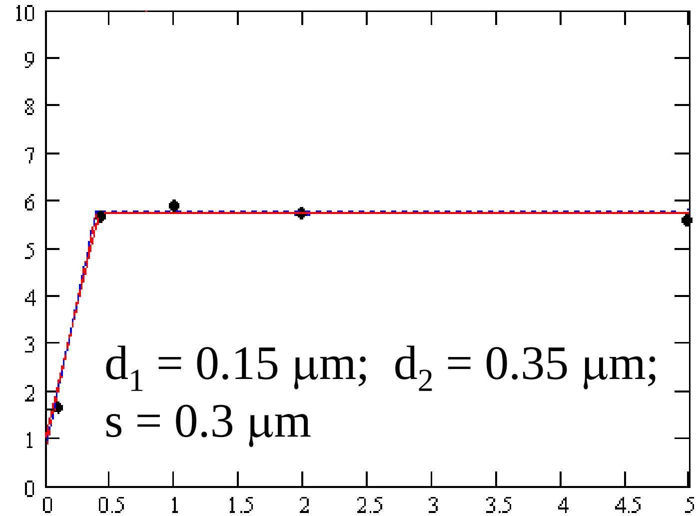

h [μm]

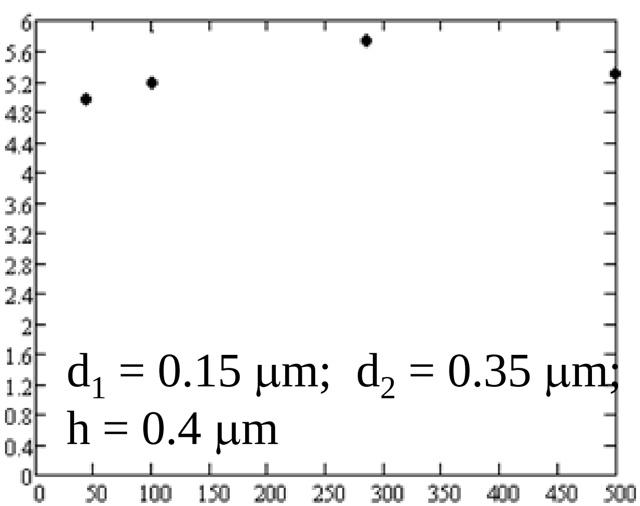

s [nm]

$$\chi \approx 1 + \frac{(d_1 / 2l_{extr})}{\sqrt{1+(d_1/2l_{extr})^2}}\left(\frac{E_0 d_L^2}{e\varepsilon_L}\right)\cdot\frac{1.4h}{(d_1+d_2)}\cdot m_e c^2 I_{18}$$

$$\chi < \chi_{\max}$$

$$\chi = \chi_{\max} \qquad \chi > \chi_{\max}$$

$$\tilde{\chi} = \frac{\chi}{1+e^{\frac{\chi-\chi_{\max}}{0.1}}} + \frac{\chi_{\max}}{1+e^{\frac{\chi_{\max}-\chi}{0.1}}}$$

Efficiency > 60%

Optimal structure target parameters

Size of electron vacuum orbit

(E_L – laser field)

$$r_{eh} = \frac{\lambda_L}{2\pi}\sqrt{\frac{1.37 I_{18}}{1+0.7 I_{18}}}$$

Optimal distance between ledges $\quad d_2 \approx 2r_{eh}$

Electron extraction length due to laser field action

$$l_{extr} \approx E_L / en_e = 4\pi \frac{c}{\omega_{pe}} \frac{\omega}{\omega_{pe}} \sqrt{1.37\, I_{18}}$$

Optimal ledge size $\quad d_1 \geq 2l_{extr}$

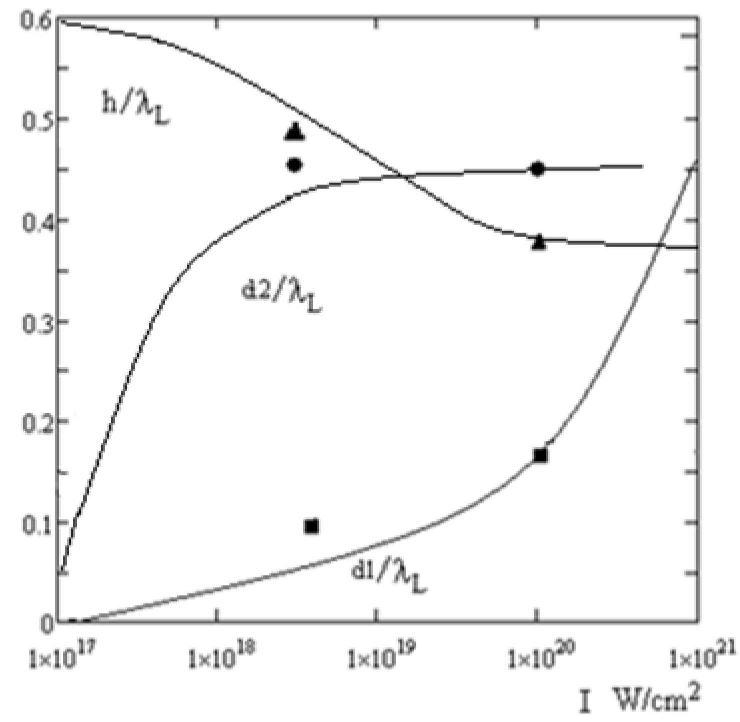

Optimal relief height *h* when vacuum electron excursion is about target period

$$h \approx 0.05(d_1 + d_2)\frac{\omega t_L}{\sqrt{I_{18}}}$$

For $\quad I_{18} = 100,\ \tau_L = 15\ fs,\ \lambda_L = 0.8\ \mu m \qquad d_1 = 0.15\ \mu m,\ d_2 = 0.4\ \mu m,\ h = 0.2\ \mu m$

It’s closed to the calculated optimum

Limitations of a nanostructure targets

Thermal (prepulse) smoothing

$$l_T \approx \sqrt{T_p \cdot \tau_p / m_e \nu_{ei}} > s \qquad T_p \sim \eta_p I_p \tau_p / Z_p n_i s$$

$$\tau_p \sqrt{Z_p T_p / m_i} = \tau_p \sqrt{\eta_p I_p \tau_p / m_i n_i s} < 0.5\, d_2$$

$$I_p \le 10^9 W / cm^2, \qquad \tau_p \le 1ns \qquad K_m \ge 10^{10}, \quad I_L \ge 10^{19} W / cm^2$$

Pondermotive (main pulse) smoothing

$$E_L^{\,2} / 4\pi < (en_e h)^2 / 8\pi$$

$$(I / 1.37 \cdot 10^{18}\, W / cm^2)^{0.5} < 2\, n_e\, h / n_{cr} \lambda_L$$

$$I_L \le 10^{21} W / cm^2$$

"Ripple" targets

J.Branzel et al. ECLIM AIP (2014)

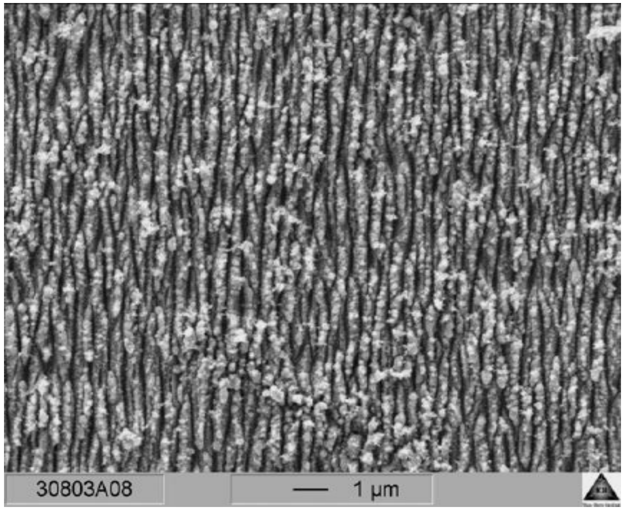

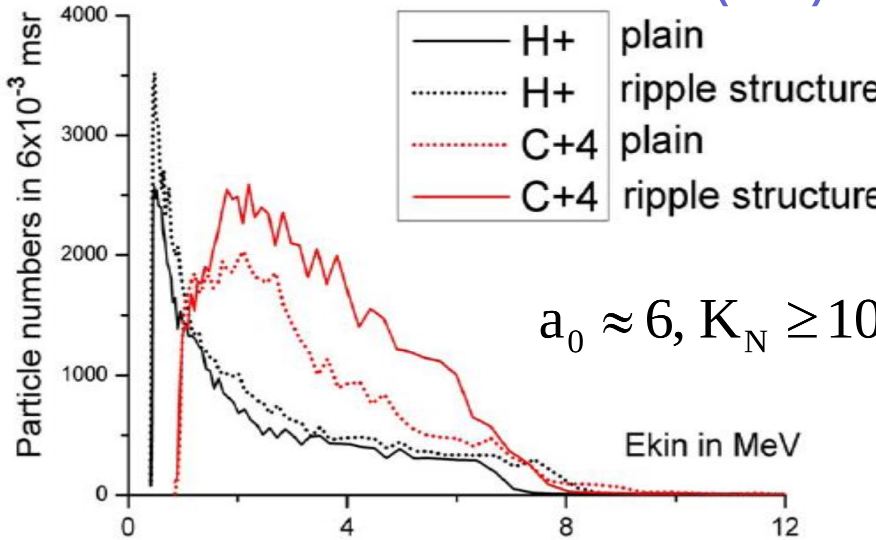

$a_0 \approx 6,\ K_N \geq 10^{10}$

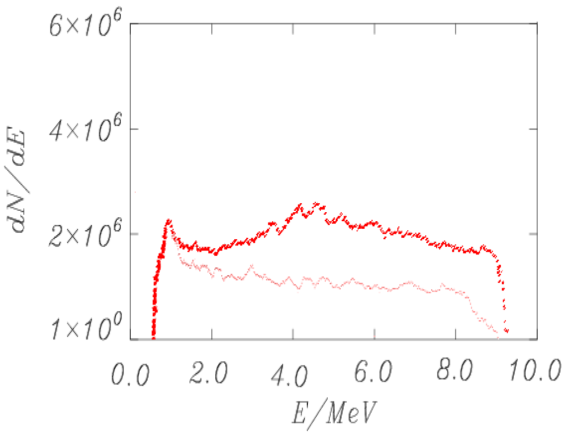

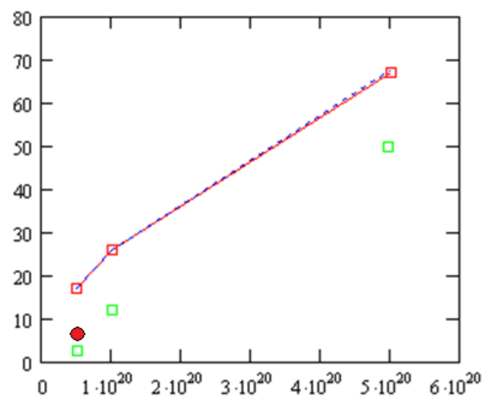

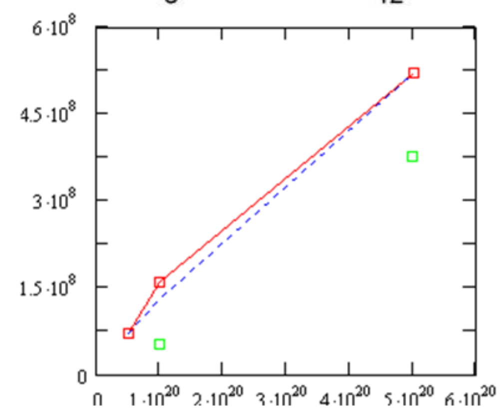

Red squares – optimal target, Green squares – plane foil

$$\varepsilon_p \approx 17(I_L / 5\cdot 10^{19} Wcm^{-2})^{0.6}[MeV]$$

$$N_p \approx 7\cdot 10^7 \cdot (I_L / 5\cdot 10^{19} Wcm^{-2})^{0.86}$$

I_L=10^{20} W/cm^2, t_L=30 fs, d_L=3mkm, d_1=200nm, d_2=100nm, h=200nm, Ti^{+15}, C^{+1}

A.Andreev et al. PP&CF (2015)

Manipulation of laser beam by reflection from relief target

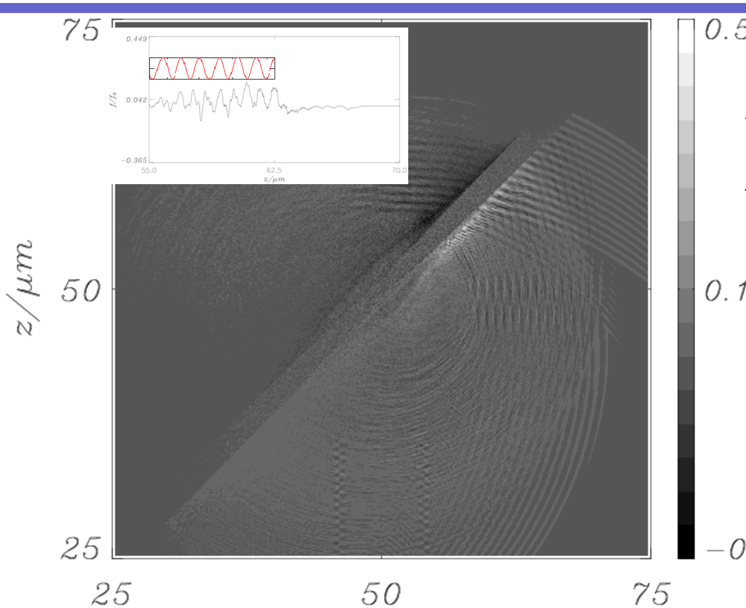

$I_L = 10^{20} Wcm^{-2}$,

$D_L = 8\lambda, t_L = 40\ fs$

100 nm relief

45^0 angle

400 nm relief

60^0 angle

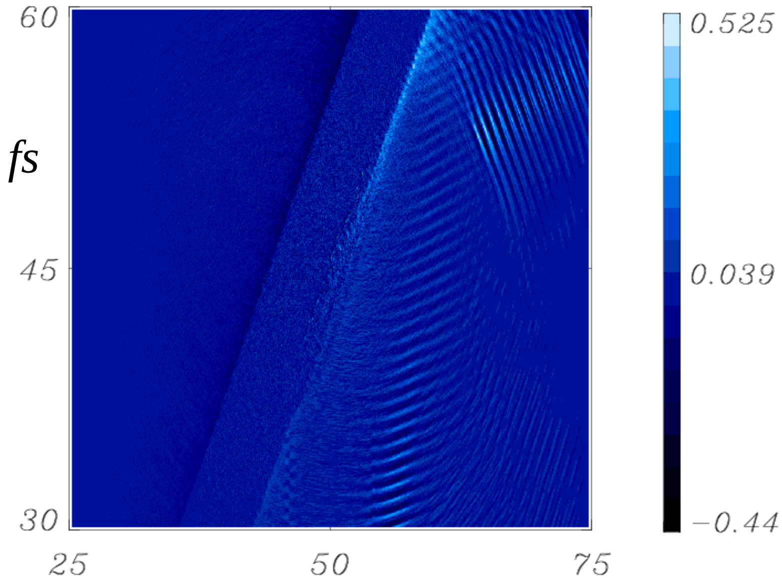

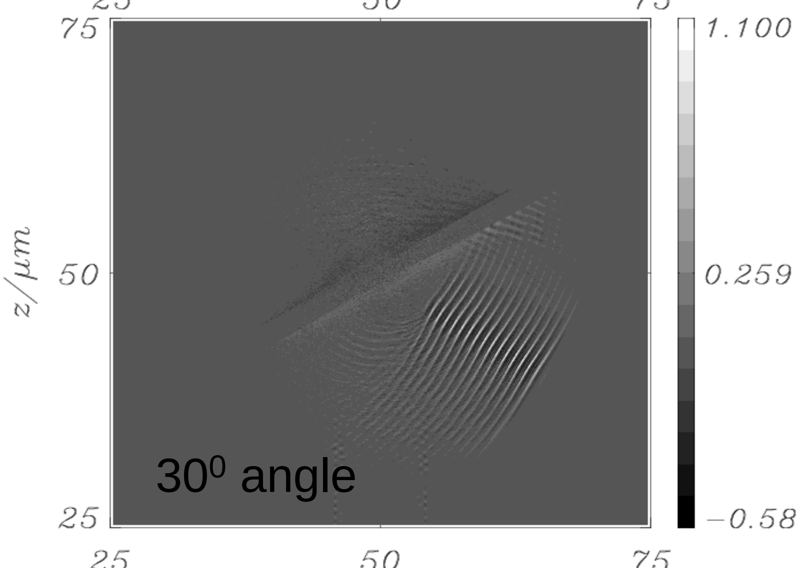

Grating equation: $d(\sin\theta_0 + \sin\theta) = n\lambda / n_{harm}$

1.Strong "surface" wave at the incidence angle θ > 45^0 for relief target due to edge diffraction
2. Backscattered wave at 60^0 for relief target
3. Atto-pulses in the "surface" and specular waves has different wave-length

X. Lavocat-Dubuis POP (2010)

Electron transport efficiency in nano-wires

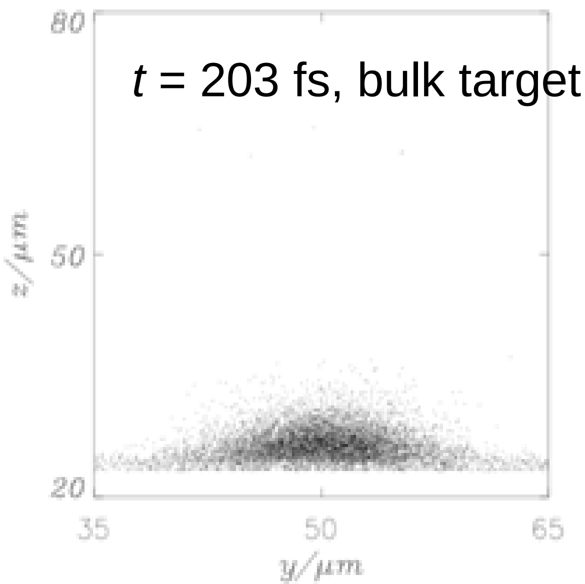

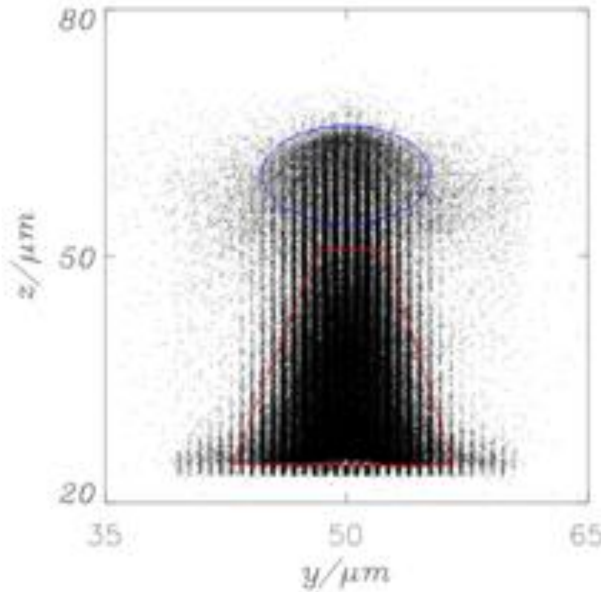

Wire solid target: C^{+6}
Length 50 microns,
d1=150 nm, d2 = 500 nm
Laser: pulse duration 45 fs,
spot size 4 microns,
intensity 3×10^{19} W/cm^2

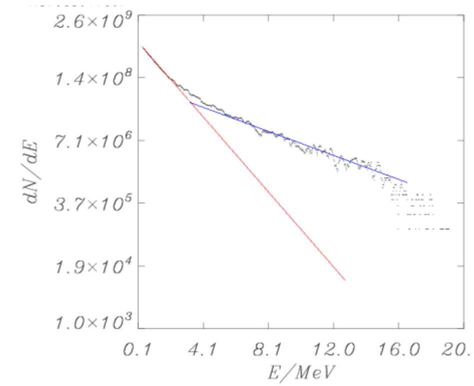

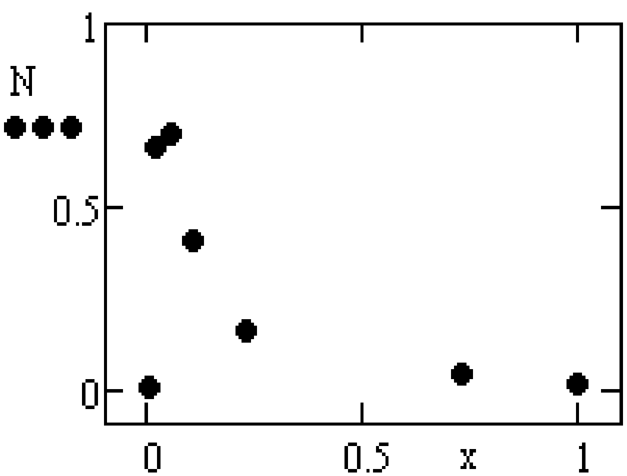

$$l_1(t) \approx \sqrt{l_{10} + \sigma_{zz}\, t\, r_{D1} l_f}$$

$$p_z \geq 0.9mc$$

N – relative number of fast electrons,
E- its relative total energy

$$x = d_1 / (d_1 + d_2)$$

A.Andreev et al. PP&CF 2014

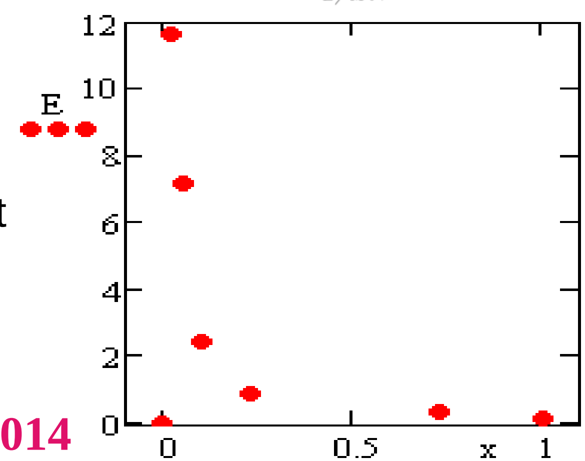

Analytical model of electron transport in “nano-wire” target

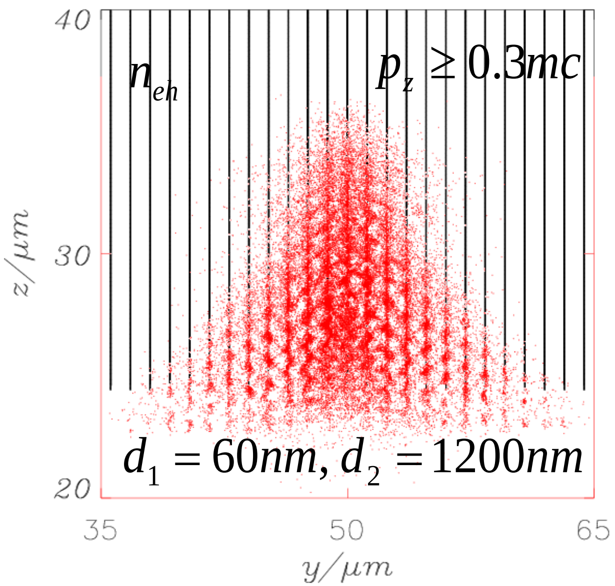

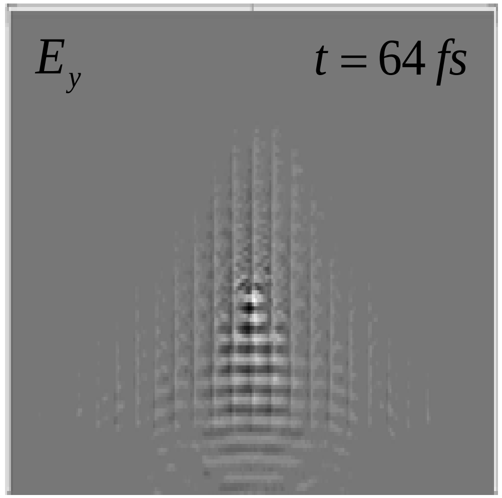

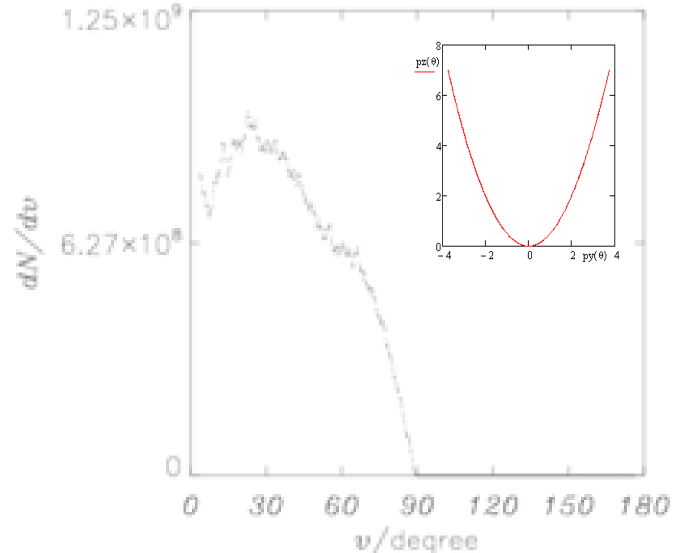

$$2\Delta\eta_e = -\eta_i + 1 + \frac{\psi}{2} - \frac{\varepsilon(\beta_z)}{2} - \frac{\beta_z a_z}{2} - \beta_z \Delta a_z$$

$$\frac{\partial^2 a_z}{\partial \xi^2} = \beta_z \eta_e + 2\kappa_{zz}\frac{\partial \eta_e}{\partial \varsigma} + \kappa_{zz}\beta_z \frac{\partial a_z}{\partial \varsigma}$$

$$\psi = |e|\varphi / T_{e0} \qquad \varepsilon(\beta_z) = mc^2((1-\beta_z{}^2)^{-1/2} - 1)/T_{e0}$$

$$\vartheta \approx \frac{p_y}{p_z} \approx \frac{\sqrt{(1+T_{e01}\psi / m_e c^2)^2 - 1}}{p_z / m_e c} \approx 10^\circ$$

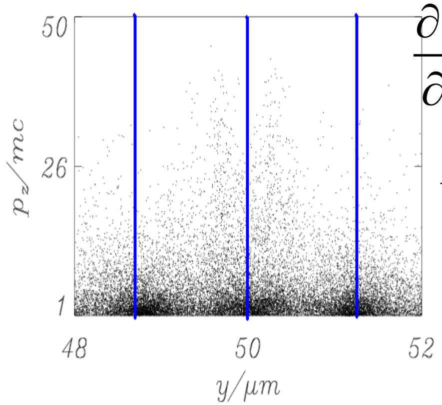

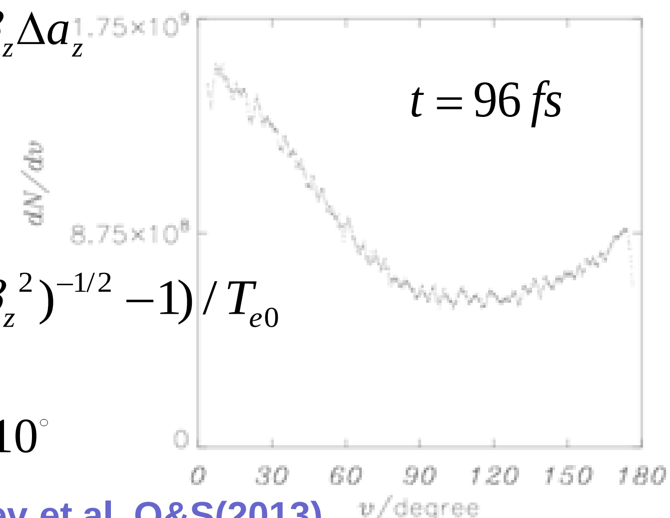

A.Andreev et al. O&S(2013)

Production of atto-pulses from nano-wire target

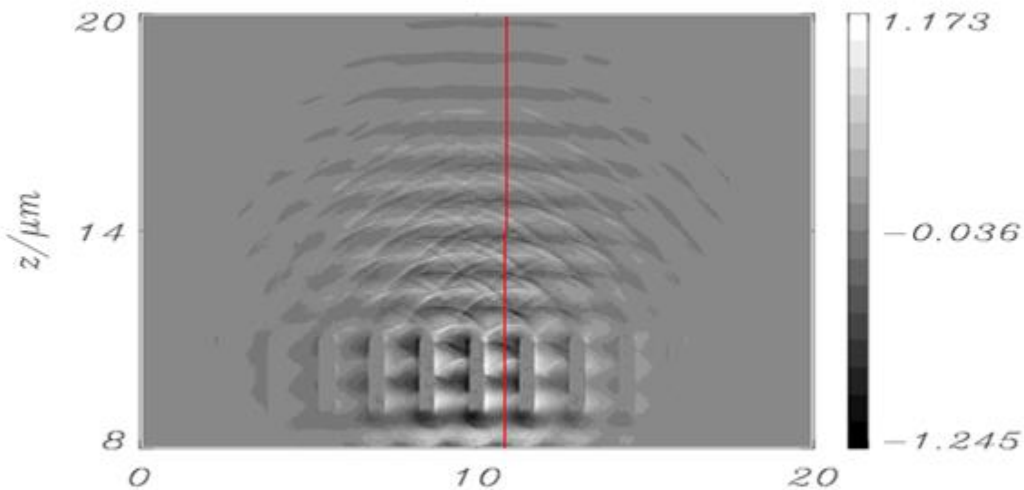

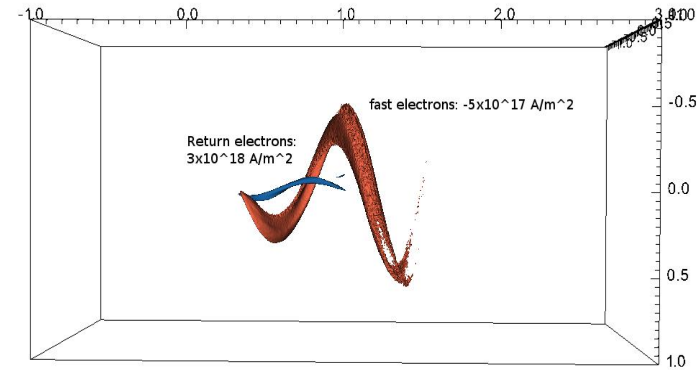

The iso-surface at10^20 W/cm2 (green) and the density of fast electrons at the iso-value 10^22 cm−3 (red), t =10 fs.

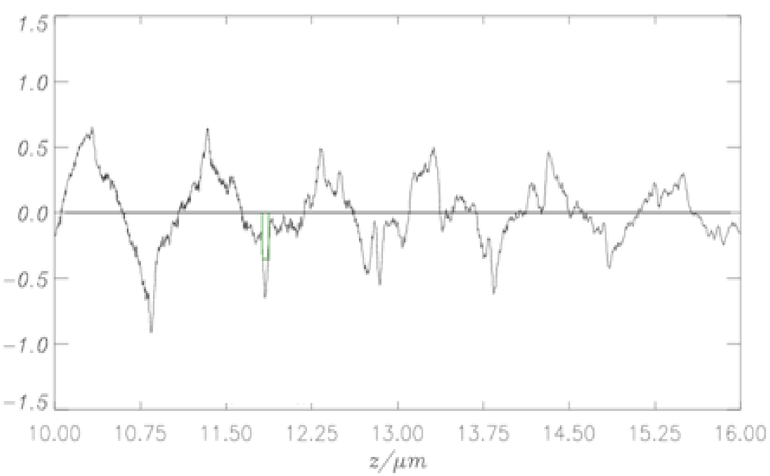

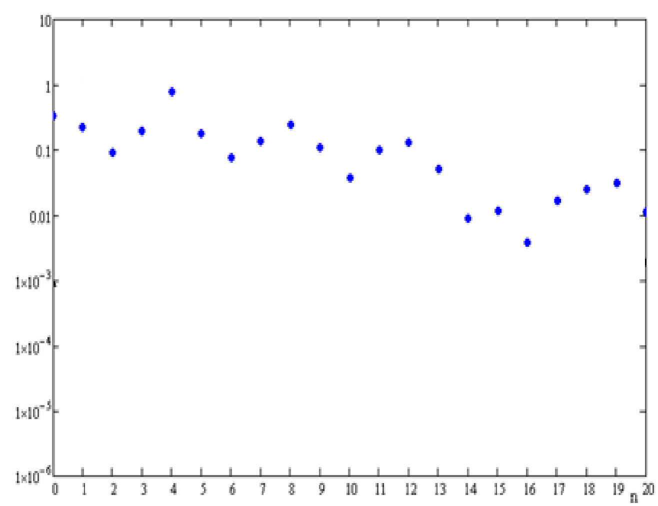

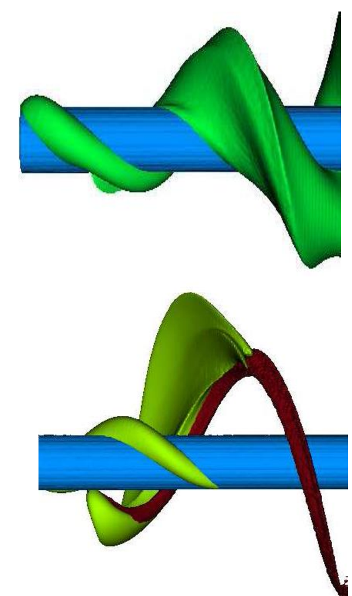

A.Andreev et al. L&PB (2013)

Laser-driven bright X/ɣ-ray emission

Electron Acceleration (Stage I)

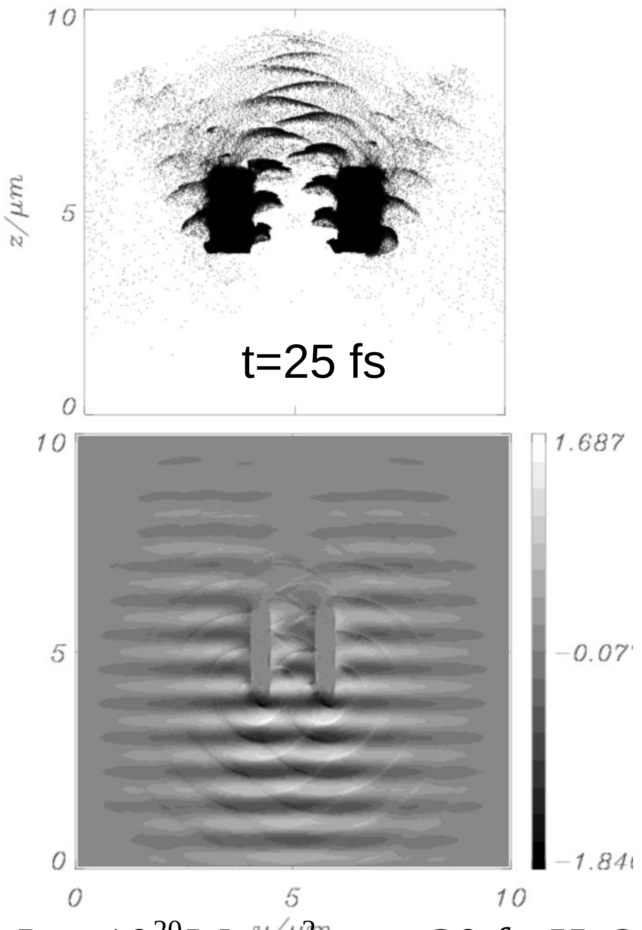

$I_L = 10^{20} Wcm^{-2}, t_L = 30\, fs, H_2O;$

$I_S = 10^{17} Wcm^{-2}, R \approx 10^{-3}$

Zhavorinkov, Andreev L&PB (2013)

Electron density distribution

$I_L = 10^{21} Wcm^{-2}, t_L = 30\, fs;$

Electron phase Space

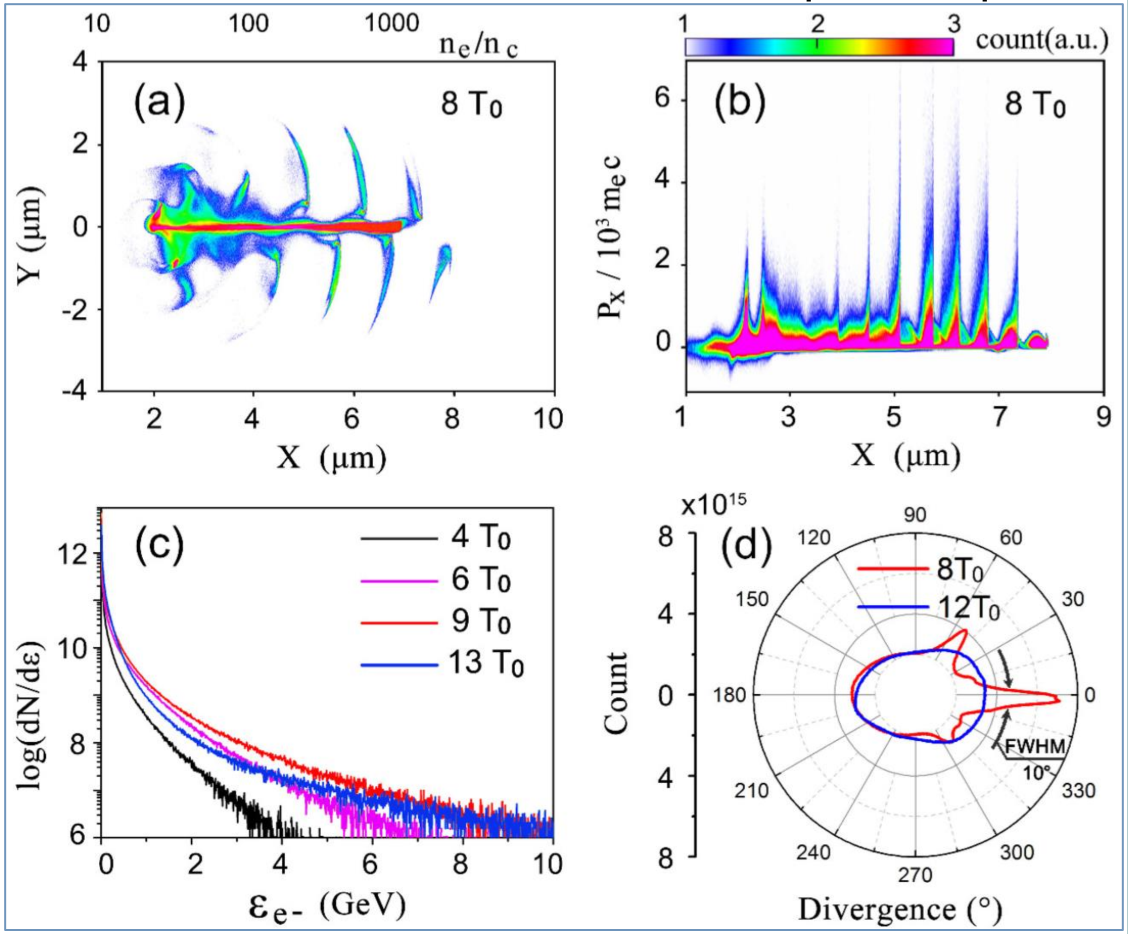

Electron energy spectrum

Electron angle divergence

Li *Opt. Express*, (2018).

Ultra-bright γ-ray flashes

Nonlinear Compton Scattering (Stage II) $I_L = I_S$

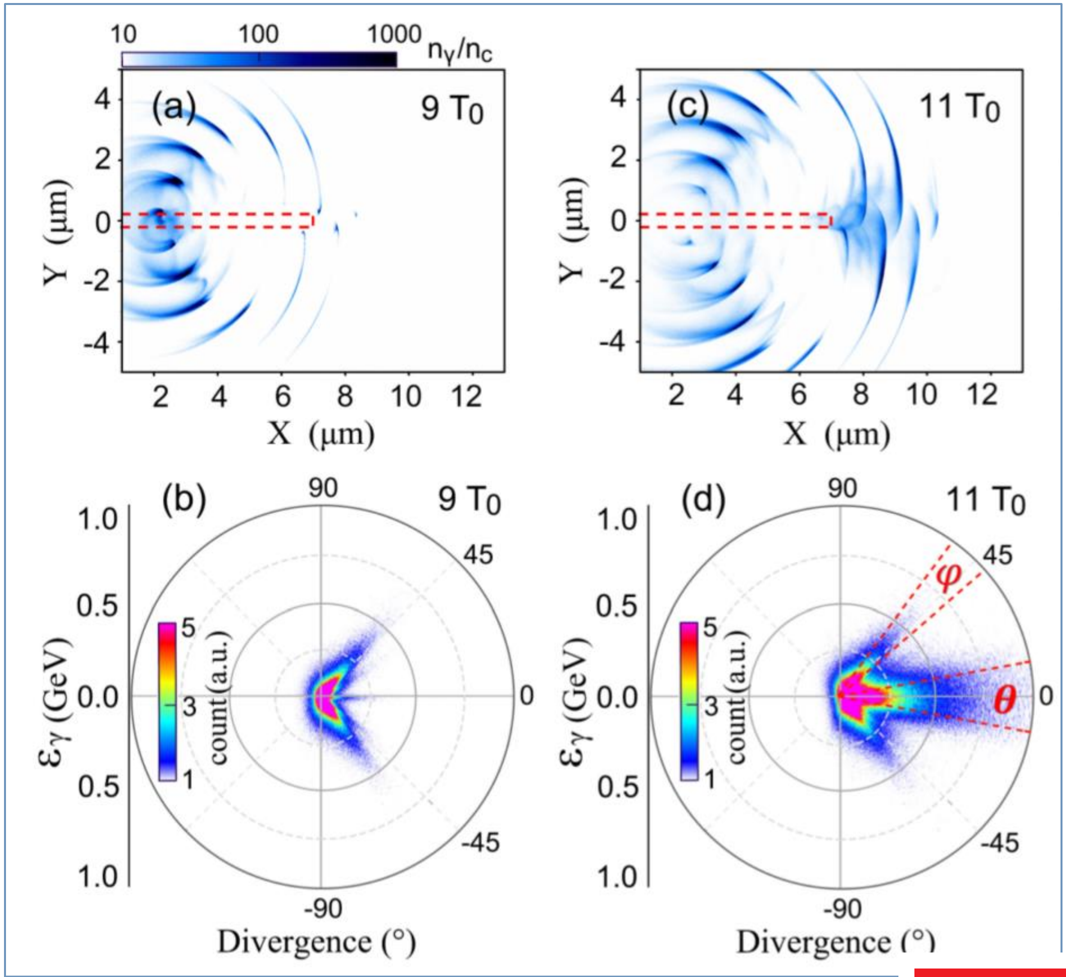

γ-photon energy spectrum

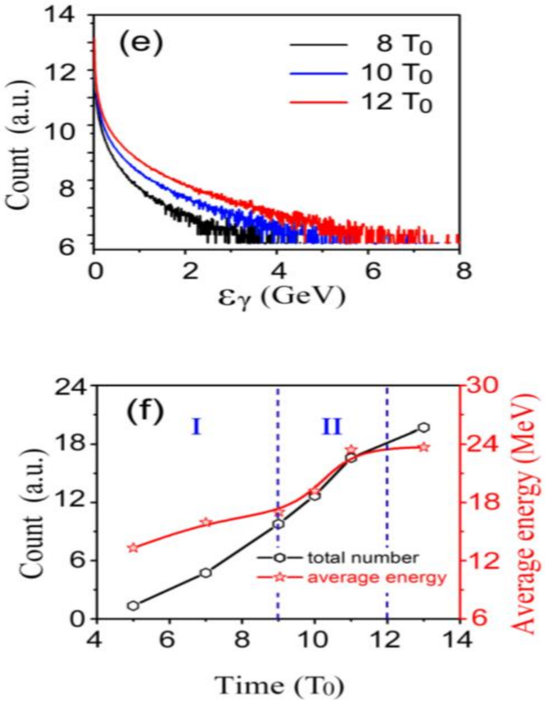

γ-photon flux evolution

Li *Opt. Express*, (2018).

10^{24}photons/s/mm^2/mrad^2/0.1%BW

Betatron radiations in nanowire targets

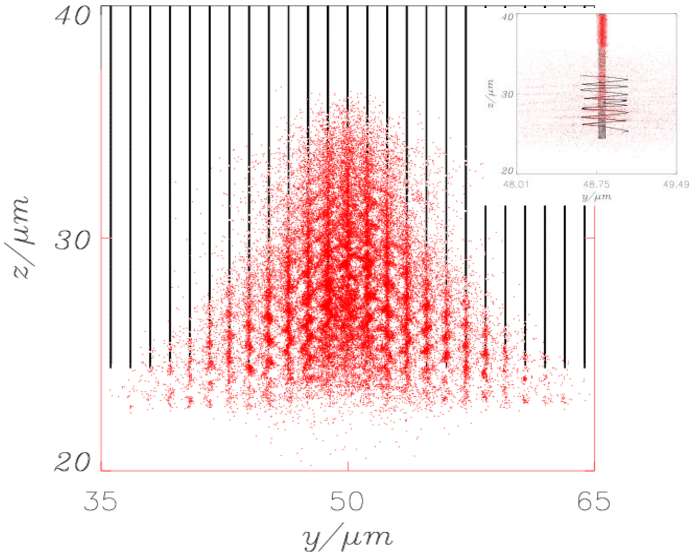

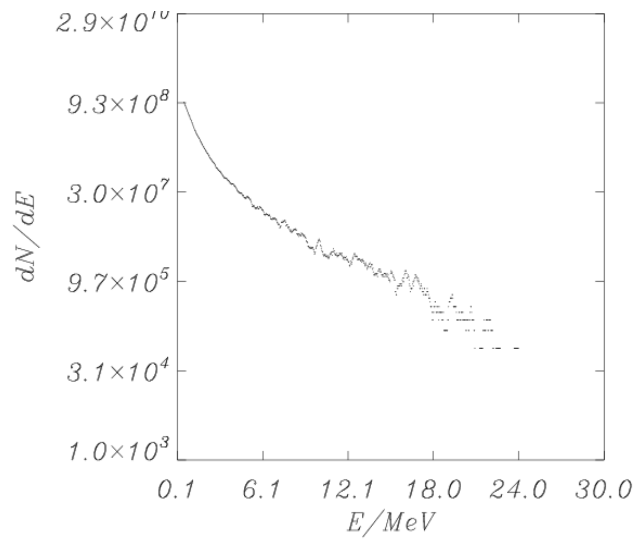

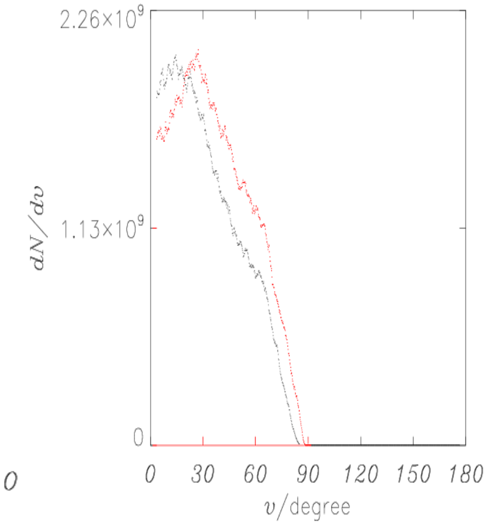

$$n_i = 6 \cdot 10^{22} \quad cm^{-3}, \; Z = 6, d_1 = 60nm, d_2 = 1\mu m, \quad I_L = 3 \cdot 10^{19} W / cm^2, t_L = 45\, fs, d_L = 4\,\mu m$$

A.Andreev et al. QE (2015)

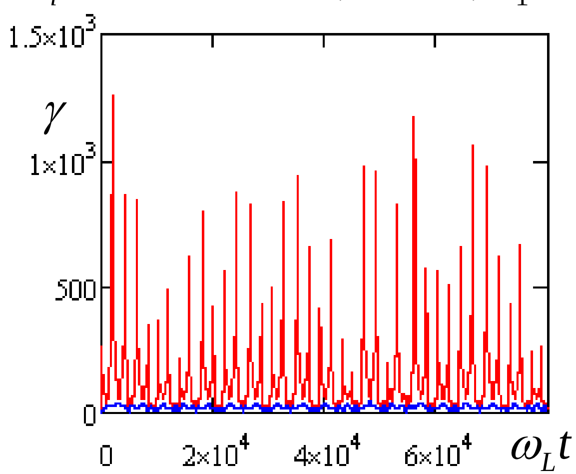

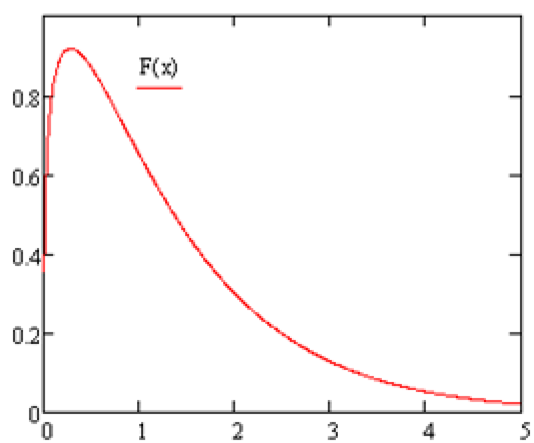

$$\frac{dP}{d\omega} = \frac{\sqrt{3} e^2 \gamma_z}{2\pi r_E} \mu^2 F\left(\frac{\omega}{3\omega_c}\right) \qquad \mu = \frac{2e^2 N_{eh}}{m_e c^3 t_L \gamma_z}$$

$$dP / d\omega \approx 400 \cdot dP^{(BG)} / d\omega$$

$$\kappa = \frac{N_{eh} P_{1e}}{I_L \pi r_{\max}^{\;\;2}} \approx 0.02$$

$$\mu_{res} \approx 0.2\gamma_z, \omega_{e,res} \sim 0.1\omega_L; \quad I_L = 10^{21} Wcm^{-2}, t_L = 30\, fs; \quad \omega_c \approx \omega_L \gamma_z^3 \pi c / \upsilon_E (1.5 + 2\mu^{-1/2}) \approx 3MeV$$

Atto-pulse enhancement by two reflections

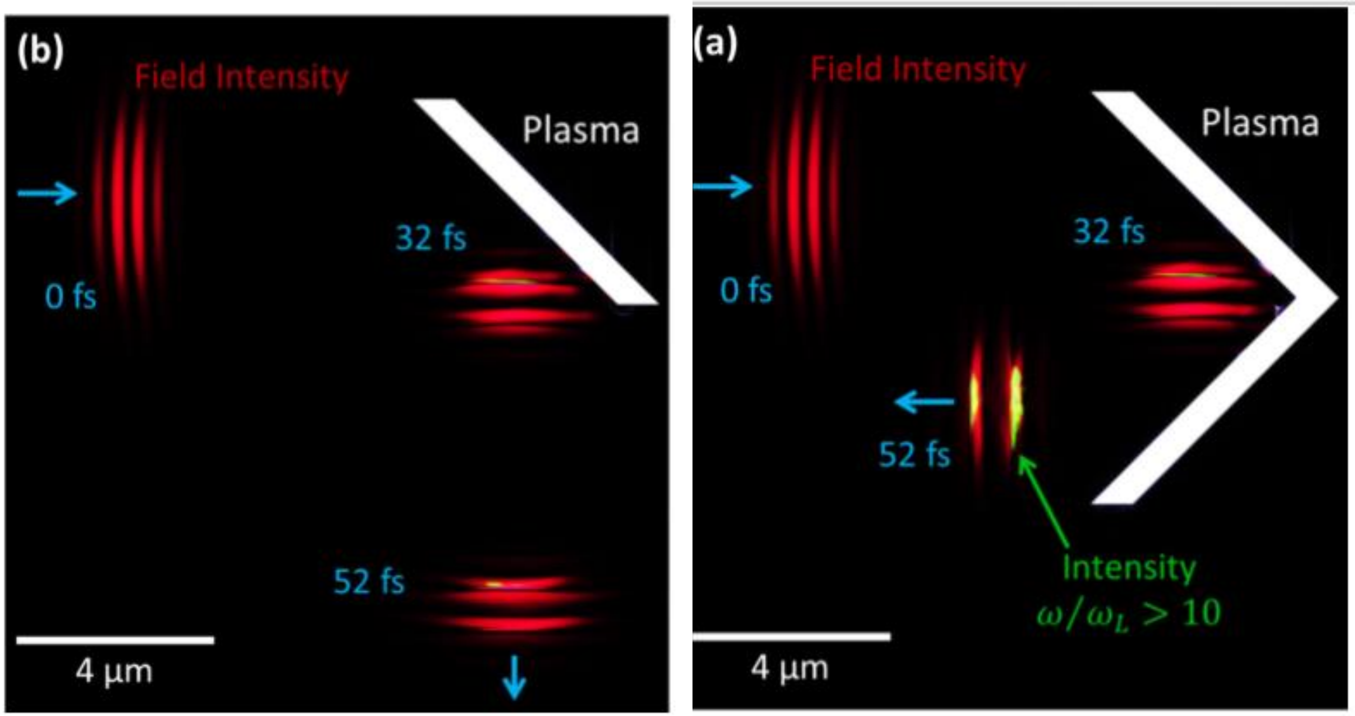

2D simulations comparing two-pass (a) and one-pass (b) interactions. An incident laser (red, a0 =20, τ =5 fs) interacts with two (a) or one (b) plasma surfaces (white, N =200), showing substantially enhanced high-order harmonics (yellow/green) in the two-pass case.

M. R. Edwards,
M. Mikhailova, PRA (2016)

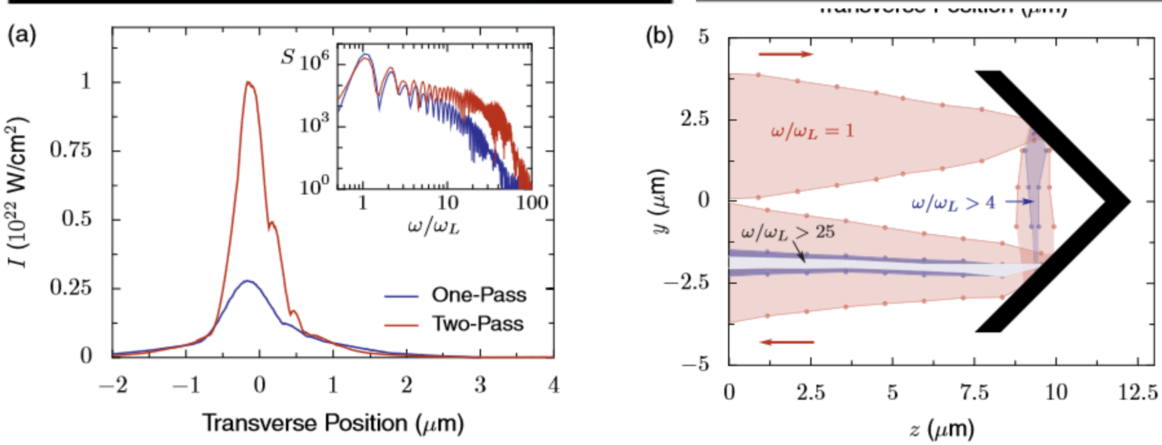

a) The transverse distribution of reflected intensity from 2D simulation, showing spatial narrowing, after one pass (blue, lower line) and two passes (red, upper line). Inset :spectra of reflected fields in both cases (b) Spatial FWHM of fundamental (red), moderate harmonics 4 < ω/ωL < 20 (blue) and high harmonics 25 < ω/ω L < 40 (gray) for focused two-pass interaction.

Amplification of Surface High Harmonics via multiple reflections of intense pulses

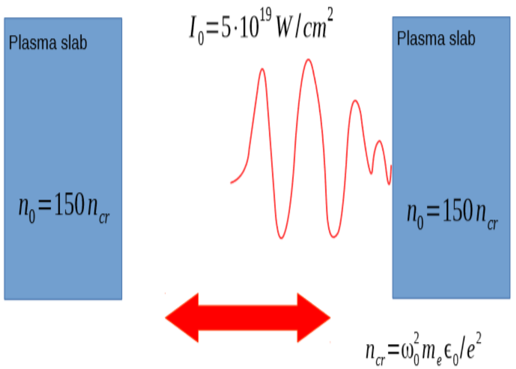

The curvature of the mirror coincides with the curvature of the wave front in the laser pulse at that position. The plane target (plasma slab) is located in the focal plane of the pulse.

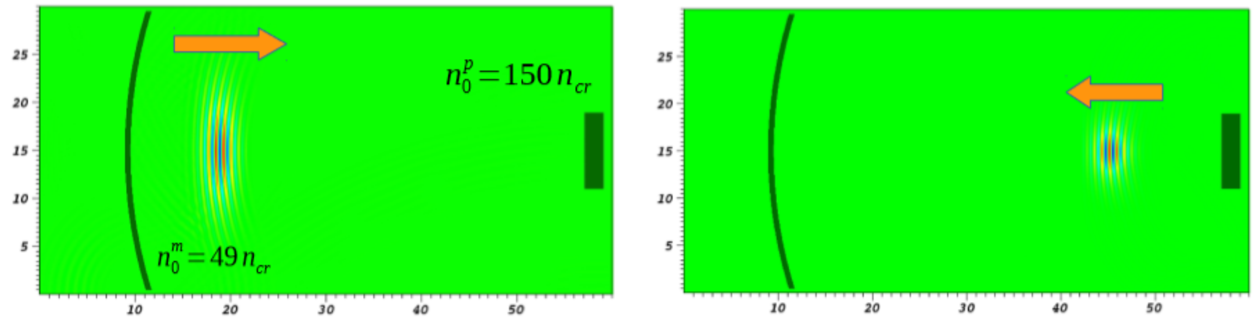

When an intense laser pulses impinges on a flat target surface it gets reflected by the ionized layer, which behaves by a longitudinally oscillating mirror. Main part is reflected back with a distorted wave front. This modulation is generated by the relativistic motion of the plasma mirror. The high frequency components appearing in the reflected spectrum are exactly the harmonics. Here we use the reflected pulse, containing its harmonics, to induce SHHG on a second clean surface.

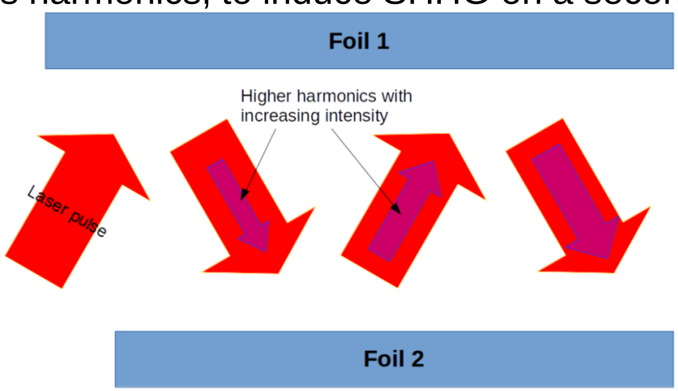

Schematics of the multiple reflection setup. The two foils are parallel and are moved perpendicular to the interaction plane with 100 cm/s velocity.

In our setup we assume a pulse of 10-100 mJ energy in the case of high repetition rate lasers, or 1-10 J in the case of high peak power lasers, compressed to about 10 fs time duration and focused to about a few tens μm2 spot area. A focal length of about 10 cm ensures a small beam divergence, smaller than the incidence angle which can be 20 degrees. **Lecz&Andreev JOSA B (2018)**

Spectral intensity of reflected pulse at normal incidence

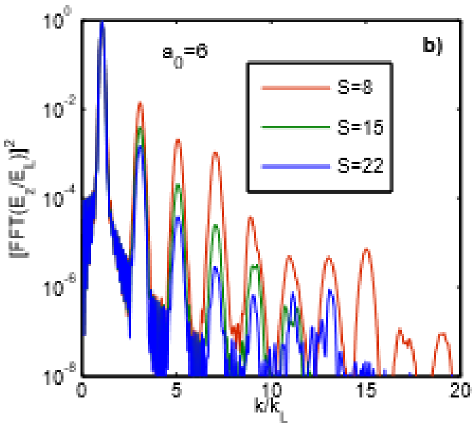

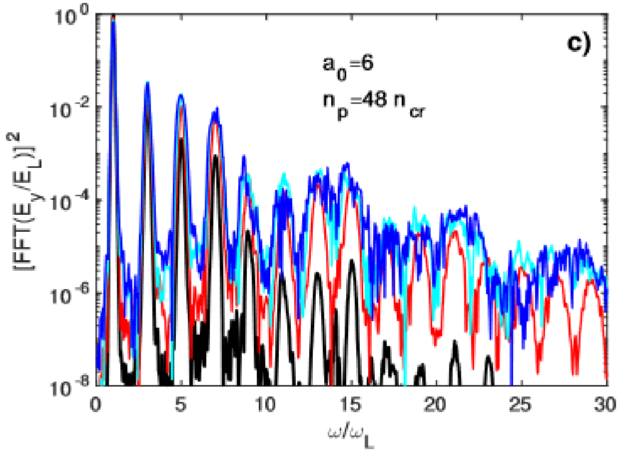

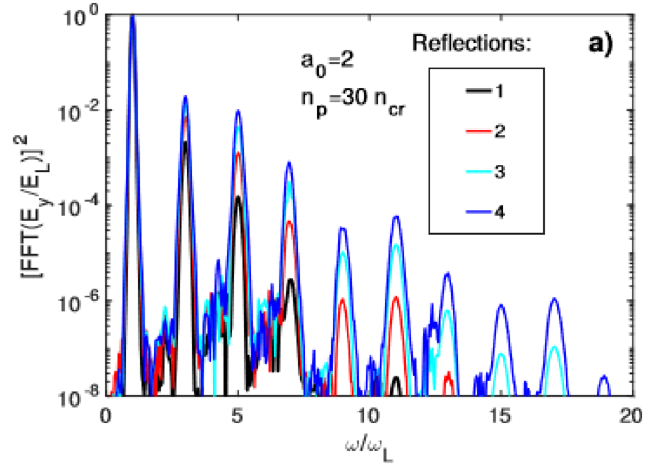

Spectra of reflected pulse for different S parameters.

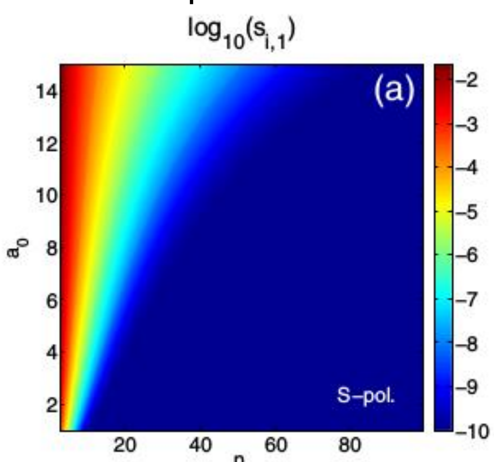

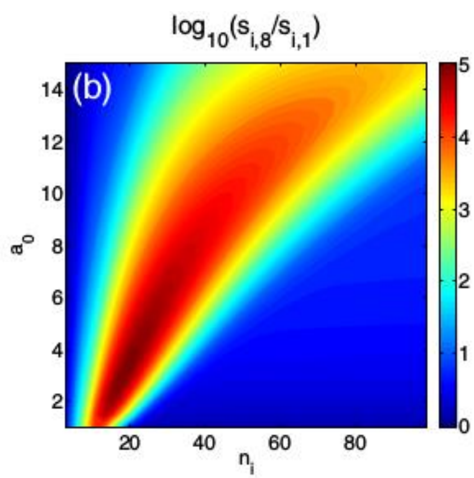

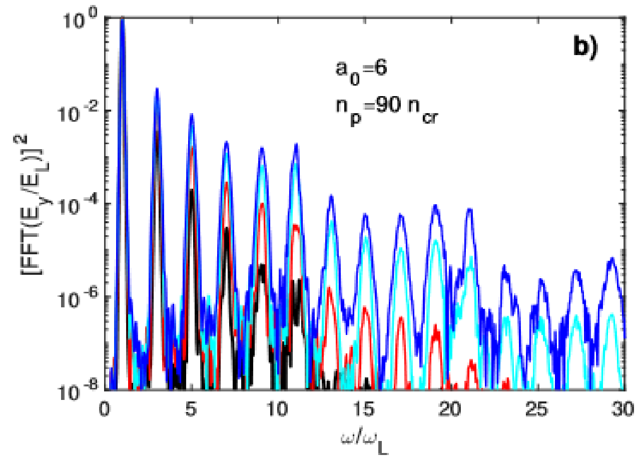

(a) Intensity distribution of harmonics (n_i) for different laser amplitudes. (b) Amplification factor of each harmonics after the 8th reflection.

Spectral intensity distribution of the pulse after reflections for different laser intensity and plasma density in the case of normal incidence.

Reflection at oblique incidence of laser pulse

Lecz&Andreev JOSA B (2018)

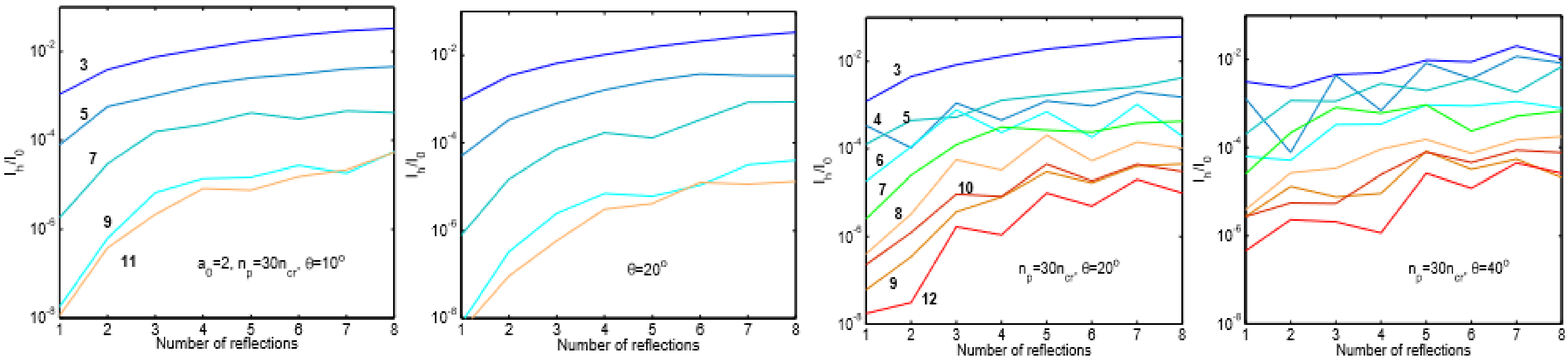

Intensity evolution of harmonics generated during consecutive reflections for a0 = 2 and for different initial incidence angles; a,b) S – polarisation; c,d) P - polarisation

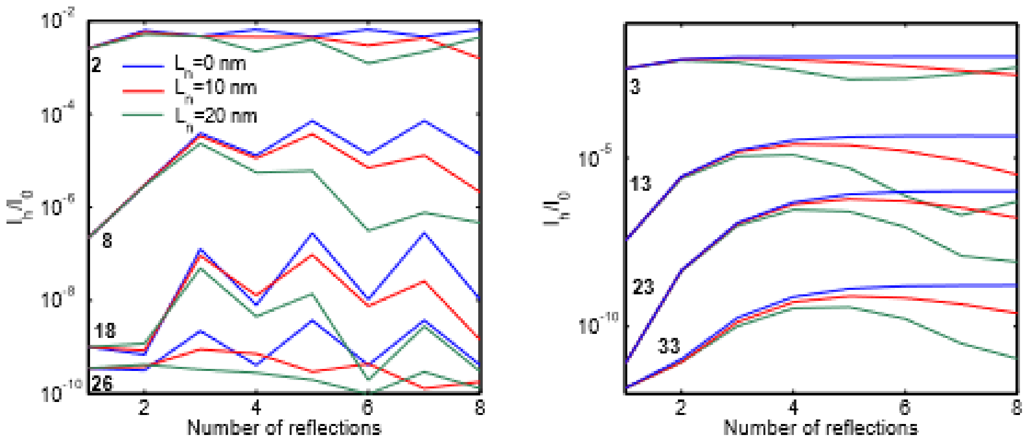

Intensity evolution of several harmonics for different plasma density scale lengths with P (l) and S (r) polarizations. Here: a0 = 3, np/nc = 45, θ = 10o.

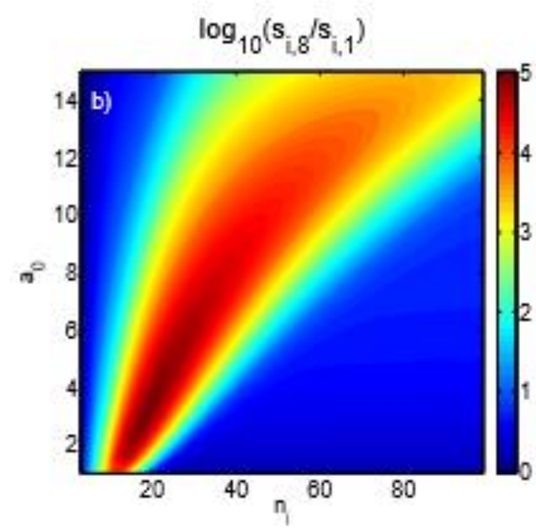

Harmonic amplification factor after 8 reflections for same density.

2D SIMULATIONS

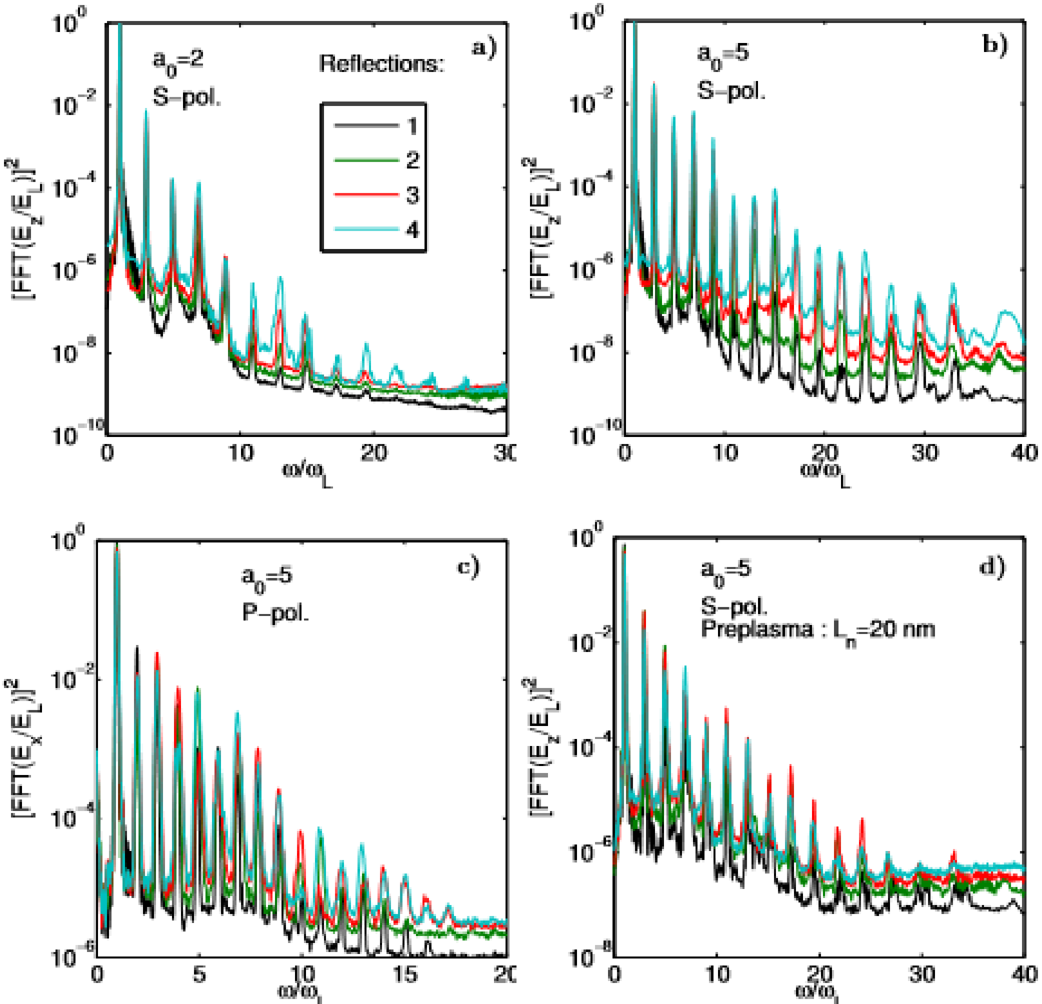

Spectra of laser pulse after consecutive reflections for S and P polarization and with preformed plasma for a0 = 5. The fields within 1 μm distance from the laser propagation axis are included.

Amplification in low density plasmas

In the second phase of ELI-ALPS operation, the secondary sources are anticipated to produce weak (~*pJ*) ultra-short (< *fs*) pulses; the tentative achievable intensity of these secondary pulses are very weak and for practical significance need to be amplified. We examine the possibility to utilize resonant Backward Raman amplification (BRA) as an efficient mechanism in plasma to amplify such weak pulses.

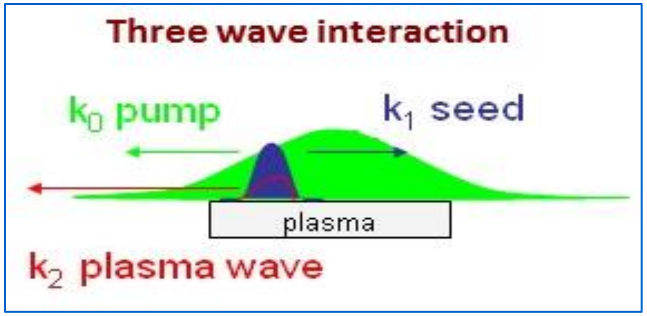

$$\boldsymbol{k_0} - \boldsymbol{k_1} = \boldsymbol{k_2} \qquad \omega_0 = \omega_1 + \omega_2$$

$$\omega_{0,1}^2 = \omega_p^2 + c^2 k_{0,1}^2 \qquad \omega_2^2 = \omega_p^2 + \upsilon_{th}^2 k_2^2$$

Approximate energy transfer: ω_2 / ω_0

A case study for ELI-ALPS parameter access

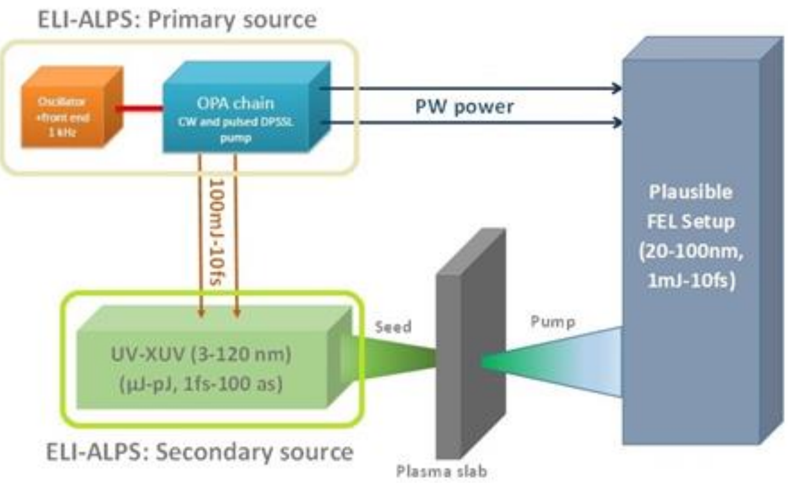

A schematic of the feasible BRA setup, relevant to ALPS infrastructure.

Primary Laser: SYLOS: Energy: 20mJ, Duration: 10fs, Spectrum: (0.3-1.3) μm
Secondary pulse: Energy: μJ-pJ, Duration: fs-as, Spectrum: (3-120) nm

Primary sources at present setup are not consistent for BRAmp processing
Alternative pump: FEL setup (driven by primary lasers) like DESY-FLASH FEL sources: 6.5-47 nm, 10-50fs, 1-5GW
Spot optimization: K-B Geometry of reflective optics (Spot: 0.01-1μm)
Plasma slab: (1-10) μm: laser illumination: isochoric heating of solid

Mishra&Andreev JOSA B (2018)

Optimization of resonant BRA physical parameters

- Applicability of SVEA to ultra-short pulses

$$\partial_t^2 A << \omega \partial_t A \Rightarrow \tau_l(as) >> (1/2)\lambda(nm) \equiv \tau_o(as) >> 5\lambda(nm)$$

- Seed-pump propagation

$$\omega_2 = \omega_0 - \omega_1 < \omega_1 \Rightarrow 1/2 < \lambda_0 / \lambda_1 < 1$$

- L-wave breaking

$$I_0 < I_{br} = (n_e / n_{cr})^{3/2} (4\omega_1\omega_0 / c^2 k_2^2) I_M, \;\; I_M \approx (n_{cr} m_e c^3 / 16)$$

- Shortest achievable duration of the seed leading spike

$$\Delta t_{s,fs} \sim 0.1(\lambda_1/\lambda_0)(\Lambda_0 \lambda_0^{nm} / I_0^{18})^{1/3}, \;\; \Lambda_0 e^{-2\Lambda_0} \approx \left[I_{1o} \Delta t_{1o}^2 (1-\lambda_0/\lambda_1)/(4m_e^2 c^3 / e^2) \right]$$

- Largest achievable intensity of the seed leading spike

$$I_{1m}^{(18)} \approx 1.2 \cdot 10^3 \left[(\lambda_0/\lambda_1)^2 / (1-\lambda_0/\lambda_1) \right] (I_0^{(18)} / \Lambda_0 \lambda_0^{nm})^{2/3}$$

Malkin et al. PRE 90, 063110 (2014). **Mishra & Andreev, PoP 23, 083108 (2016);**

Parametric space for laser/ plasma parameters to achieve efficient resonant BRA

PIC simulation results (with ELI-ALPS configuration)

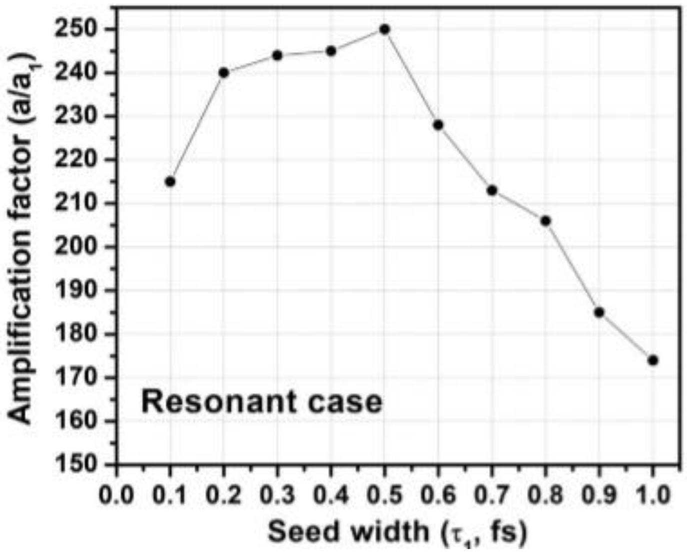

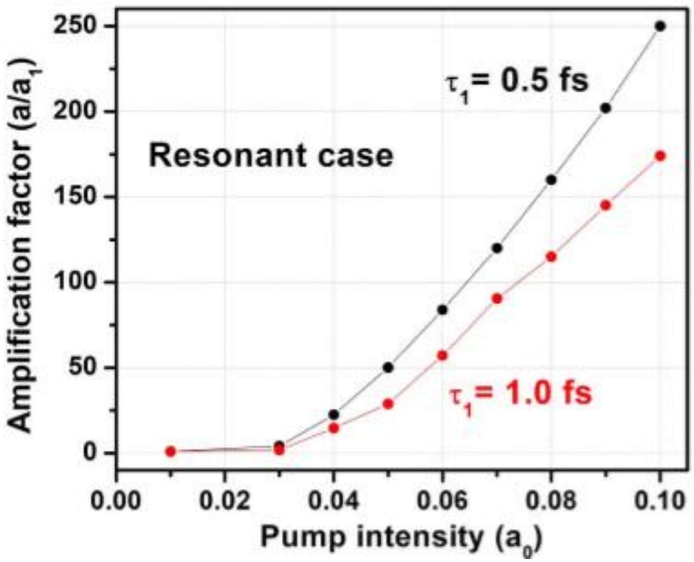

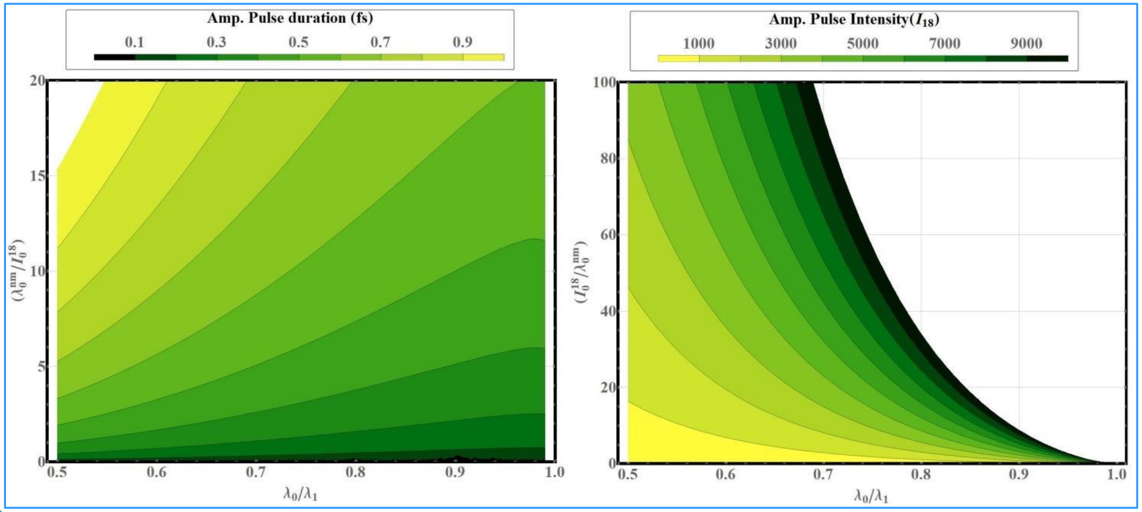

Resonant amplitude amplification factor as a function of seed pulse width (τ1);
Resonant amplitude amplification factor as a function of the pump pulse amplitude,
the calculations refer to λ=30 nm, τ0=10 fs, and a1=0.001.

Mishra&Andreev JOSA B (2018)

Plausible resonant BRAmp configuration

Plausible Pump laser parameters	
wave length λ_0	~40 nm
Pulse freq. ω_0	~4.71×10^{16} s^{-1}
Pulse length τ_0	~10 fs
Peak intensity (I_0)	~ 10^{17} W/cm^2 (spot size ~10 μm)
Plausible seed laser parameters	
wave length λ_1	60 nm
Pulse freq. ω_1	3×10^{16} s^{-1}
Pulse length τ_1	0.8 fs
Pulse energy ε_1	~10 nJ
Peak power W_1	~10 MW
Peak intensity I_1	~10^{14} W/cm^2 (spot size ~10 μm^2)
Output results	
Wave breaking Int. I_{br}	1.2×10^{19} W/cm^2
Plasma density	7.8×10^{22} cm^{-3}
L-w freq.	1.57×10^{16} s^{-1}
Pulse duration ( )	0.9 fs
Output fluence w_{1m}	1.6×10^{4} J/cm^2
Output intensity I_{1m}	7×10^{18} W/cm^2
Amplification factor ( )	7×10^{4}
Maximum amplification time ( )	160 fs
Maximum plasma thickness ( )	48 μm

Conclusion

- **Optimal structure of the considered targets permits to get almost total absorption of laser pulse. Profile shape has a weak influence on the absorption. In our case, degradation of a structure by a laser prepulse is the most important factor. For this scheme to work, one needs a very high-contrast laser-pulse and a nanosecond laser pre-pulse duration**
- **It is shown that relativistic intensity laser wave can be effectively (~ percent) converted into sequence of atto-pulses of minimal duration at the reflection from a foil with a big angle of incidence.**
- **We have shown a line splitting in the harmonic spectra. Our simulations demonstrated that an additive accelerated motion of the oscillating plasma surface during laser pulse is causing the substructure in the harmonic spectra. The surfaces movement and so the substructure in the harmonic spectra, increases with the plasma density gradient.**
- **Nano-wires exhibit a large coefficient of laser energy conversion to kinetic energy of a fast electrons. Its bunch can propagate as far as several hundred micrometers in such targets.**
- **The obtained atto-pulse generation and focusing with energy conversion efficiency of a few percent by cone-shaped target enables the peak intensity of the filtered fields in the focus to reach the value of the incident radiation.**
- **It may be concluded that the BRA schema operating in XUV regime may efficiently be utilized to amplify and compress the weak ultra-short pulses to EW/cm^2 and sub fs time scale.**
- **It is shown that in the weakly relativistic regime the intensity of high harmonics can be amplified by three orders of magnitude with help of the method of multi-reflections thus, significantly increase the generated weak atto-pulses.**

Contributors

Thank you to them

Z.Lecz, S.Mishra (ELI-ALPS)
M.Schnuerer's group (Max Born Institute),
K.Yu.Platonov (SPb State University),

THANK YOU FOR YOUR ATTENTION!

SZÉCHENYI 2020
Hungarian Government
European Union European Regional Development Fund
INVESTING IN YOUR FUTURE